

Global-Local Finite Element Analysis
of Laminated Composites

by

Marco A. Vidussoni

Thesis submitted to the Faculty of the
Virginia Polytechnic Institute and State University
in partial fulfillment of the requirements for the degree of
Master of Science
in
Engineering Mechanics

APPROVED:

O. H. Griffith / Chairperson

J. N. Reddy

E. R. Johnson

July 11, 1988
Blacksburg, Virginia

**Global-Local Finite Element Analysis
of Laminated Composites**

by

Marco A. Vidussoni

O. H. Griffin, Chairperson

Engineering Mechanics

(ABSTRACT)

A Global-Local finite element approach was used to investigate the interlaminar stresses in laminated composite plates with a central circular hole. Detailed solutions were sought for the interlaminar normal stress distributions close to the free straight edge of the plate as well as around the edge of the hole. The Global model was analyzed as a two-dimensional problem. The displacements obtained a distance away from the regions of interest in the two-dimensional model were used as imposed boundary conditions to the three-dimensional models of the edges.

The results obtained were found to be accurate, thus demonstrating the validity and strength of the Global-Local technique. The results further concluded that for symmetric cross-ply laminated plates with large central circular holes, the interlaminar normal stresses at the free edges are affected to a small degree by the size of the hole.

The CSM Testbed and ANISAP were the two finite element analysis programs used throughout this investigation. The CSM Testbed element library was augmented with 16, 20, 24 and 32 node displacement formulation based elements which were implemented as Experimental elements.

Acknowledgements

This research was accomplished under support from the Computational Structural Mechanics Group at NASA-Langley Research Center through Grant NAG-1-675.

Appreciation is gratefully extended to Dr. O. H. Griffin, Jr. for many hours of helpful discussions and for all the support he provided. The author expresses his thanks to Dr. J. N. Reddy and Dr. E. R. Johnson for serving on his graduate committee.

Thanks are further extended to Dr. N. F. Knight, Jr., Dr. M. Aminpour, Ms. C. Lotts and Ms. S. McCleary of the Computational Structural Mechanics Group at NASA-Langley Research Center for the help provided during the course of this investigation as well as to Dr. M. Williams and Ms. E. N. Lau of the Virginia Polytechnic Institute and State University Computing Center for their support during the final stages of the research.

Table of Contents

Chapter 1: Introduction and Literature Review	1
1.1 Introduction	1
1.2 Literature Review	4
1.2.1. Finite Element Analysis Programs Used	4
1.2.2. Elements Implemented in the CSM Testbed	5
1.2.3. Elements Through the Thickness Study	6
1.2.4. Global/Local Analysis	6
1.2.5. The Free Edge Problem	10
1.2.6. The Hole Edge Problem	13
Chapter 2: Element Implementation	14
2.1. Description of the Elements	14
2.1.1. - 16 Node Element	17
2.1.2. - 20 Node Element	17
2.1.3. - 24 Node Element	17
2.1.4. - 32 Node Element	19
2.2. Element Verification	19
2.3. Conclusions	23

Chapter 3: Element Aspect Ratio Study	25
3.1. Comparative Discussion	26
3.2. Conclusion	29
Chapter 4: Elements Through the Thickness Study	30
4.1. CSM Testbed S81 element	33
4.2. Experimental Elements	35
4.2.1. - 16 Node Element	35
4.2.2. - 20 Node Element	37
4.2.3. - 24 Node Element	44
4.2.4. - 32 Node Element	46
4.3. ANISAP Elements	50
4.4. Comparative Discussion	50
4.5. Conclusion	51
Chapter 5: Global-Local Analysis	52
5.1 The Global Model	53
5.2 The Local Models	55
5.3. Straight Free Edge Problem	57
5.3.1. Location of the Global-Local interface	57
5.3.2. Free edge stresses	60
5.4. Hole Free Edge Problem	74
5.4.1. Location of the Global-Local interface	80
5.4.2. Hole edge stresses	85
5.5. Discussion	95
5.6. Conclusion	103
Chapter 6: Conclusion to the study	104

References	106
Appendix A. FORTRAN Listing for Element Routines	109
Vita	130

List of Illustrations

Figure 1. Schematic for Global-Local analysis	3
Figure 2. Geometry of the Focus Problem	7
Figure 3. Force components at laminate interfaces close to free edges	11
Figure 4. Definition of the characteristic angles for a lamina	16
Figure 5. Geometry of the experimental elements	18
Figure 6. Test model for verifying the element implementation	20
Figure 7. Schematic of the benchmark model	22
Figure 8. Finite element model used for the aspect ratio study.	27
Figure 9. Model for the study of elements through the thickness, $[0/90]_s$ and $[90/0]_s$	32
Figure 10. σ_{zz} at midplane for S81 element, $(0/90)_s$, 4 elements/ply	34
Figure 11. σ_{zz} at midplane for 16 node element, $(0/90)_s$, 4 elements/ply	36
Figure 12. σ_{zz} at midplane for 20 node element, $(0/90)_s$, 1 element/ply	38
Figure 13. σ_{zz} at midplane for 20 node element, $(90/0)_s$, 1 element/ply	39
Figure 14. σ_{zz} at midplane for 20 node element, $(0/90/0/90)_s$, 1 element/ply	40
Figure 15. σ_{zz} at midplane for 20 node element, $(0/90)_s$, 2 elements/ply	41
Figure 16. σ_{zz} at midplane for 20 node element, $(90/0)_s$, 2 elements/ply	42
Figure 17. σ_{zz} at midplane for 20 node element, $(0/90/0/90)_s$, 2 elements/ply	43
Figure 18. σ_{zz} at midplane for 24 node element, $(0/90)_s$, 4 elements/ply	45
Figure 19. σ_{zz} at midplane for 32 node element, $(0/90)_s$, 1 element/ply	47
Figure 20. σ_{zz} at midplane for 32 node element, $(90/0)_s$, 1 element/ply	48
Figure 21. σ_{zz} at midplane for 32 node element, $(0/90/0/90)_s$, 1 element/ply	49

Figure 22. Schematic of the Global model, NSPOKES = 40, NRINGS = 3	54
Figure 23. Schematic showing the position of the Local models	56
Figure 24. Local straight edge model	58
Figure 25. T2.0-II mesh, Sigma zz at midplane for d = 6.0", (0/90)s	61
Figure 26. Sigma zz at midplane for d = 0.0", (0/90)s	63
Figure 27. Global model with no hole	64
Figure 28. Sigma zz at midplane for d = 1.0", (0/90)s	65
Figure 29. Sigma zz at midplane for d = 2.0", (0/90)s	67
Figure 30. Sigma zz at midplane for d = 3.0", (0/90)s	68
Figure 31. Sigma zz at midplane for d = 4.0", (0/90)s	69
Figure 32. Sigma zz at midplane for d = 5.0", (0/90)s	70
Figure 33. Sigma zz at midplane for d = 6.0", (0/90)s	72
Figure 34. Sigma zz at midplane for d = 6.0", (90/0)s	73
Figure 35. Sigma zz at midplane for d = 6.0", (0/90/0/90)s	75
Figure 36. Local hole edge model, NSPOKES = 24, NRINGS = 4, Z scale = 10 : 1	76
Figure 37. Deformed mesh for Local problem with d = 0.1"	78
Figure 38. Sigma zz vs. theta for (0/90)s, d = 0.1"	79
Figure 39. Sigma xx vs. theta for (0/90)s, d = 0.1"	81
Figure 40. Sigma yy vs. theta for (0/90)s, d = 0.1"	82
Figure 41. Sigma zz vs. Theta for (0/90)s, d = 6.0", rings = 4, spokes = 32	83
Figure 42. Sigma zz vs. Theta for (0/90)s, d = 6.0", rings = 4, spokes = 24	84
Figure 43. Sigma zz vs. Theta for (0/90)s, with d = 1.0"	87
Figure 44. Sigma zz vs. Theta for (0/90)s, with d = 2.0"	88
Figure 45. Sigma zz vs. Theta for (0/90)s, with d = 3.0"	89
Figure 46. Sigma zz vs. Theta for (0/90)s, with d = 4.0"	90
Figure 47. Sigma zz vs. Theta for (0/90)s, with d = 5.0"	91
Figure 48. Sigma zz vs. Theta for (0/90)s, with d = 6.0"	92
Figure 49. Sigma zz vs. Theta for (90/0)s, with d = 6.0"	94

Figure 50. Sigma zz vs. Theta for (0/90/0/90)s, with d = 6.0"	96
Figure 51. Normal inplane stresses vs. Theta for (0/90)s, with d = 6.0"	97
Figure 52. Plot of the Global deformed mesh	98
Figure 53. Sigma zz at the interface, d = 6.0", [0/90]s	101
Figure 54. Sigma zz vs. z at the straight edge, d = 6.0", [0/90]s	102

List of Tables

Table 1. Mechanical Properties of T300/5208 Graphite/Epoxy	21
Table 2. Summary of benchmark results	23
Table 3. Summary of aspect ratios for the elements, results for the test problem	28
Table 4. Summary of tests performed on the elements for the thickness study	31
Table 5. Summary of the results obtained for the elements/layer study	50
Table 6. Summary of optimal interface location for straight edge problem	60
Table 7. Summary of analyses performed on the straight free edge	62
Table 8. Summary of analyses performed on the hole free edge	85

Chapter 1: Introduction and Literature Review

1.1 Introduction

Analysis of composite laminates by the finite element method provides a high degree of control over the detail and accuracy of the predicted stress fields. When a laminate of finite size is stressed by inplane loading, two regions of primary interest can be differentiated: 1. the region away from, and 2. the region close to, discontinuities. These can be a free unloaded edge or any kind of geometric or material anomaly. In the regions away from the discontinuities the stress fields are fairly uniform and may be predicted satisfactorily even with simple analysis tools such as the classical laminated plate theory (Whitney¹). However in the regions close to the discontinuities all components of stress have characteristically high gradients (Pipes and Pagano²). As a generally accepted rule, (Pipes and Pagano², Wang and Crossman³) the presence of the discontinuity affects the stresses to a distance approximately one laminate thickness away from the free edge.

Analytical models have been proposed to solve this problem. These were based on both elasticity formulations (Pipes and Pagano⁴) and variational methods (Tang⁵). However, their capabilities were restricted to very simple and specific cases. To analyze a more generic type of problem, the

most viable alternative was to perform a full three-dimensional finite element analysis of the laminate, with a high element density close to the areas of critical interest. The appropriate approach to model these regions can be chosen from the following two alternatives:

1. to utilize a large number of low interpolation order elements, or
2. to utilize a smaller number of higher order elements.

When the finite element analysis is performed in three-dimensions on an arbitrary laminate, a large amount of computer resources is involved even for the simplest geometries and loading cases. This large investment in resources is a result of the large number of elements required to model the problem accurately. Each laminate orientation requires a number of elements through the thickness in order to simulate the displacements correctly in a fully three-dimensional loading situation.

Unless absolutely required, full three-dimensional analysis of laminates can be a waste of resources. When considering the problem of a laminated plate with some sort of discontinuity, the response for most of the regions in the plate away from the crucial areas can be predicted by a much less sophisticated and economical type of analysis, such as a two-dimensional finite element analysis or even from classical laminated plate theory.

The basic concept of "Global-Local analysis" is to perform a simple analysis on a global region, and a more accurate analysis on a local region of high interest. The interface between the two analyses is provided by a common boundary to which the global displacements are applied as boundary conditions to the local model, as shown in Figure 1. The boundary is chosen a distance away from the critical regions in order to maintain accuracy of the simplifying assumptions upon which the method is based.

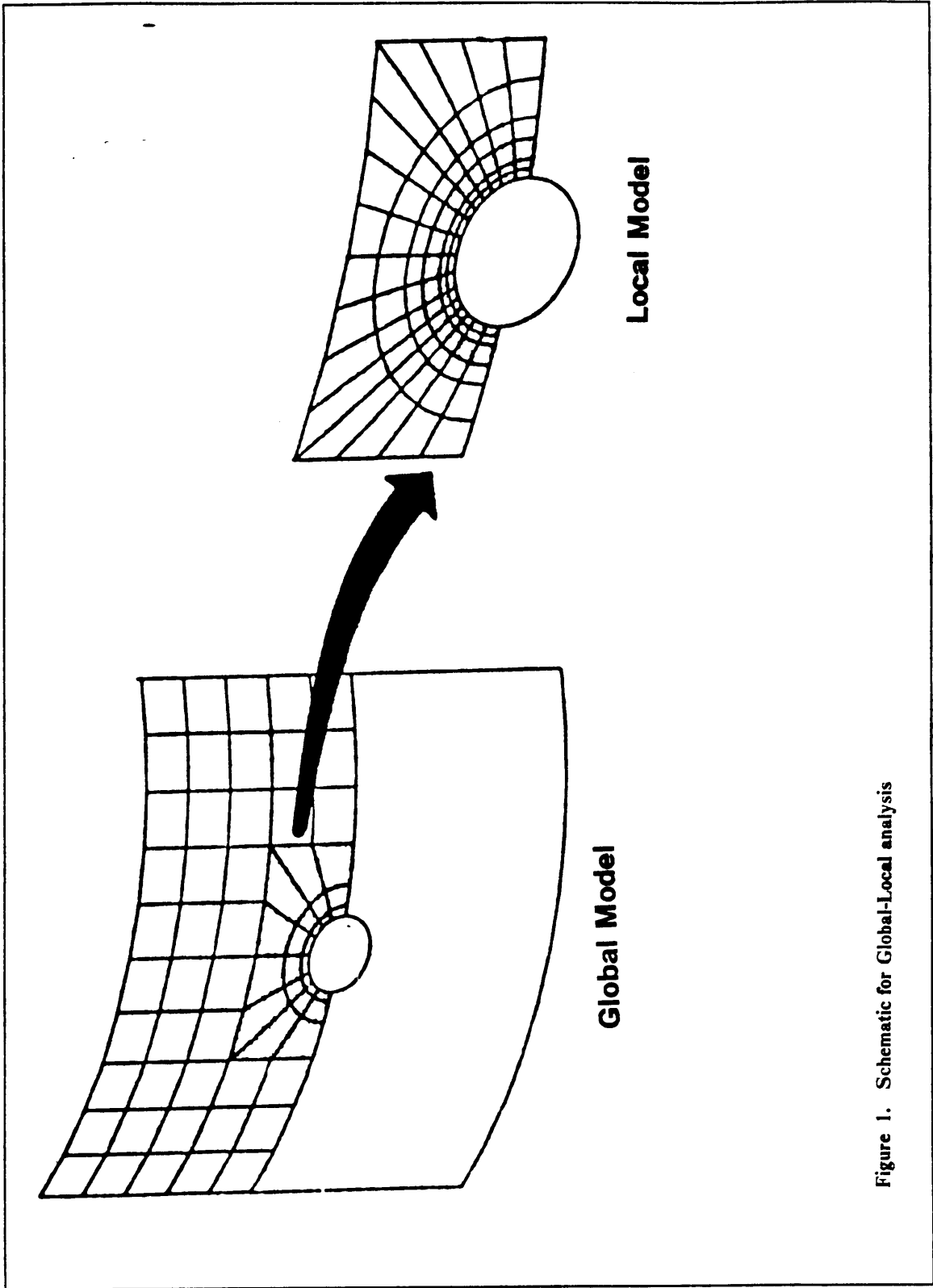


Figure 1. Schematic for Global-Local analysis

For the purpose of this study, a global analysis based on two-dimensional plate elements was used, with a full three-dimensional local analysis. Other possible combinations of analysis are presented in section 1.2.4.

The problem chosen for analysis during the course of this study was a laminated plate with a centrally placed circular hole. The Global-Local investigation was further extended to include a study of the optimal positioning of the Global-Local boundary for the models under consideration.

The finite element programs which were utilized throughout the course of the study were the CSM Testbed (Lotts et al.⁶) and ANISAP (Burns⁷). SPAR (Whetstone⁸), the predecessor of the CSM Testbed had only one three-dimensional brick element available, designated as the "S81" element. In order to perform a more accurate analysis, a family of three-dimensional isoparametric displacement elements were implemented in the the CSM Testbed. To fully verify the capabilities of these elements, studies were performed on the maximum element aspect ratio (the ratio of element side length to thickness) possible for various cases, as well as on the minimum number of elements through the thickness necessary to model three-dimensional laminates satisfactorily.

1.2 Literature Review

1.2.1. Finite Element Analysis Programs Used

As has been mentioned in the previous section both the CSM Testbed and ANISAP were employed during the course of the investigation.

The CSM Testbed is based on NICE/SPAR, a public domain program which has been extensively updated and improved by the Computational Structural Mechanics (CSM) Group at NASA

Langley Research Center. The overall structure of NICE/SPAR was maintained in the CSM Testbed. It is comprised of two parts, the finite element analysis section "SPAR", and the executive control language "NICE". The latter was developed at Lockheed (Palo Alto)⁹, whereas the former originated from Engineering Information Systems¹⁰.

ANISAP (ANISotropic Analysis Program) is a three-dimensional finite element code based on STAP (Static Analysis Program) developed by Bathe and Wilson¹¹. ANISAP was created at Virginia Polytechnic Institute and State University by Burns⁷. The code is capable of modeling fully anisotropic materials. The version utilized during the investigation was modified by the author. The extent of the changes were in the complete implementation of the 24 and 32 node elements as well as improved output options, post-processing capabilities and out of core storage of the stiffness matrix.

1.2.2. Elements Implemented in the CSM Testbed

The original version of the CSM Testbed had only one three-dimensional brick element available in its library⁸. During the course of the investigation, four new isoparametric displacement formulation elements were implemented as "External Experimental Elements"¹². These were :

16 Node Element - with quadratic interpolation in the plane and linear interpolation through the thickness (Bathe et al.¹¹),

20 Node Element - with quadratic interpolation in all three directions (Zienkiewicz¹³),

24 Node Element - with cubic interpolation in the plane and linear interpolation through the thickness (Bathe et al.¹¹),

32 Node Element - with cubic interpolation in all three directions (Zienkiewicz¹³).

1.2.3. Elements Through the Thickness Study

No detailed study seemed to have been performed on the minimum number of three-dimensional elements necessary to model composite laminates satisfactorily. A proposal for such a study was put forward by Knight, Greene and Stroud¹⁴. Burns⁷ performed a limited comparison on the responses obtained with the 16 and 20 node elements installed in ANISAP. The results suggested two 20 node elements were necessary to model the thickness of a laminate with accuracy.

1.2.4. Global/Local Analysis

Although the concept of Global/Local analysis is not new, very little specific work has been carried out to develop the technique and quantify the parameters to a satisfactory degree, especially when performing analyses on composite laminates.

There is an entire spectrum of possible associations for performing Global-Local analyses. Reddy proposes various combinations of such methods: analytical, variational, finite difference, finite element and boundary element¹⁵. Reddy presents typical problems which are well suited to Global-Local analysis such as:

- free edge stress analysis of laminates,
- contact stress problems,
- stress analysis of structures with discontinuities, and
- blade stiffened panel with a discontinuous stiffener - the "focus problem" shown in Figure 2.

The suitability of the focus problem to the Global-Local technique is discussed by Knight et al.¹⁴. They identified this suitability based on various characteristics of the model: a discontinuity, ec-

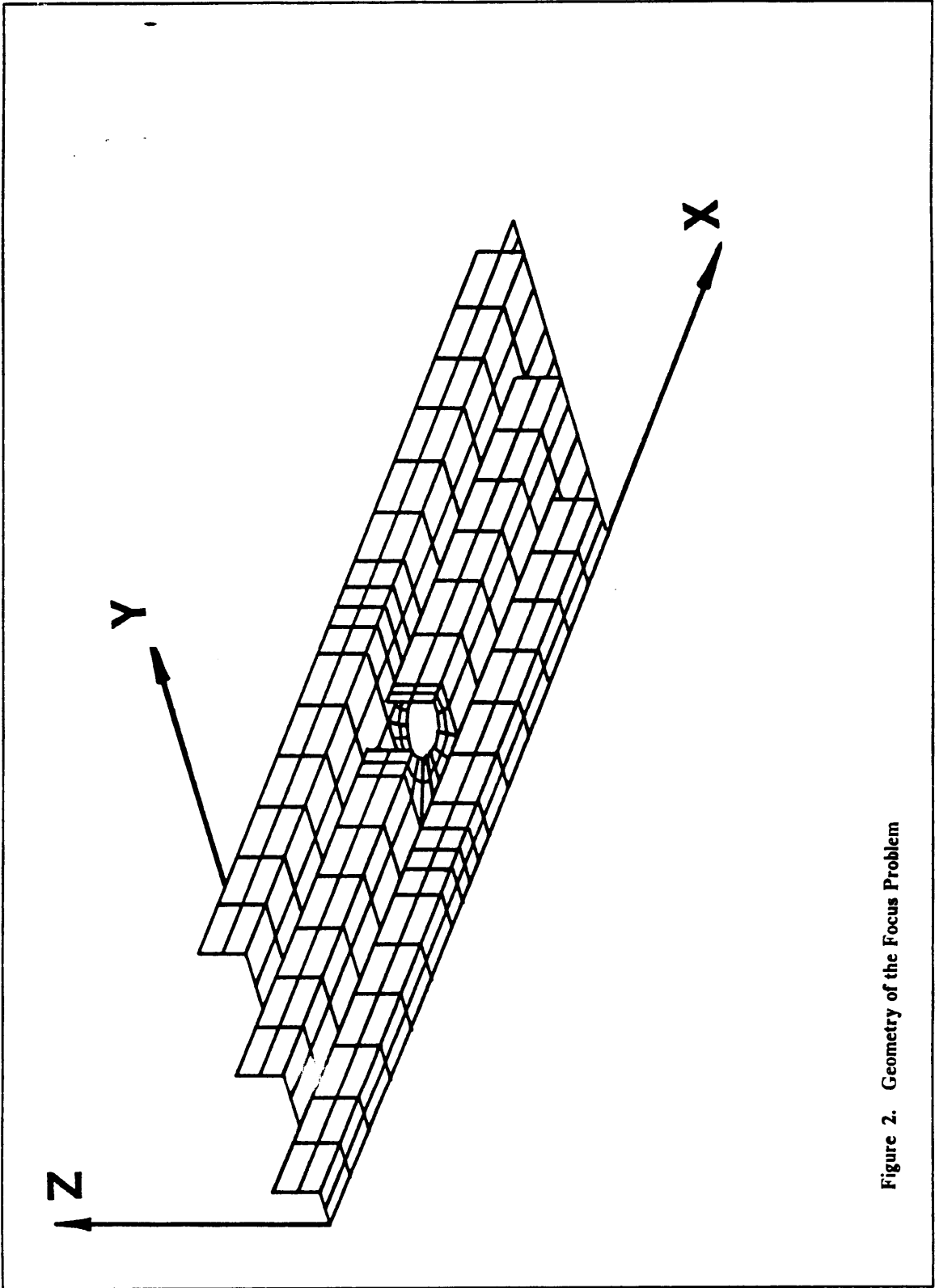


Figure 2. Geometry of the Focus Problem

centric loading, large displacements, large stress gradients and high inplane loading. For the solution of the focus problem Reddy¹⁵ suggested a global two-dimensional analysis be combined to a local three-dimensional finite element analysis. Dong¹⁶ prescribed the same approach.

Dong illustrates many cases in which Global-Local Finite Element Methods (GLFEM) are advantageous, these include the analysis of a laminated plate with a hole¹⁷, crack growth, wave scattering and the focus problem¹⁶.

Dong describes a very specific development of the Global-Local method. It consists of a combination of Ritz functions for the global domain, which capture the essential behavior of the overall region, together with a local finite element analysis in order to obtain the specific behavior in particular sections. Dong's approach to GLFEM results in a simultaneous solution of both the global and local regions. The accuracy and effectiveness of the method is dependent on the quality of the global functions.

Nelson specifies stresses around holes in composite laminates as one of the ideal cases for Global-Local analysis¹⁸. Knight, Greene and Stroud provide a general definition for GLFEM for composite panels, where "global" refers to the overall panel response and "local" is the response near the hole¹⁴. They identified four areas of research associated with Global-Local methodologies:

- discretization procedures,
- refined theories.
- classical and closed-form solutions, and
- hybrid techniques.

One important consideration Dong specifies as essential for the success of the analysis is that continuity requirements for displacements and rotations be completely satisfied at the Global/Local interface¹⁷. Knight et al.¹⁴ recommended a study be performed on the definition of the interface region between the global and the local models. Reddy¹⁵ identified possible problem areas when performing GLFEM, these were:

- interfacing between regions,
- interfacing between methods,
- selection of regions, and
- changing regions and interfaces.

Noor¹⁹ stated the method could be limited by the errors for the boundary data on the local analysis. Ransom²⁰ suggested some guidelines for two-dimensional GLFEM by suggesting some "Rules of thumb", which were found to be applicable during the analysis of laminated plates with central circular holes. These required that: 1. the local boundary should be placed farther from the hole than the innermost ring in the global analysis, and 2. the local model should be chosen to have nodes which coincide with the position of nodes in the global model.

Knight et al.¹⁴ applied a zooming technique to the focus problem, by analyzing successively finer grids in specific regions, in order to solve for the stress distribution. The analysis was two-dimensional throughout. The stresses obtained in the local region were used to calculate constants for the point stress failure criterion (Whitney and Nuisimer²¹). They noted that only a fully three-dimensional analysis could reveal the interlaminar stress components within the local region.

Noor approached the solution of the postbuckling behavior of the focus problem by the GLFEM¹⁹. The problem is highly non-linear which results in very large computer requirements. To reduce these requirements the Global-Local method was employed. By the application of this method the displacement and strain distributions were found.

Nelson¹⁸ proposed that the next generation of finite element analysis software have complete analysis capabilities such as linear and non-linear analysis, one-, two- and three-dimensional models as well as mixed dimensional models. Importance is also placed on program modularity.

1.2.5. The Free Edge Problem

When a composite laminate of finite dimensions is loaded, the components of stress which are created can be subdivided into 2 groups:

- Intralaminar stresses - σ_x , σ_y and τ_{xy}
- Interlaminar stresses - σ_z , τ_{xz} and τ_{yz}

Away from free edges and discontinuities of sorts the intralaminar stresses can be predicted by the classical laminated plate theory¹. This theory does not, however, provide any indication of the possible magnitudes of the interlaminar stresses.

The early works of Pipes and Pagano⁴ showed that away from a free (unloaded) edge, the interlaminar stresses are negligible. However when one focuses onto the stress components close to a free edge the existence of a "boundary layer" was demonstrated.

Interlaminar stresses arise when differences in Poisson's ratios occur between adjacent layers. At the interfaces continuity of displacements must be satisfied, which results in the creation of non-zero interlaminar shear stresses τ_{yz} along the interface (fig. 3.a). These shear stresses are kept in force equilibrium by σ_y and in moment equilibrium by the interlaminar normal stress σ_z (fig. 3.b).

Thus the free edge stresses are governed by the extent of material properties mismatch between neighboring layers. It is possible in fact to design laminates with no material mismatch. The simplest solution is achieved with a unidirectional laminate. However Herakovich²² showed that it was possible to have no mismatch in material properties even when dealing with symmetric angleply laminates $[\pm\theta]_s$.

Previous investigations have shown that within the boundary layer all the stress components have large gradients. These result in large decreases in absolute magnitude of the intralaminar stresses

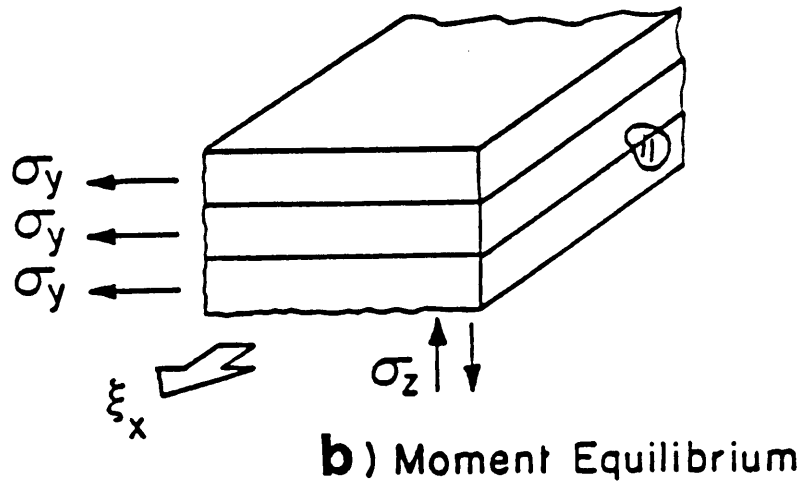
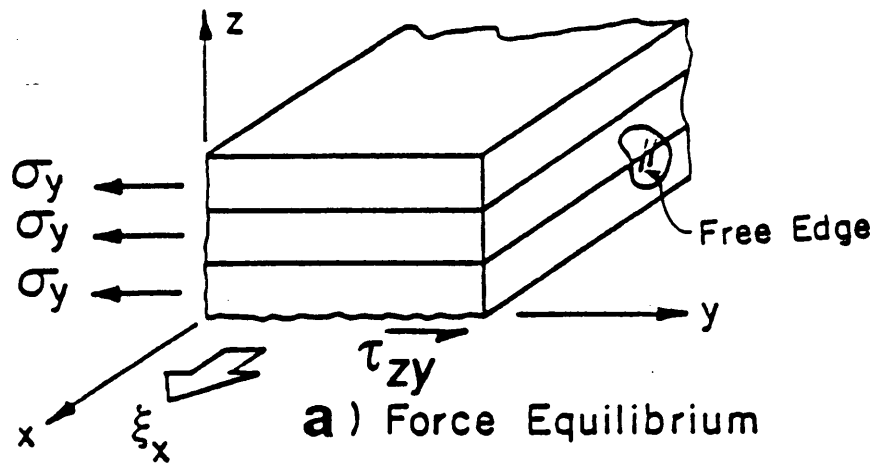


Figure 3. Force components at laminate interfaces close to free edges

and in large increases of the interlaminar components. Pipes and Pagano² showed that significant interlaminar stresses exist within one laminate thickness of the edge. Historically, this has been considered the approximate boundary layer thickness.

Most of the methods employed for evaluating interlaminar stresses utilize an "effective modulus" formulation, whereby each layer is described as a homogeneous anisotropic material (Salamon²³). Such an assumption neglects completely the existence of fibers and matrix materials as constituents, and as such it models perfect bonding and uniform material distribution within each layer. However if there is no particular need or interest in the micromechanics of the laminate this assumption is a very good one.

Pipes and Pagano² developed a rigorous elasticity solution assuming that stresses were independent of the x-coordinate in Figure 3, which reduced the independent variables from three to two. Renieri and Herakovich²⁴, during the course of an investigation on linear and nonlinear materials, revealed a number of inconsistencies with the results of Pipes and Pagano².

Pagano later derived a higher order theory²⁵ which satisfied the requirements for a vanishing shear stress at the free edge interface junction. This theory, however, is limited in the possible number of layers to be modeled. The degree of limitations with analytical solutions caused many investigators to resort to three-dimensional finite elements for the analysis of composite laminates. The free edge extension problem has been solved thoroughly with standard results provided by Rybicki²⁶ and Stanton²⁷.

Wang and Crossman³ provided results for $[90/0]_S$ laminate which supported those provided by Herakovich et al.²⁸, although neither could satisfy the traction-free edge conditions. Griffin²⁹ produced results for the normal interlaminar stress at the interfaces of $[0/90]_S$ laminates for both Boron/Epoxy and Graphite/Epoxy material systems. Again the presence of high interlaminar stresses was predicted at the edges of the laminates in question.

1.2.6. The Hole Edge Problem

The problem of a layered plate with a hole is fully three-dimensional in character. The presence of the hole creates free edge effects which disturb not only the inplane fields but also the interlaminar effects. Griffin²⁹ concluded that these problems can be solved for by the use of three-dimensional finite element analysis. Salamon²³ conducted an assessment of edge effects in laminates with holes, finding that the sign of the interlaminar normal stress cannot be determined intuitively from equilibrium considerations. He also noted that the maximum interlaminar stresses may occur not at the hole but at a nearby straight edge. These observations were obtained by consulting the results presented by Barker et al³⁰ and Rybicki et al³¹.

During another investigation, Dana³² concluded that the maximum interlaminar normal stress varies from 30% to 15% of the farfield inplane normal stress for crossply laminates. Rybicki and Schmueser³³ demonstrated that both the sign and distribution of the interlaminar stresses change considerably by varying the layup sequence in crossply laminates. Griffin et al.³⁴ investigated the changes in the interlaminar normal stress at the straight free edge of a plate with a 2.0" diameter hole as compared to the stresses in a plate with no hole. The results which were presented showed very little changes between the two cases.

Tang³⁵ provided an analytical solution for the extension of an infinite plate with a circular hole. The results obtained compared well with finite element solutions. He also solved the problem by employing a variational formulation; the results however displayed large discrepancies with existing solutions close to the edge of the hole.

Chapter 2: Element Implementation

2.1. Description of the Elements

As it has already been mentioned, the original version of the CSM Testbed had only one three-dimensional brick element installed; the "S81"⁸. This element is based on a hybrid stress formulation. It has 8 nodes (one in each corner), with 3 displacement degrees of freedom per node.

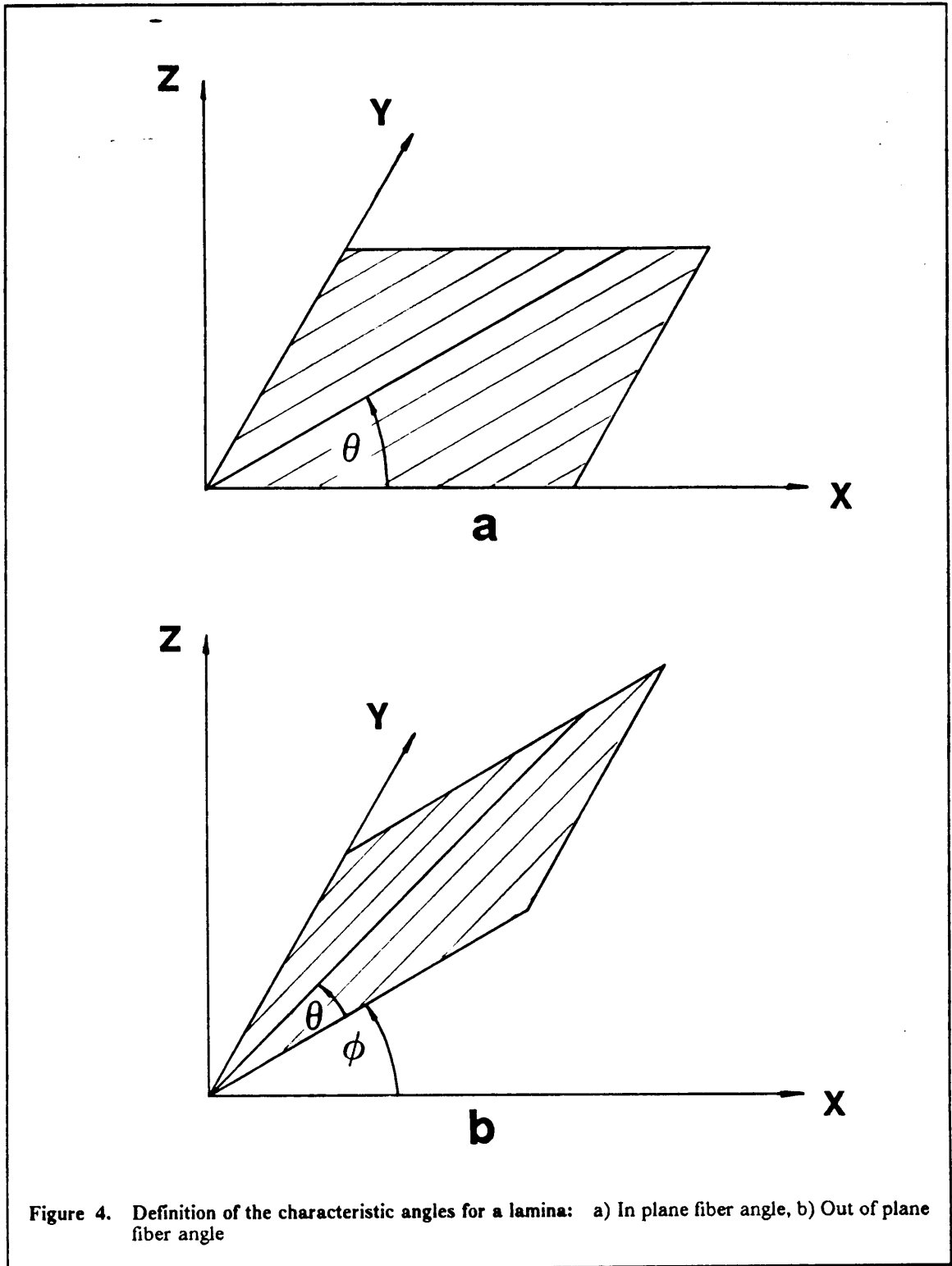
For the purpose of modeling composite laminates, the S81 element was found not to perform satisfactorily. Its biggest shortcoming was found to be its low order of integration (one point), the lowest possible for a brick element. Such a low order resulted in extremely large models required to analyze even simple laminate problems, and completely erroneous results for non-parallel element faces.

Although it is not true that a higher degree of interpolation results in a better element, it was felt that for the specific purpose of modeling composite materials a reasonable balance between degree of interpolation and size of the element stiffness matrix should be achieved.

To satisfy these requirements, four elements were installed in the CSM Testbed as "Experimental Elements"¹². These are displacement formulation based isoparametric (Serendipity) elements with 16, 20, 24 and 32 nodes per element. Each node has three degrees of freedom; the displacements in the three-dimensions. The element stiffness matrix is calculated by performing Gauss integration over the whole element. The number of Gauss points within each element can be selected by the user specifying the number of Gauss points to be used in the plane (local x-y plane) and through the thickness (local z axis). This selection enables the user to modify the stiffness response of the element by selecting various combinations of Gauss points within the element. The choice of order of integration is of the utmost importance to the accuracy of the results¹¹. By using a reduced integration order from the order required for an exact solution, a less stiff element can be achieved. This may result in a closer behavior of the system to the actual response, although the boundedness of the solution is destroyed. Integration orders which are too low yield erroneous results, and those which are too high model a too stiff response¹¹. Throughout the course of the investigation a 3x3x3 Gauss integration was employed for each element.

All the experimental elements are capable of modeling fully anisotropic materials independently of the CSM Testbed processors. Generally composite laminae are transversely isotropic, with orientations described by an in-plane rotation θ (fig. 4.a). However, it is conceivable for a composite to possess a second characteristic angle which represents an elevation of the in-plane properties into the third dimension. Such an angle can be defined by ϕ (rotation about y), as shown in Figure 4.b.

The SPAR Experimental Element facility¹² requires that 15 constants be supplied each time this specific element routine is called. These constants are the 9 elastic properties, the angles θ and ϕ as defined in Figure 4, and the out of plane angle between the global axes and the local element axes. The remaining 3 constants define the specific weight and the order of Gauss integration in the plane and through the thickness.



2.1.1. - 16 Node Element

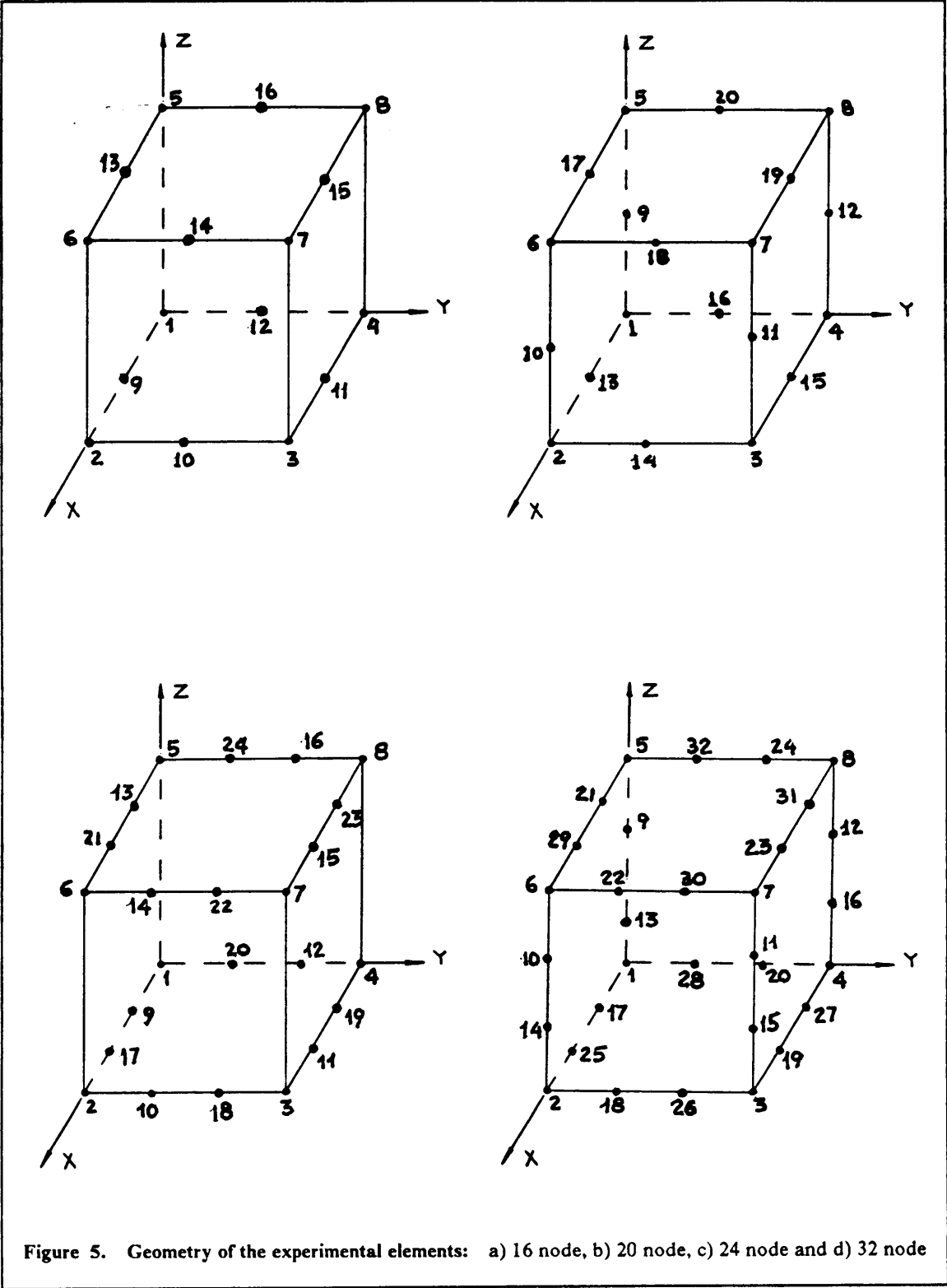
The 16 node element is shown in Figure 5.a. It has quadratic interpolation in the plane and linear interpolation through the thickness. The full element stiffness matrix is [48 x 48].

2.1.2. - 20 Node Element

This element has quadratic interpolation in all three directions. It is shown in Figure 5.b. The full element stiffness matrix is [60 x 60]. This is a very good element to use because of its higher than linear degree of interpolation in all directions.

2.1.3. - 24 Node Element

The 24 node element has cubic interpolation in the plane and linear interpolation through the thickness (fig. 5.c). The element stiffness matrix has dimension [72 x 72]. This type of element is not very well suited to model composites because of its linear interpolation through the thickness, however it should prove to be a good element for uniform materials such as isotropic, or materials with a slight degree of orthotropy.



2.1.4. - 32 Node Element

This element is the most complex one implemented (fig. 5.d). It has cubic interpolation in all three directions. The full element stiffness matrix is [96 x 96]. This element should prove to be very good for any type of material provided a convenient pre-processor is available for mesh generation; Otherwise, generating a mesh of 32 node elements could become a very cumbersome process.

2.2. Element Verification

Since the experimental elements are all well known and tested (Lin³⁸, Dana³² and Zienkiewicz¹³), it was felt that it was only necessary to demonstrate satisfactorily that results obtained with the experimental elements on the CSM Testbed were comparable to those obtained for the same cases on ANISAP. Thus a very limited number of tests were performed during the 'element verification' stage. The cases were analyzed by loading the model shown in Figure 6 in the following manner:

1. 1 parallelepiped element, Gr/Ep material properties at 30° off the x-axis with an imposed displacement of 0.01 in. in the x-direction,
2. 1 parallelepiped element, Gr/Ep material properties at 30° off the x-axis with an imposed displacement of 0.01 in. in the x-direction and an imposed displacement of 0.005 in. in the y-direction.

All the tests were performed for each element type.

Once the comparative tests were completed, each experimental element was tested in the benchmark problem, shown in figure 7. This is a very simple model in which two elements share a common face which can be rotated through an angle thus distorting both elements. The skew

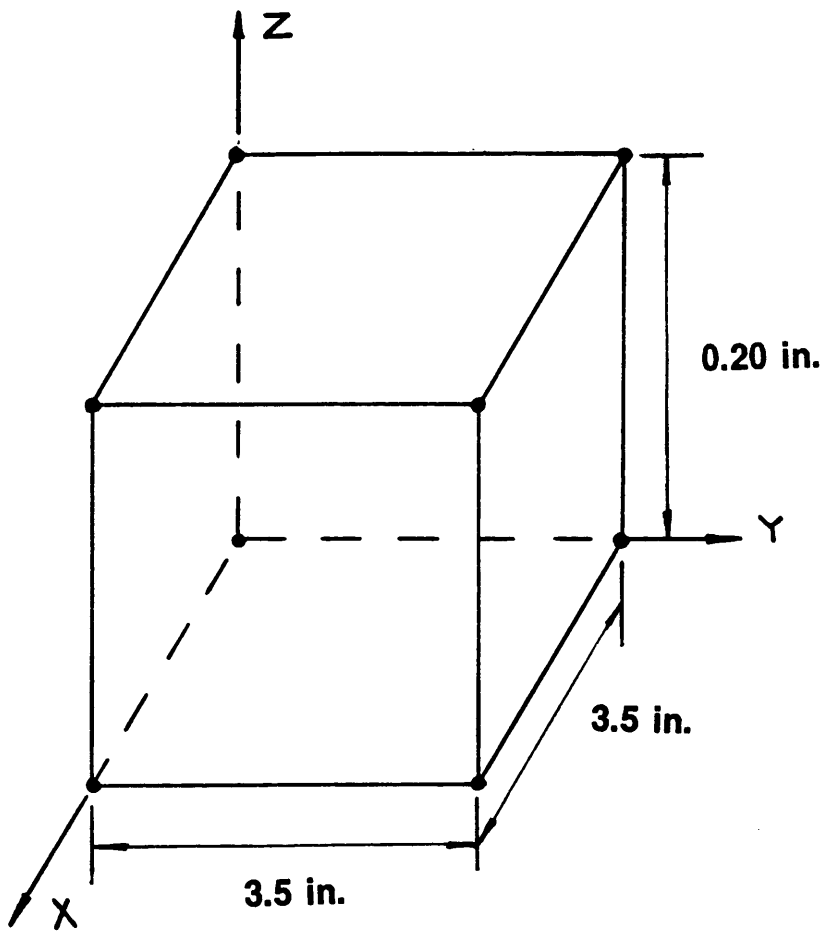


Figure 6. Test model for verifying the element implementation

angle θ , is a measure of the extent to which the particular type of element can be distorted. The model is loaded by both external loads and displacements in such a manner that the result is a constant x-direction stress with all other components zero. The purpose of the benchmark was to measure the performance of the three-dimensional elements when distorted. The reason the S81 was discarded as a candidate element for use during the course of this investigation was due to its poor performance when opposite sides of the element were not parallel to each other.

The material properties for the T300/5208 Graphite-Epoxy material system used throughout the course of the investigation are presented in Table 1 (Griffin³⁶).

Table 1. Mechanical Properties of T300/5208 Graphite/Epoxy

E_1	E_2	E_3	G_{12}	G_{13}	G_{23}	ν_{12}	ν_{13}	ν_{23}
19.2 Msi	1.56 Msi	1.56 Msi	0.82 Msi	0.82 Msi	0.54 Msi	0.239	0.239	0.45

Table 2 summarizes the results obtained with the benchmark for the elements under consideration. The maximum skew angle is a measure of the maximum deformation which can be imposed on the element before the element stiffness matrix becomes singular and the program halts execution due to a division by zero.

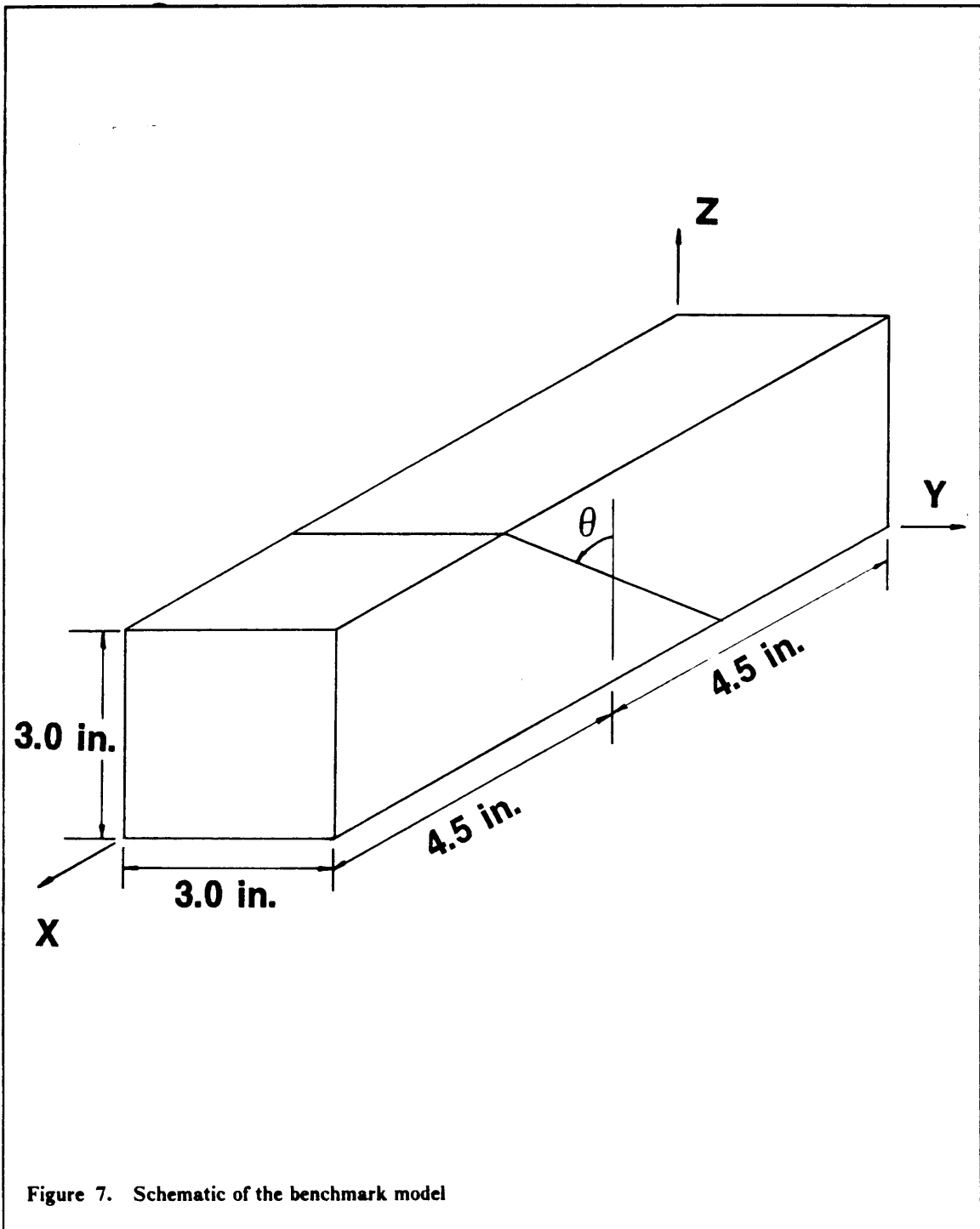


Table 2. Summary of benchmark results

Element Type	Max. Skew Angle (deg.)
S81	67.0
16 Node	71.56
20 Node	71.56
24 Node	71.56
32 Node	71.56

2.3. Conclusions

All the computer runs with both ANISAP and the CSM Testbed yielded identical results. Any discrepancies were attributable to machine accuracy. The results obtained from the benchmark show the incapability of the S81 to deal properly with highly deformed geometries similar to those modeled by the benchmark. The maximum skew angle was limited by the geometry of the model to 71.56°. To impose a larger angle on the model would result in an impossible mapping, and the Jacobian for some of the Gauss points would be negative. The maximum skew angles obtained with the experimental elements seem to have achieved a satisfactory size to ensure proper behavior even under extremely distorted geometrical conditions. All of the experimental elements still produced correct results at 71.56°. Larger angles weren't imposed on the benchmark because the size of the smallest side was extremely close to creating a singularity.

The tests performed in the next two chapters are necessary for proving satisfactorily the viability of using these elements for the modeling of composite materials at the lamina level. More specif-

ically, Chapter 3 will deal with the study of the maximum possible aspect ratio for each element under different loadings and layups. In the next study the number of elements through the thickness necessary to correctly model composites is determined, and this study is discussed in Chapter 4.

Chapter 3: Element Aspect Ratio Study

Once the Experimental elements were implemented successfully, it was found necessary to perform preliminary tests to assess their adaptability to composite materials. One of the limitations with the use of finite elements for analyzing composite laminates is the relative small size of the thickness of each layer when compared to the x-y plane dimensions.

A dimensionless quantity was defined as the "aspect ratio" for a particular element which is the ratio of the characteristic element side length to the element thickness. The aspect ratio is defined as:

$$AR = L / t , \text{ as shown in Figure 8.}$$

A series of simple models were prepared and solved to find the maximum aspect ratio attainable by the various elements available, before signs of instability were detected in the results. The instabilities were traced back to the relative order of magnitude of the element thickness when compared to machine accuracy. This instability manifested itself as an ill-conditioning of the stiffness matrix.

The model used for the test is shown in figure 8. It consists of a 2x2 square mesh in the plane, with one element through the thickness. The simplification introduced by selecting only one element through the thickness for modeling each fiber orientation is acceptable since the present study

is not aimed at obtaining significant values for the interlaminar stresses, but only in searching for the limit in the stability of the results for a particular element, loading case and layup.

Two loading conditions were applied to the model:

1. x-direction applied displacement of 0.01 (load case I),
2. x-direction applied displacement of 0.01 and y-direction applied displacement of 0.005 (load case II).

All the layups analyzed were symmetric crossplies, more specifically:

1. $[0/90]_s$.
2. $[90/0]_s$.
3. $[0/90/0/90]_s$.

The results obtained for each element type are presented in Table 3 and are discussed in the following section. All of the results obtained were compared to the performance of the original S81 element.

3.1. Comparative Discussion

The results presented in Table 3, are indicative of the performance of the elements; indicative of the order of magnitude of the critical aspect ratio. The tests which were performed on the elements are very simplistic. As such the aspect ratios obtained are certainly not the minimum attainable values for each element type but are only specific values obtained from the model in question. In no way was such a model thought to be extremely demanding and as such the results should be considered in their correct context. The S81 element is quoted reaching an aspect ratio of 2000. It was actually

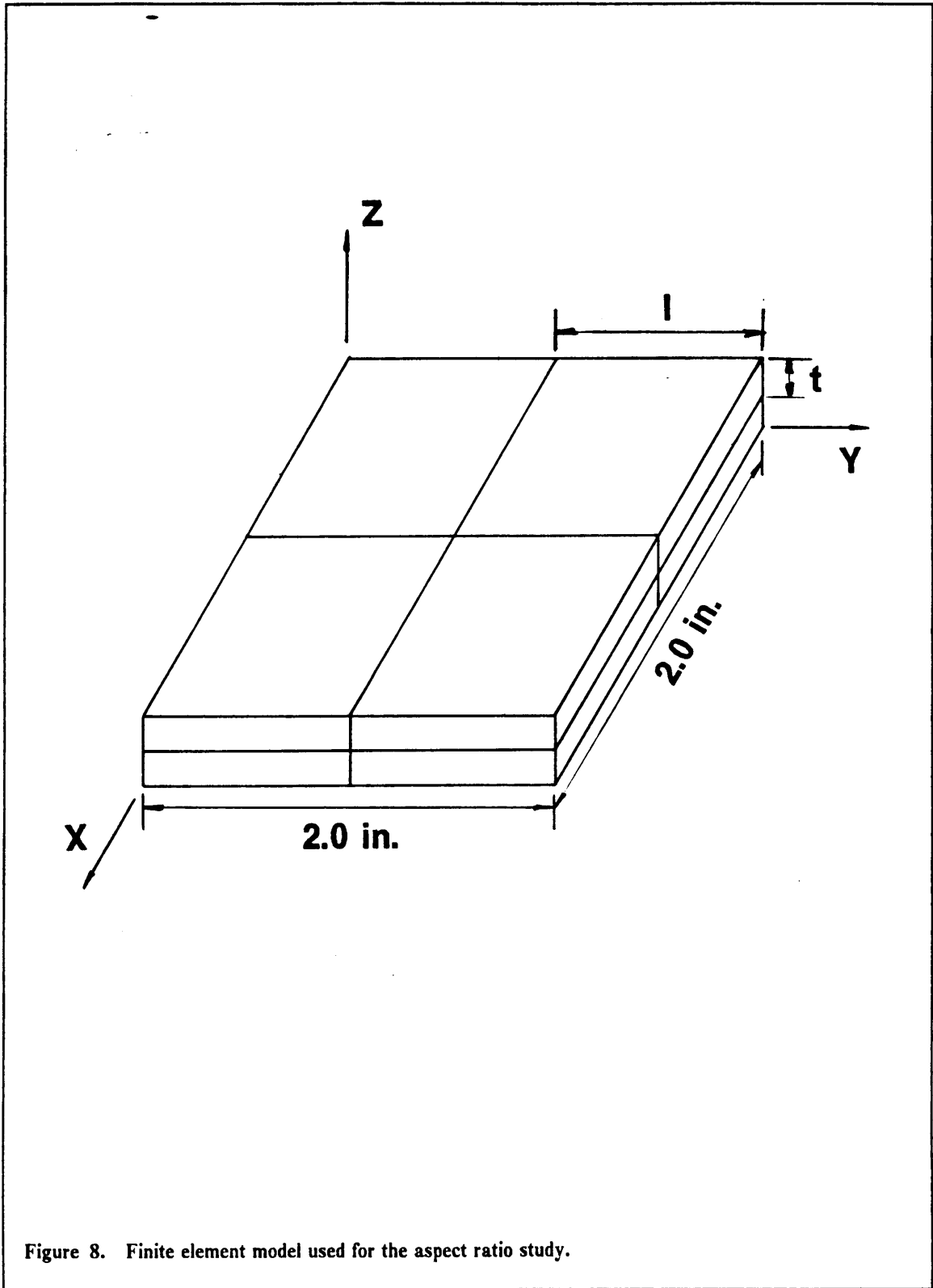


Figure 8. Finite element model used for the aspect ratio study.

Table 3. Summary of aspect ratios for the elements, results for the test problem

Element	Layup	Load case I	Load case II
S81	[0/90] _s	2000	2000
	[90/0] _s	2000	2000
	[0/90/0/90] _s	2000	2000
16 Node	[0/90] _s	1000000	1000000
	[90/0] _s	1000000	1000000
	[0/90/0/90] _s	1000000	1000000
20 Node	[0/90] _s	1000000	1000000
	[90/0] _s	1000000	1000000
	[0/90/0/90] _s	1000000	1000000
24 Node	[0/90] _s	1000000	1000000
	[90/0] _s	1000000	1000000
	[0/90/0/90] _s	1000000	1000000
32 Node	[0/90] _s	1000000	1000000
	[90/0] _s	1000000	1000000
	[0/90/0/90] _s	1000000	1000000

found that for an aspect ratio of 2000 the element operated correctly whereas for an aspect ratio of 3000 it failed, thus the exact aspect ratio would lie somewhere between these two values. All the experimental elements attained the same order of magnitude in aspect ratio of 1000000. Again the accurate value can be found to lie between 1000000 and 2000000. It is not the purpose of this study

to provide accurate figures for the critical aspect ratios of the elements but just to supply some indication of the correct orders of magnitude.

It is interesting to note that within a specific element type the response is not affected by layup or loading. The order of magnitude of the aspect ratios attained by the experimental element family is so large that the eventual failure of the elements can be attributable only to machine accuracy, ie. the order of the sizes involved in the calculations are of the same order or at least very similar to the actual accuracy of the machine.

The result that element aspect ratio is not affected by the type of loading is of great importance when dealing with composite laminates because this could suggest that even complex loadings would not place restrictions on the aspect ratios of the elements involved. Of course to support fully such an assertion it would be necessary to perform a similar type of analysis with various models of increasing loading complexity. Since the failure is due to the singularity of the stiffness matrix it would seem evident from a 'continuum' point of view that the failure be independent of the loading condition. However, when one considers a discretized model, such a statement ceases to be obvious, and for such a reason both loading conditions were considered.

When comparing the aspect ratios obtained with the S81 and the experimental family, it becomes evident that the S81 is not well suited for use in the modeling of composite materials.

3.2. Conclusion

The analysis of the maximum possible attainable aspect ratio for all the element types available revealed that the experimental element family was vastly superior to the existing S81 element, especially when dealing with composite laminates.

Chapter 4: Elements Through the Thickness Study

A common form of failure in composite laminates is by delamination. The origins of such a mechanism can be traced back to high interlaminar stresses near free edges. In order to obtain accurate values of such stresses and the related gradients, it is necessary to have a fine grid close to the edges under investigation. It is, however, not sufficient to have a detailed grid in the plane of the laminate. One must have a sufficient degree of resolution through each layer thickness. A layer thickness corresponds to a lamina or a number of adjacent laminas with equal fiber angle.

The study consisted of investigating the distribution of interlaminar normal stress near the free edge of a laminate. This was achieved by increasing the number of elements used to model the thickness of each layer. This process was repeated for all element types including the S81. The S81 element was considered for comparative purposes. The results were compared to those obtained with the 32 node element with two or more elements per layer, which were assumed to achieve the best possible solution for the given mesh. As a further means of verification computer runs of selected problems were performed on ANISAP. The free edge model used is shown in figure 9. All stresses are independent of the x-direction because the applied displacement is in that direction, and therefore only one element is required to model the laminate in the x-direction. The mesh was designed with four elements with finer intervals between them in the y-direction. This disposition allows a smoother recovery of the stress components. The thickness of the laminate was modeled by a

variable number of elements depending on the specific laminate under consideration and the effective number of elements needed to represent each layer.

Each element type was subjected to a total of nine test cases which were decided upon by combining various laminates with a certain number of elements per layer. Only crossply laminates were considered: $[0/90]_5$, $[90/0]_5$ and $[0/90/0/90]_5$. The choice of such laminates made it possible to impose symmetric boundary conditions on all 3 planes at the origin. The final model was simplified considerably which resulted in modeling of only one eighth of the actual problem.

The total number of elements through the laminate thickness was increased from 2 to 8 in steps of 2. A summary of all the tests performed on each element type is presented in Table 4.

Table 4. Summary of tests performed on the elements for the thickness study

Total number of layers in the model	$[0/90]_5$	$[90/0]_5$	$[0/90/0/90]_5$
2	Yes	Yes	No
4	Yes	Yes	Yes
6	Yes	Yes	No
8	Yes	No	Yes

All the results were presented on three dimensional plots of the interlaminar normal stresses at the midplane. The plots were visually compared and the better results were kept as reference against which the others were discussed. These reference plots were the assumed solution to the problem.

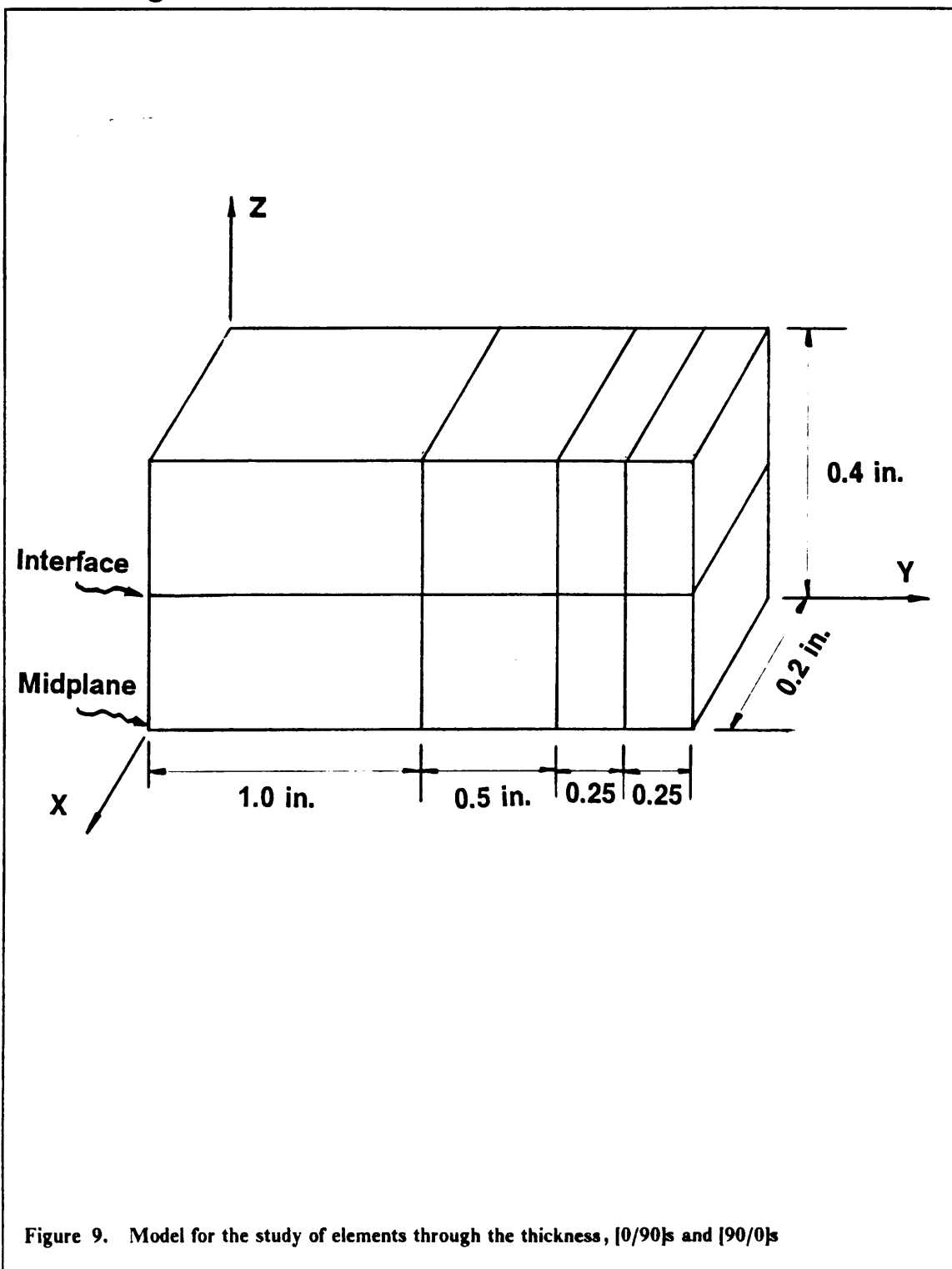


Figure 9. Model for the study of elements through the thickness, [0/90]s and [90/0]s

4.1. CSM Testbed S81 element

As a first observation it is important to note that the S81 element provides stress values only at the node points, and not at the Gauss points as do all the experimental elements. This resulted in a considerably smaller number of plottable points in the plane (10 points) than the experimental elements (36 points).

The S81 is a low order element with linear interpolation functions along all the edges. When this consideration is coupled to the small number of stress points available the performance expectations for the S81 were very limited. The best results were obtained from the analysis of the $[0/90]_5$ laminate (shown in fig. 10), with 4 elements per ply. This model consisted of eight elements through the thickness; four through the 0° layer and four through the 90° layer. The plot followed the generally accepted distribution for the interlaminar normal stress at the edge of a laminate. However, there was a large amount of unevenness in the results which suggested that more than four elements would be necessary in order to produce more reliable results. The differences between this plot and those employing a lesser number of elements were not very large, suggesting that maybe the element converged to a close solution but not the correct one or otherwise required a much more detailed mesh.

When the $[90/0]_5$ laminate was analyzed, the response at 3 elements per thickness was found to be unacceptable since it did not reach the peak at the edge attained by the higher order elements. Finally the $[0/90/0/90]_5$ laminate was analyzed and the results obtained with 2 elements per thickness were a poor representation of the actual stress state. This was considered an extremely negative factor since the $[0/90/0/90]_5$ has gradients which are much smaller than those encountered in the other two laminates and thus convergence to an acceptable solution should be facilitated. Again all the plots for the last two laminates displayed large disturbances in the results.

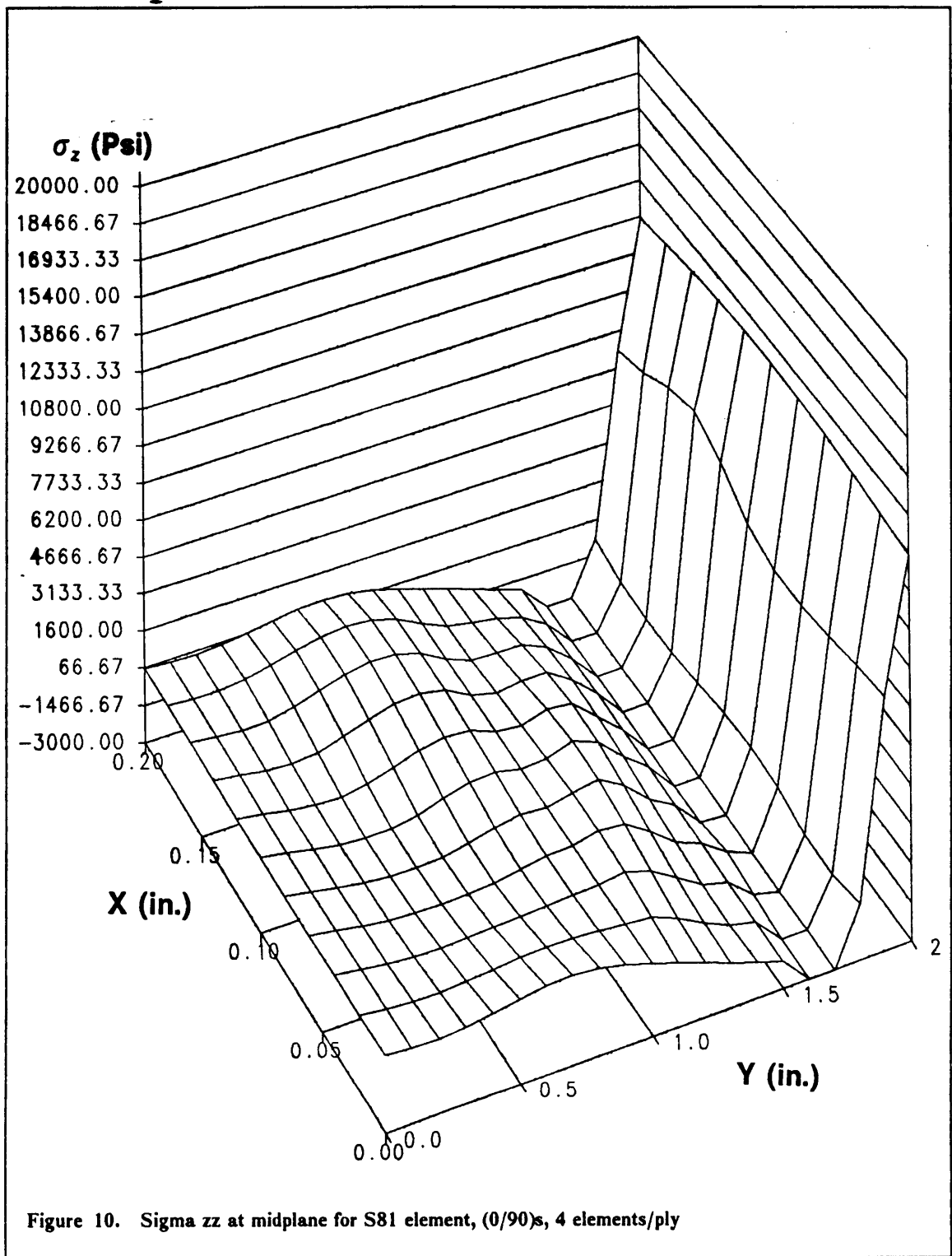
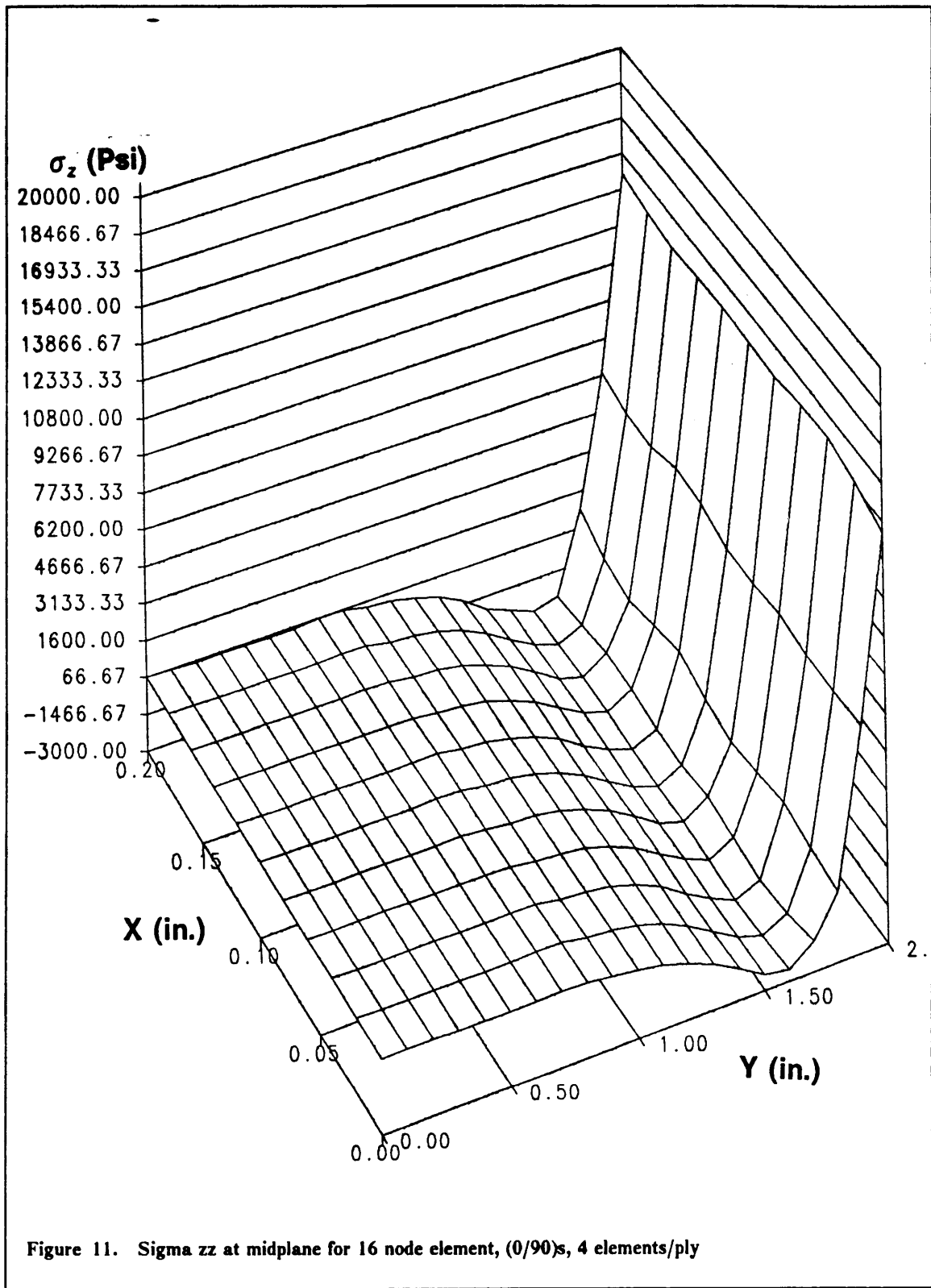


Figure 10. Sigma zz at midplane for S81 element, (0/90)_s, 4 elements/ply

4.2. Experimental Elements

4.2.1. - 16 Node Element

This is the lowest order element implemented in the experimental family. The analysis of the $[0/90]_5$ laminate was very successful when 4 elements per layer were utilized (fig. 11). However the responses obtained for the lower number of elements per layer were all of surprising quality. When the analysis was performed on both the $[90/0]_5$ and the $[0/90/0/90]_5$ the responses were found to be not as close to the assumed solution as one would want even when using the maximum number of elements per layer available for that particular laminate. The maximum possible number of elements in the model was limited exclusively by computation time considerations and the relative importance of the results obtained when the number of elements in the model was doubled. These differences could suggest that this particular element requires at least 4 elements per layer to model edge effects properly.



4.2.2. - 20 Node Element

This element was found to be very successful. All of the analyses were completed with a high degree of accuracy when compared to the results obtained for the 32 node element. Also the plots were very smooth, indicating a good reliability of the results. It is interesting to note that the response of the 1 element per thickness case resulted in very close representations of the actual stress distribution independent of the laminate type (figs. 12, 13 and 14).

When 2 elements per ply were used to model each layer the results duplicated those obtained with the 32 node element (figs. 15, 16 and 17).

Rough calculations of the forces above and below the $\sigma_z = 0$ plane showed that force equilibrium was satisfied for all the laminates under consideration. This is the basic requirement necessary for the stresses at the edges of a laminate to maintain both force and moment equilibrium.

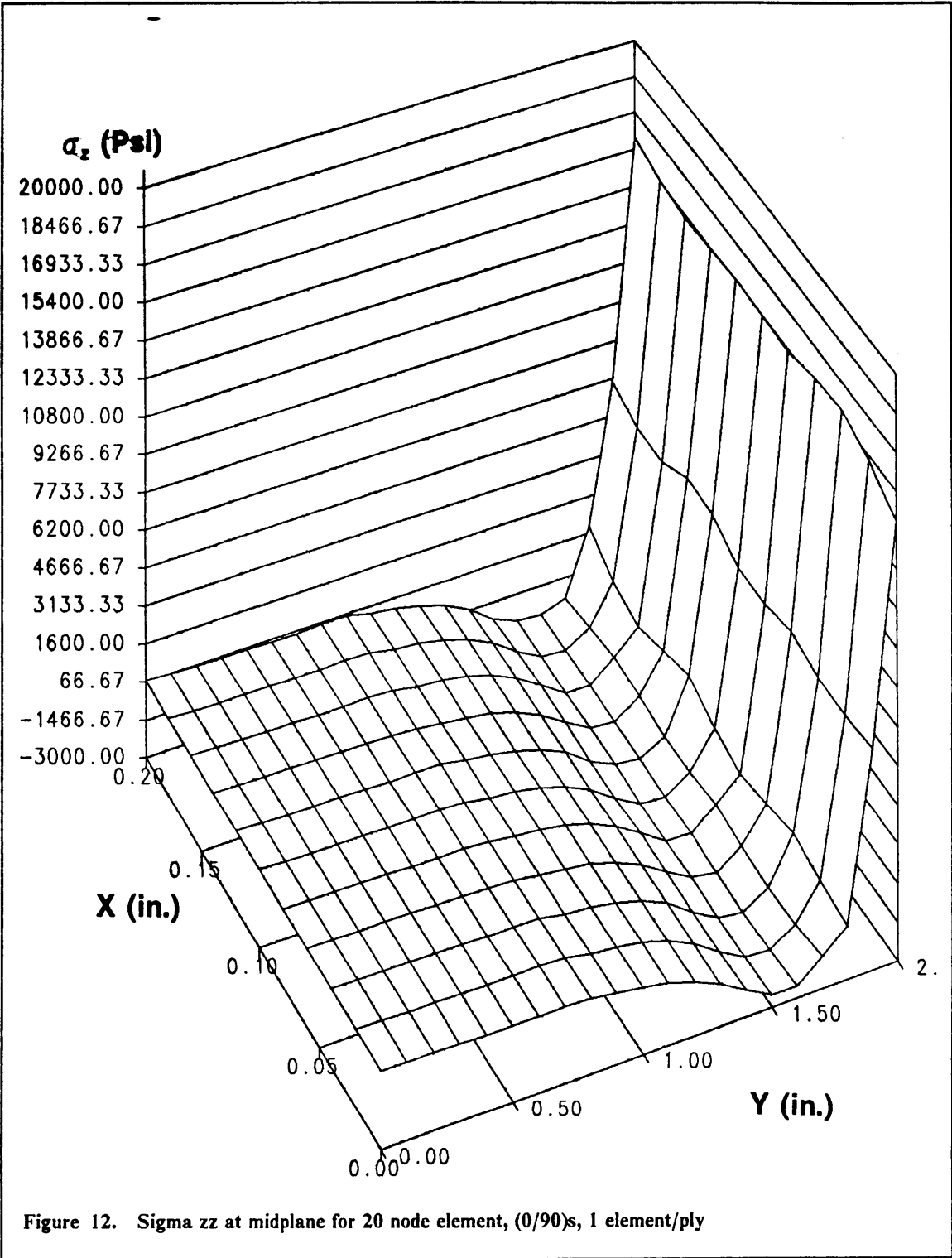


Figure 12. Sigma zz at midplane for 20 node element, (0/90)s, 1 element/ply

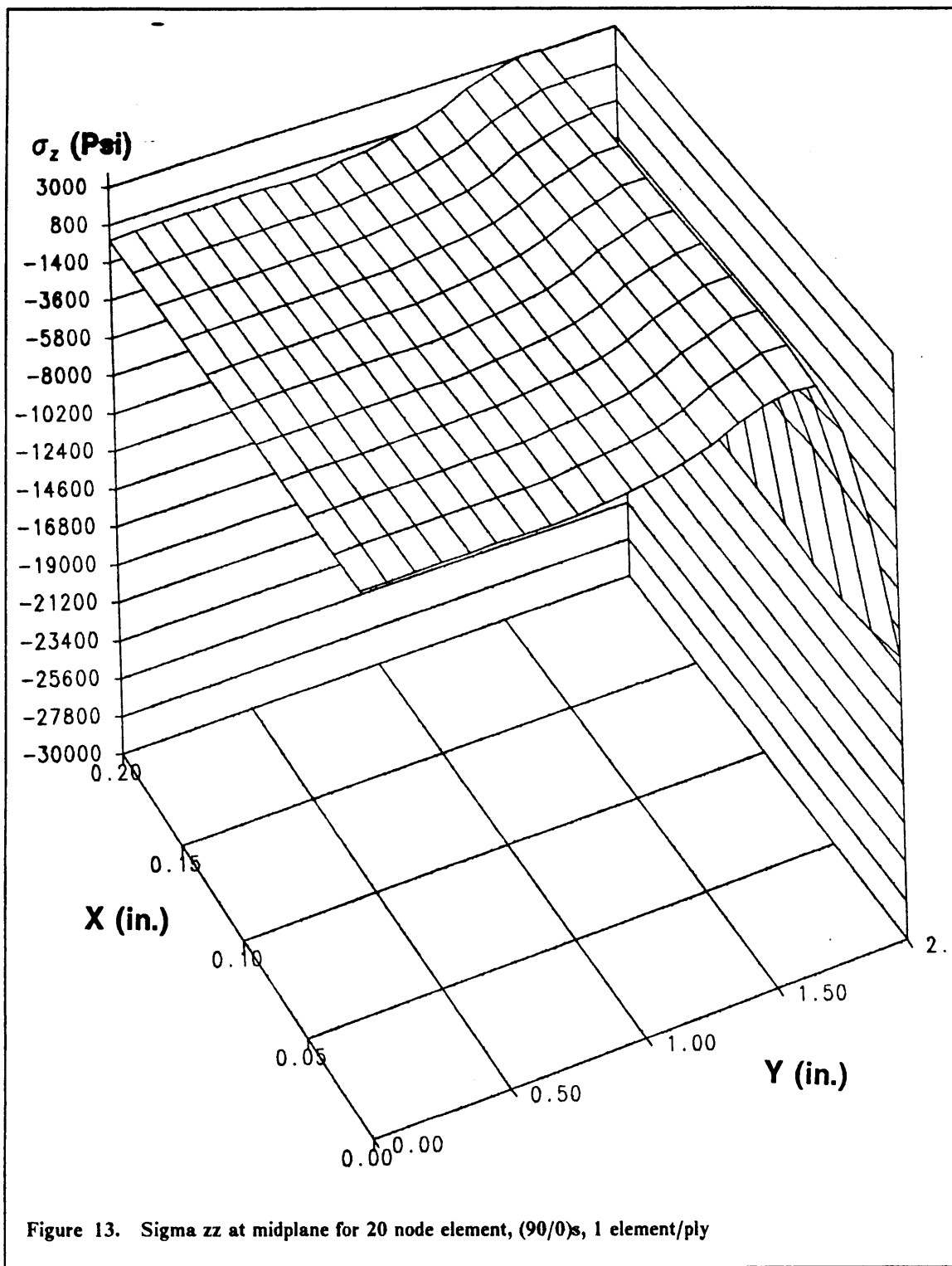


Figure 13. Sigma zz at midplane for 20 node element, (90/0)s, 1 element/ply

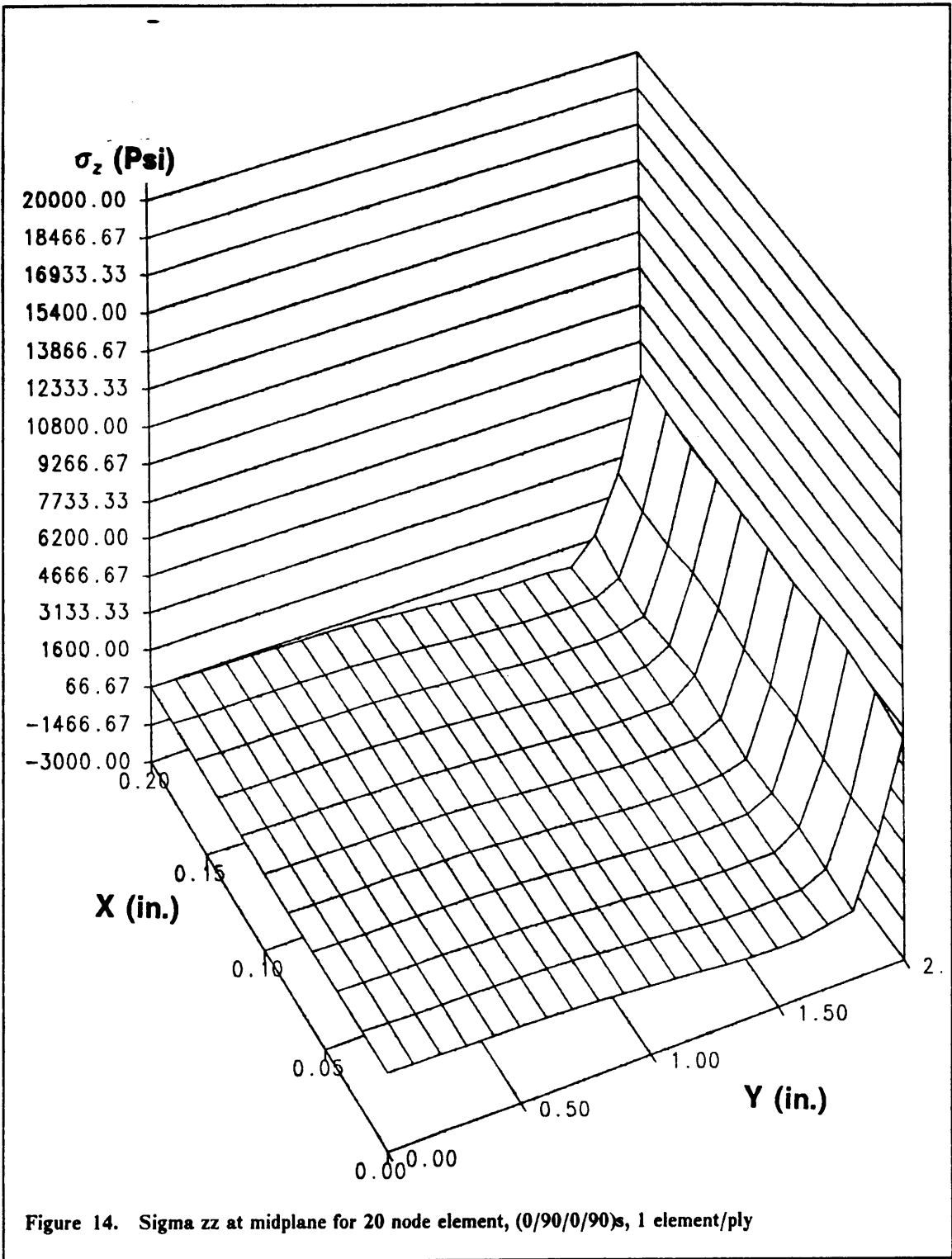


Figure 14. Sigma zz at midplane for 20 node element, (0/90/0/90)s, 1 element/ply

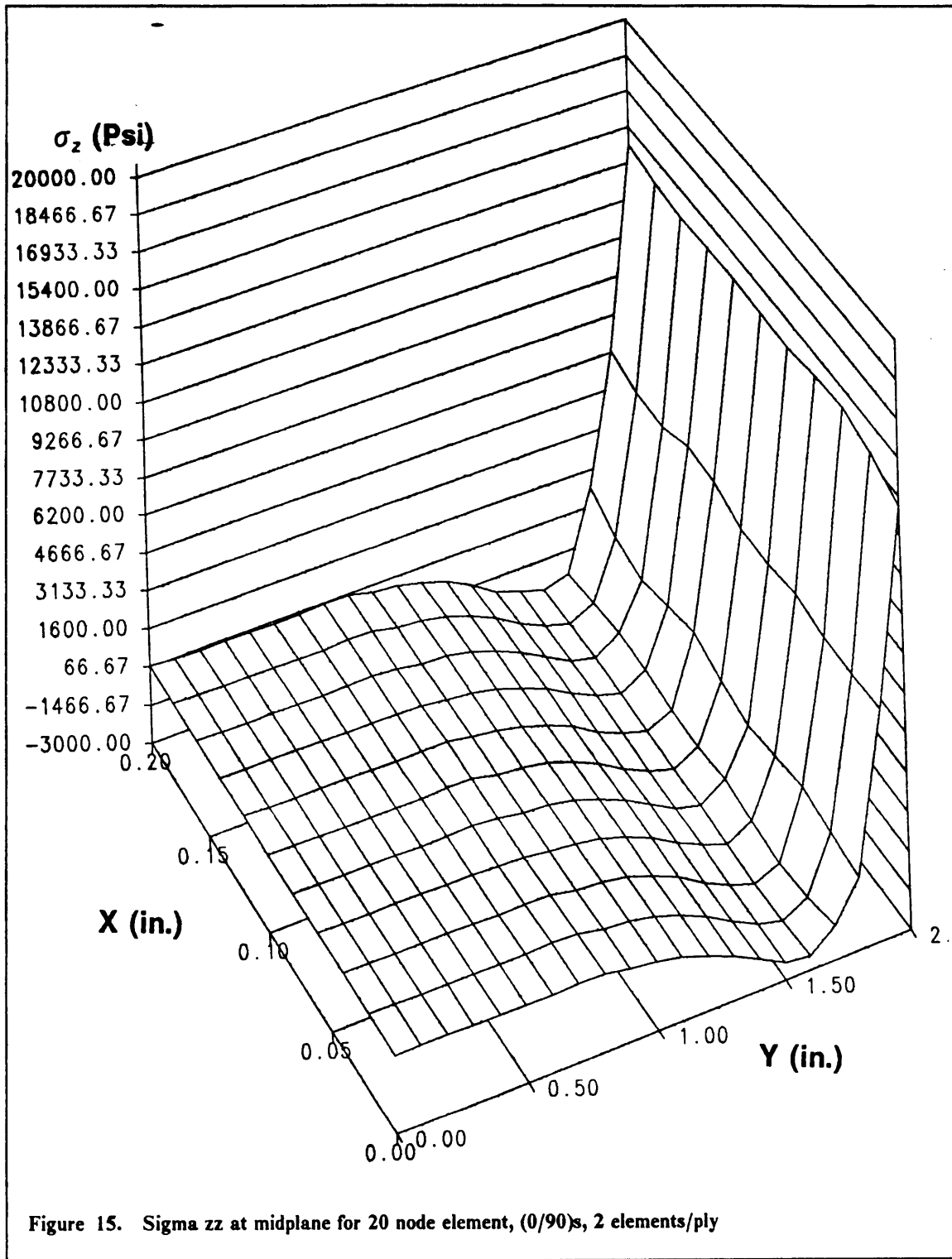


Figure 15. Sigma zz at midplane for 20 node element, (0/90)_s, 2 elements/ply

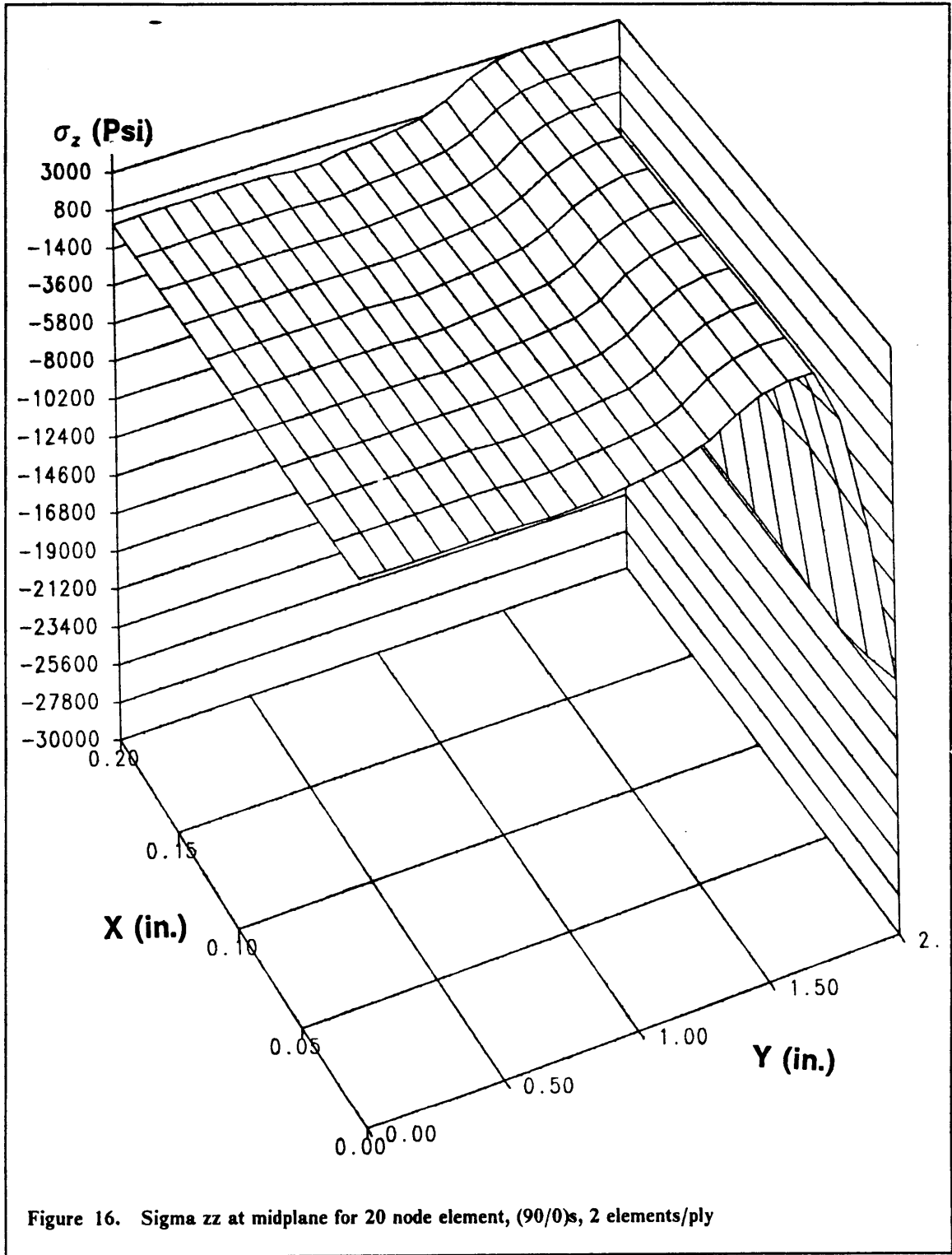


Figure 16. Sigma zz at midplane for 20 node element, (90/0)s, 2 elements/ply

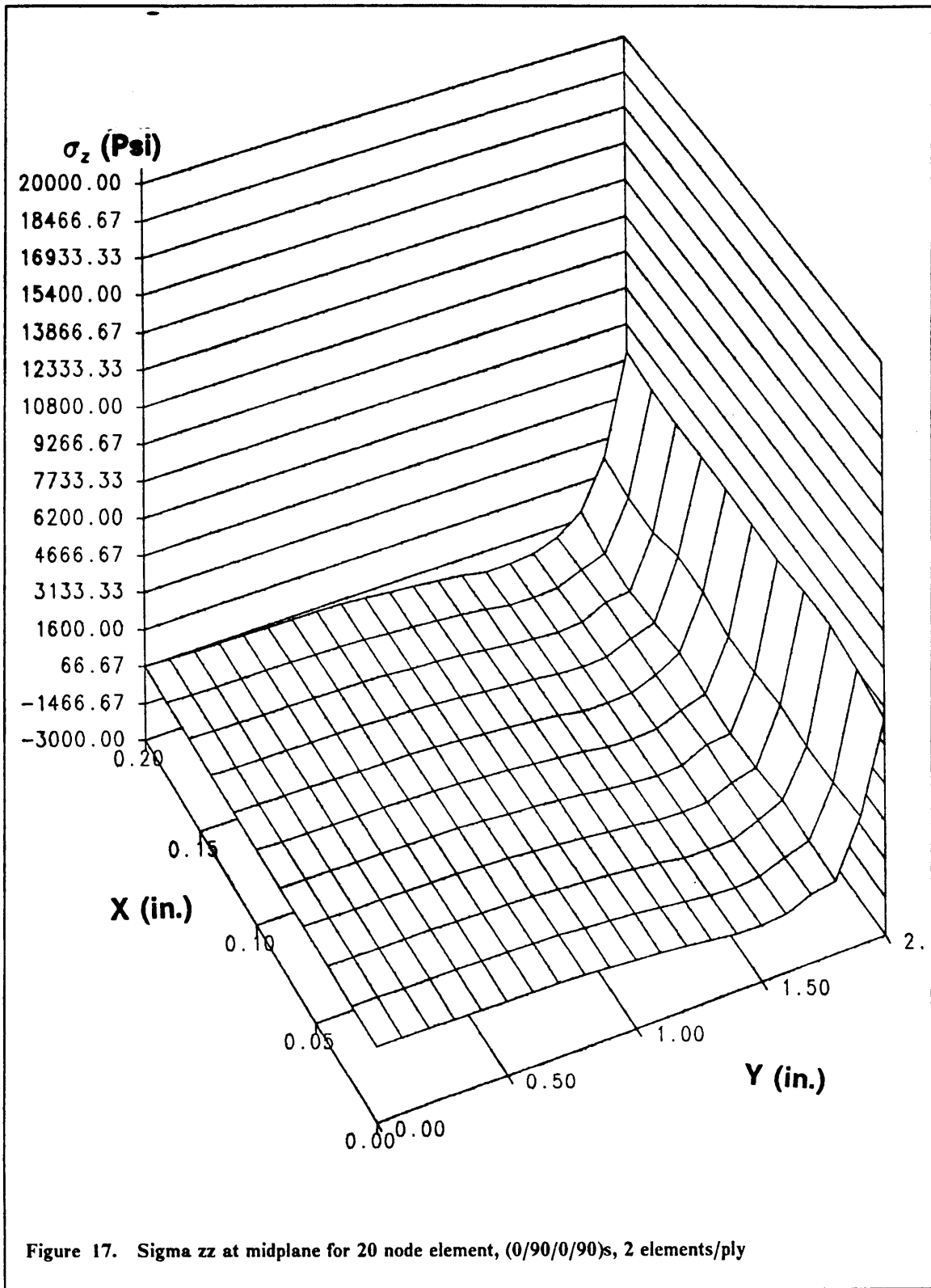


Figure 17. Sigma zz at midplane for 20 node element, (0/90/0/90)s, 2 elements/ply

4.2.3. - 24 Node Element

The 24 node element has linear interpolation functions through the thickness thus the response should be very similar to that obtained for the 16 node element. When the $[0/90]_5$ laminate was analyzed a satisfactory response was obtained with 3 elements per layer, however, when the number of elements was increased to 4 the results were basically duplicated. The analysis of the remaining laminates was not found to be satisfactory even when using the maximum possible number of elements through the thickness. This limitation was based on the assumption that by using a sufficient number of elements any element type would eventually approach the assumed solution, but with a high cost in computational time.

It is interesting to see that the 16 node element and the 24 node element both achieved the same results in terms of number of elements per ply, even though the 24 node element has more nodes.

It would seem more than natural to expect the $[0/90]_5$ and the $[90/0]_5$ laminates to require the same number of elements. The results which were obtained for the latter laminate with 3 elements per ply were accurate enough not to discourage the possibility that 4 elements would provide a correct solution to the problem.

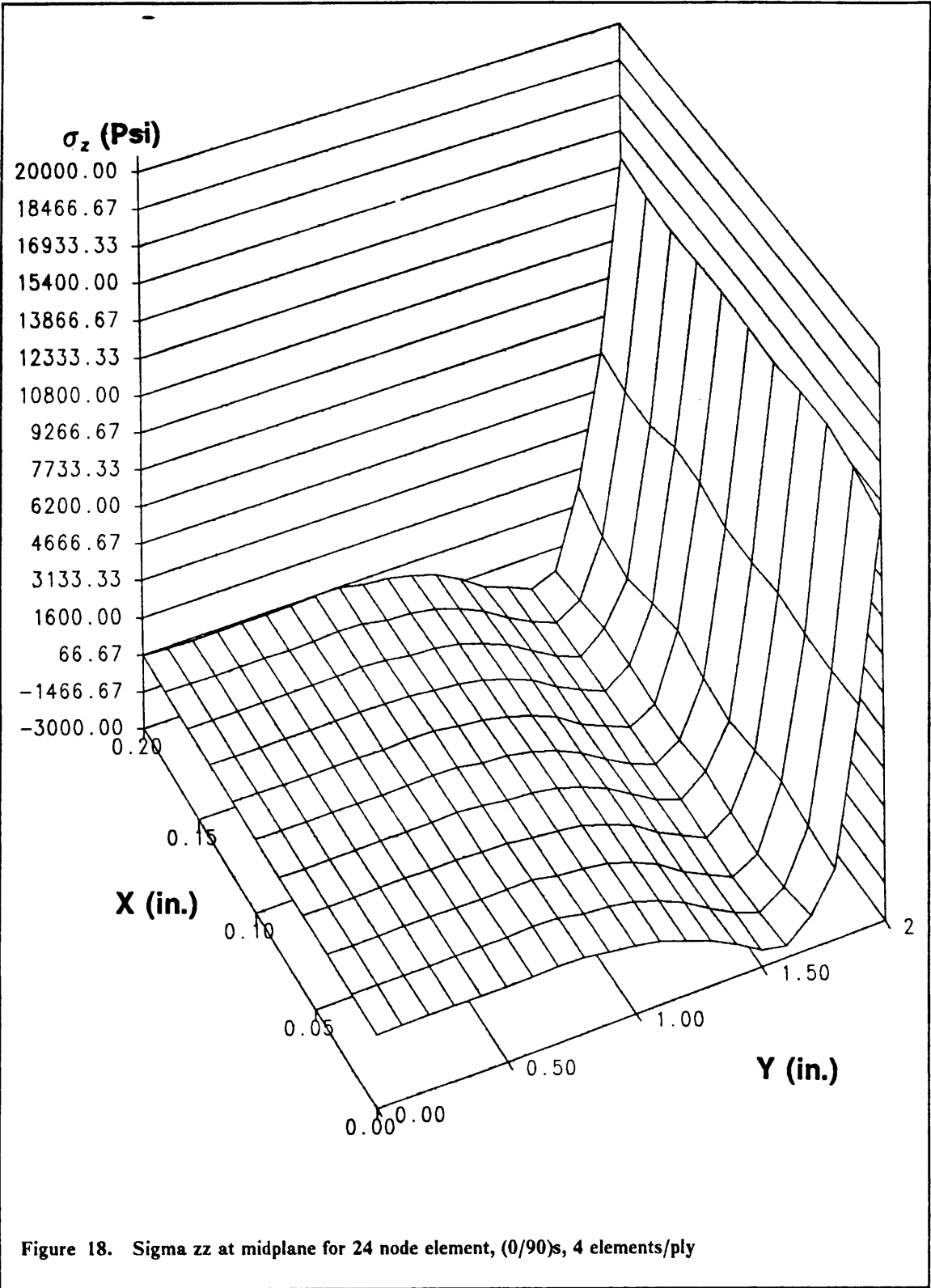


Figure 18. Sigma zz at midplane for 24 node element, (0/90)s, 4 elements/ply

4.2.4. - 32 Node Element

The 32 node element is the highest order element implemented in the experimental family. Intuitively it was expected that one element per thickness would have been sufficient to model all of the laminates under consideration, especially after analyzing the results obtained with the 20 node element. However from the results obtained with one element per thickness it was evident the response was very good (figs. 19, 20 and 21) but did not duplicate those obtained when employing two 20 node elements. Of course when the analysis was performed on the laminates with two 32 node elements per layer the stress distribution was found to coincide with those obtained with the 20 node element as well as those found with larger number of 32 node elements per thickness.

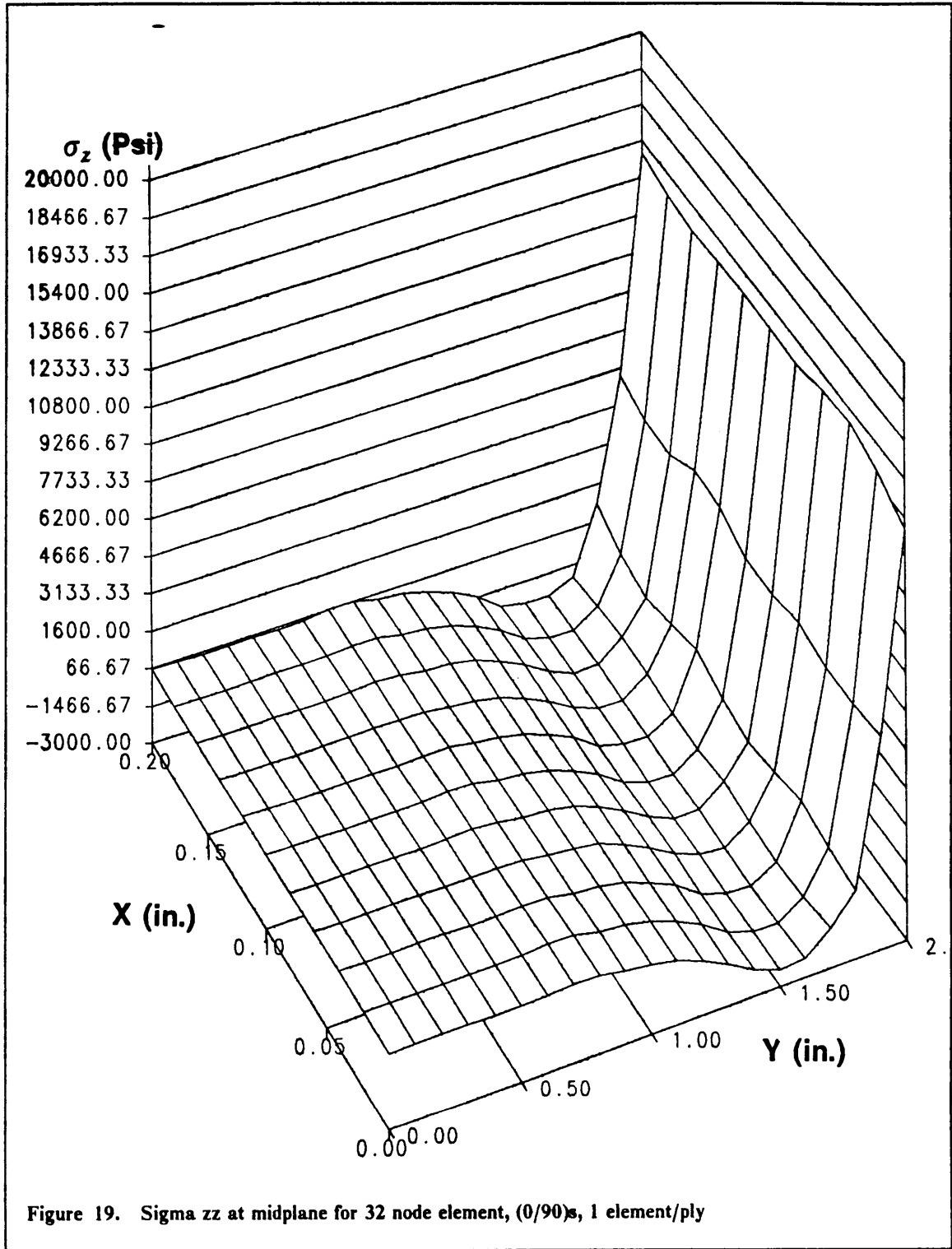
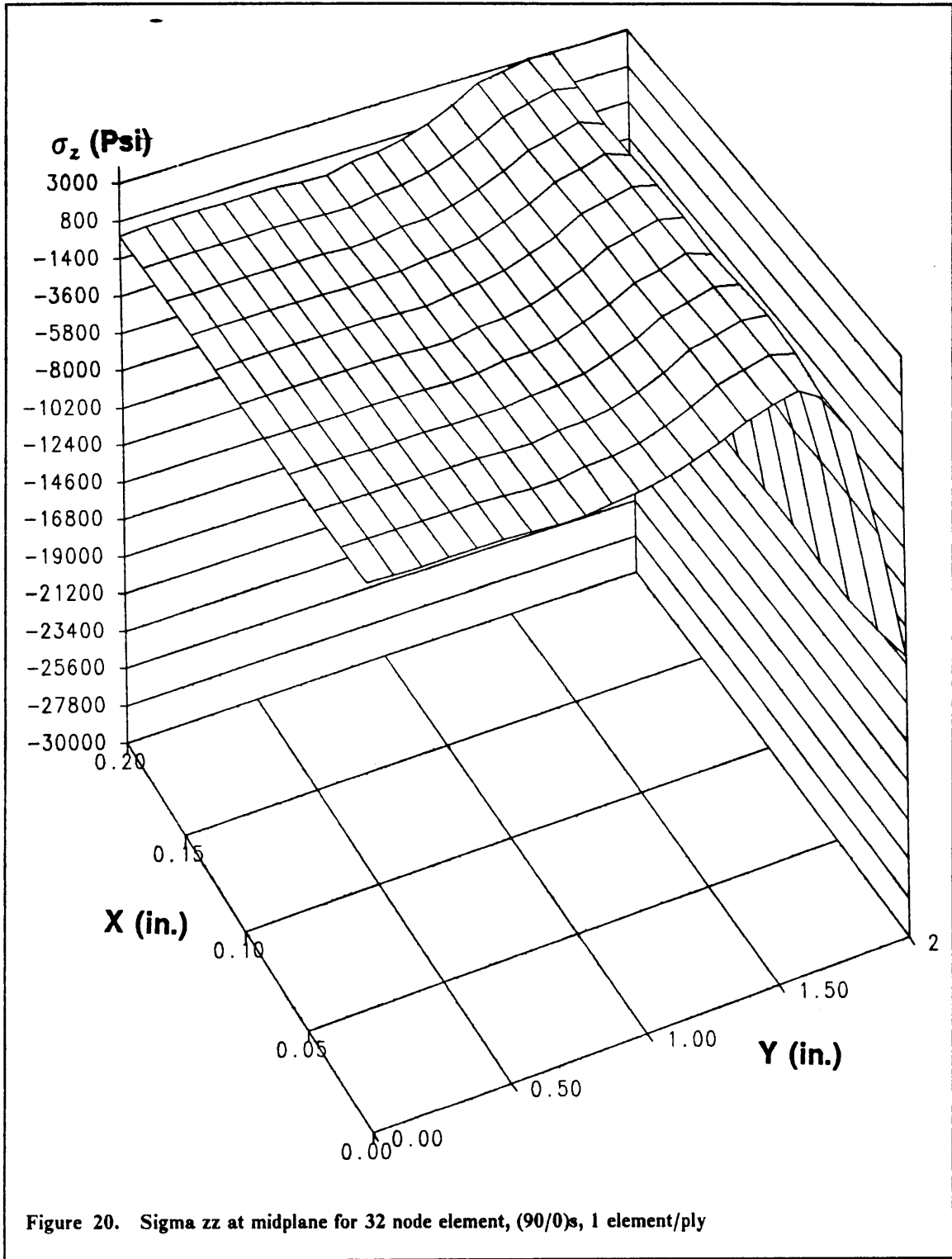


Figure 19. Sigma zz at midplane for 32 node element, (0/90)_s, 1 element/ply



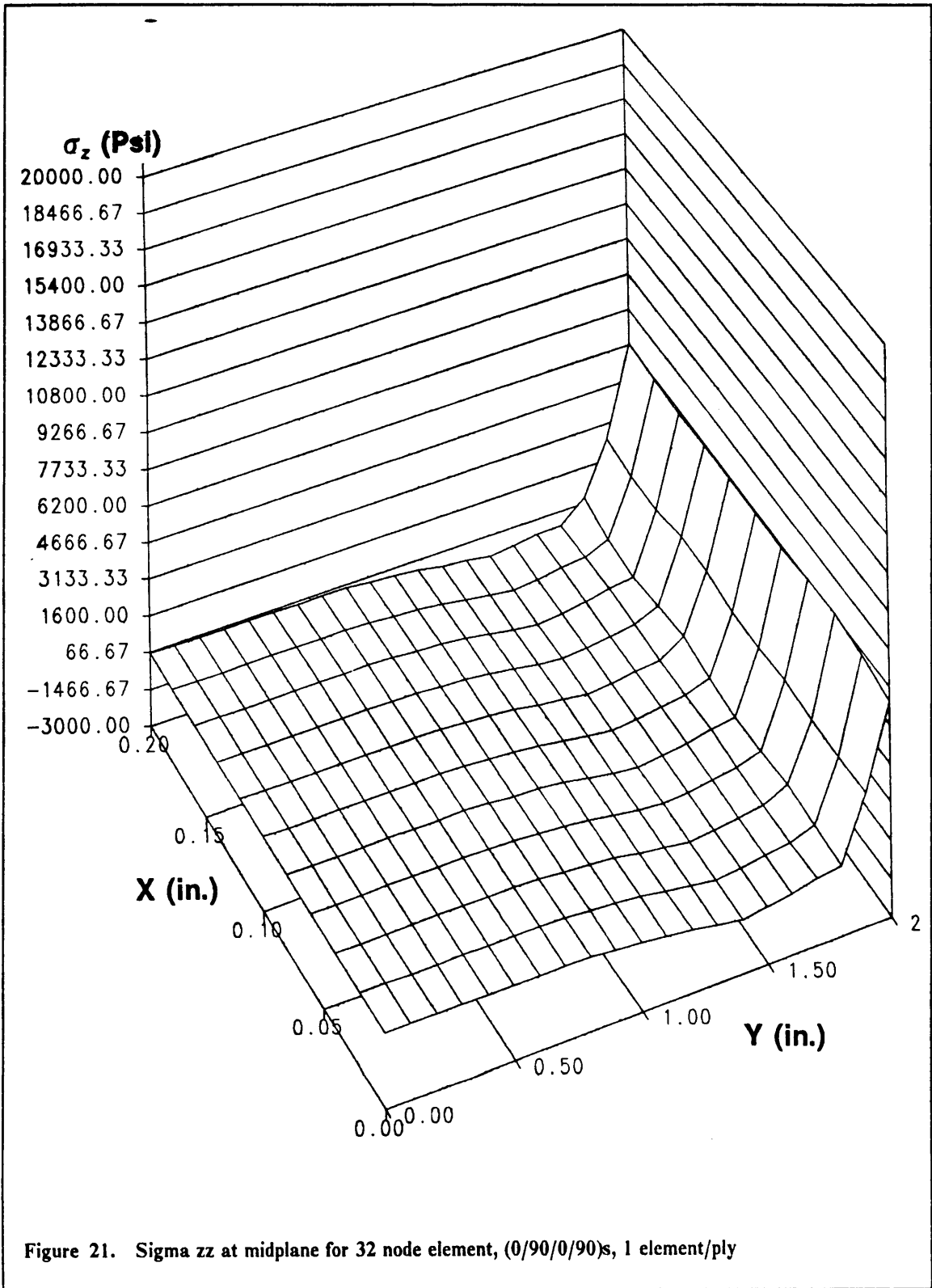


Figure 21. Sigma zz at midplane for 32 node element, (0/90/0/90)s, 1 element/ply

4.3. ANISAP Elements

Only the 20 node experimental element was verified for this specific model on ANISAP. All of the laminates under consideration were analyzed, and the results for two layers per thickness agreed with the general results obtained during the course of this study. More specifically the plots for these cases were identical to those obtained on the CSM Testbed.

4.4. Comparative Discussion

The results obtained in the study are summarized in Table 5. The numbers in the table indicate the optimal number of elements per layer required to model each laminate under consideration. The plus sign indicates that the results obtained for that specific case need a number of elements greater than the one printed in the table, but the actual number required was not determined during the course of the study.

Table 5. Summary of the results obtained for the elements/layer study

Element Type	$[0/90]_s$	$[90/0]_s$	$[0/90/0/90]_s$
S81	4 +	3 +	2 +
16 Node	4	3 +	2 +
20 Node	2	2	2
24 Node	4	3 +	2+
32 Node	2	2	2

From Table 5 it is evident that the S81 is not a good element to be used when modeling composite laminates. Similarly the 16 node and 24 node elements require too many elements per layer in order to achieve satisfactory stress distributions, resulting in very large models.

The results obtained for the 20 node element and the 32 node elements are very similar. The 32 node element approximates the response slightly better when one element per layer is used, however the differences are so small that it might not be worth the additional computational effort. When the two elements per layer distributions are considered the responses are identical.

It is interesting to note that all the element types seemed to have less difficulty in modeling the $[0/90]_5$ laminate than the other laminates considered. This was apparent when comparing the results for one or two elements per layer. The $[0/90]_5$ laminate always offered better responses than the $[90/0]_5$ and $[0/90/0/90]_5$ laminates.

4.5. Conclusion

For an approximate yet significant analysis the use of a single 20 node element per layer is suggested for crossply laminates. If the analysis needs to be more accurate then it is more appropriate to employ two 20 node elements per layer.

All the other elements were found to perform poorly or be too expensive in terms of computer resources when compared to the performance provided by the 20 node element. The remainder of the investigation will be carried out entirely using exclusively the CSM Testbed in conjunction with the 20 node element.

Chapter 5: Global-Local Analysis

The procedure employed in the present work for performing Global-Local finite element analysis of laminated plates can be described by the following steps:

1. Select the location of the Global-Local boundary,
2. analyze the full Global model as a two-dimensional problem,
3. extract the displacements at the boundaries of the Local regions,
4. create a three-dimensional model of the local regions with full three-dimensional imposed displacements,
5. analyze the Local models by means of a full three-dimensional analysis, and
6. post-process the results.

For the Global as well as both Local models three layups were considered: $[0/90]_6$, $[90/0]_5$ and $[0/90/0/90]_5$.

5.1 The Global Model

In this investigation a laminated plate with a centrally placed hole was analyzed. The amount of literature available for such a problem is extensive and thus provided numerous cases against which the results could be compared. All analyses were linear elastic.

The Global model was generated using processor "CSM1"⁶ of the Testbed, which produces a mesh to model a crossply laminated plate with a central circular hole. The quantities defined in Figure 22, were assigned the following values for the present study:

$L = 18.0$ in.,
 $W = 12.0$ in.,
 $h = 0.1$ in. (plate thickness),
 $\Lambda = 7.0$ in.,
 $d = 6.0$ in.,
 $l_{bs} = 5.8$ in.,
 $l_c = 0.2$ in.,
 $NEIX = 4$,
 $NEIE = 3$,
 $NRINGS = 3$ or 4 , and
 $NSPOKES = 32$ or 40

The quantity NRINGS represents the total number of element rings in the model contained in the region defined by "A". NSPOKES is the total number of radial lines emanating from the center of the hole. NSPOKES must always be a multiple of 4 for the CSM1 processor to complete execution. The variables NRINGS and NSPOKES have two possible values assigned depending on the particular Local region being analyzed.

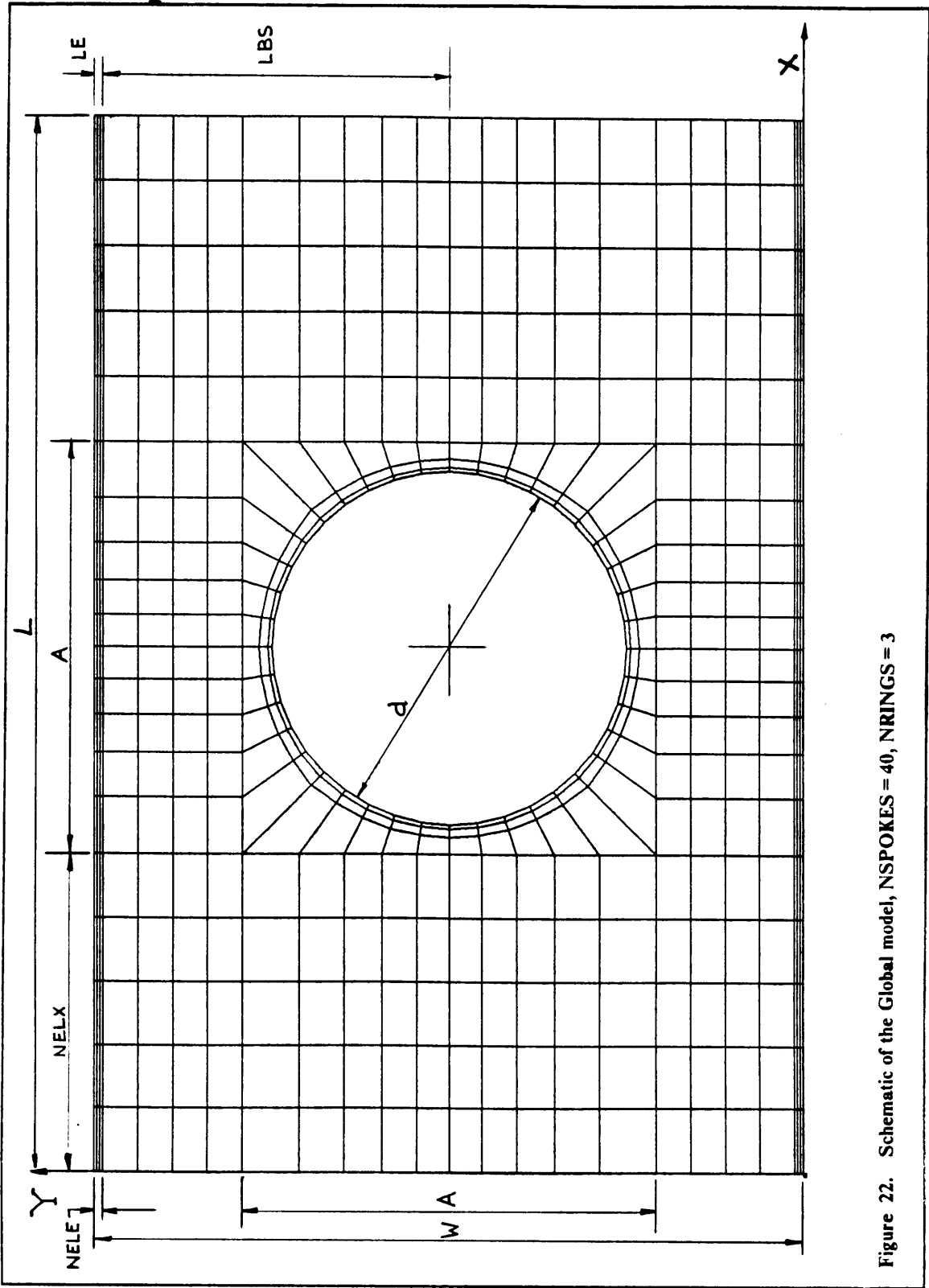


Figure 22. Schematic of the Global model, NSPOKES = 40, NRINGS = 3

The Global model was loaded in compression by imposing a uniform x-displacement of 0.1 in. at the $x = 0.0$ edge and restraining movement in the x-direction at the $x = 18.0$ in. edge. Both corner nodes along $y = 0.0$ were also restrained from movement in the y-direction.

To solve this model the EX41³⁷ element was utilized. This is a displacement formulation based four node, two-dimensional element, available as an experimental element in the CSM Testbed. An experimental element had to be used since when the original computer runs were performed with the E43, the standard two-dimensional Testbed element, erroneous deformations were obtained.

During the course of the entire study only $[0/90]_5$, $[90/0]_5$ and $[0/90/0/90]_5$ laminates were considered with a total thickness of 0.1". The far field average stress was calculated to be 57667 psi.

5.2 The Local Models

Two local regions were selected as being of critical interest to the investigation. The first was the edge of the plate close to the hole, region I in Figure 23, and the other was selected around the edge of the hole, region II.

Each region was extracted from the Global model with the corresponding boundary displacements. A three-dimensional model was generated. The Local meshes only modeled one half of the laminate thickness since all of the layups and loadings were symmetric. Also, the appropriate displacements at the axes of symmetry were imposed, such that the resulting model would emulate correctly the problem at hand. At the free edges no displacements were imposed in order not to force the over-simplified response of the global model. Typical three-dimensional models are shown in Figure 24 and Figure 35. These Local regions would allow a detailed investigation to be

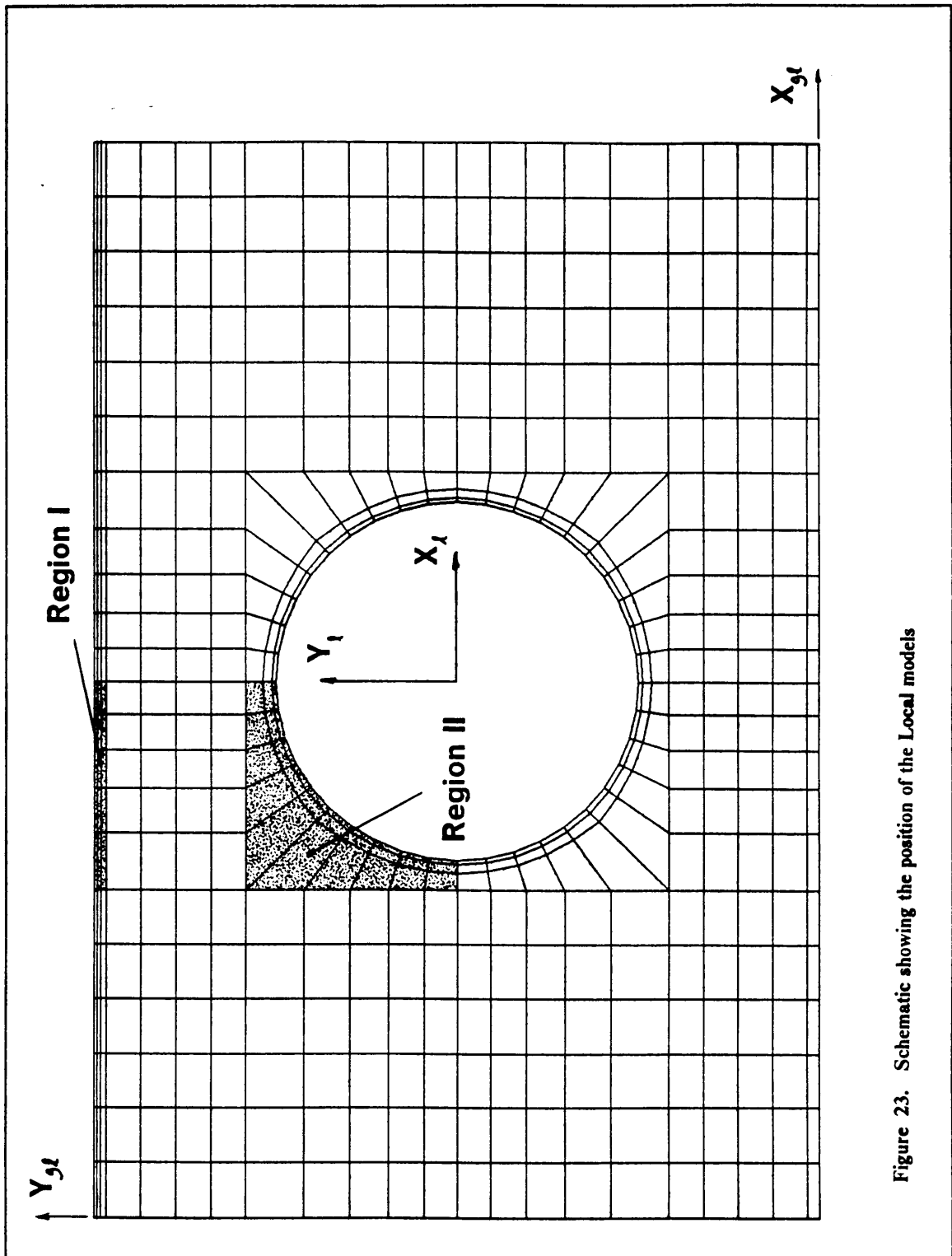


Figure 23. Schematic showing the position of the Local models

carried out on the magnitude and variation of interlaminar stresses in the presence of a circular aperture.

A preliminary study showed that it would only be necessary to specify displacements in one direction at the interface, since the local analysis would return the correct displacements for the other components. However, all the possible x and y displacements were imposed at the boundary, except at the free edges which were completely unloaded. The imposition of the maximum number of displacements resulted in lower computational times for the 3-dimensional models. When performing the analysis on the straight edge, there was no need for a high accuracy in the results around the hole, therefore $NRINGS = 3$ (see fig. 22) was sufficient, but it was necessary to have $NSPOKES = 40$ to allow the stresses to converge and provide smoother boundary conditions at the edge interface. When analyzing the stresses around the hole it was necessary to use $NRINGS = 4$ in order to transfer more evenly the displacements from the outer fields, but to use $NSPOKES = 40$ would result in an extremely large model. As will be discussed later in the chapter, the choice for $NSPOKES = 32$ was made based on a compromise between the quality of the results and the computing times involved.

5.3. Straight Free Edge Problem

5.3.1. Location of the Global-Local interface

The Local three-dimensional model at the straight edge is shown in Figure 24. The Local x-direction was originally modeled using only three elements. However during preliminary analyses it was found that when the hole diameter was large, sharp stress variations appeared at the Global-Local interface coincident with element boundaries. It was thus resolved to increase the number of elements across the model by increasing the number of spokes around the hole to 40.

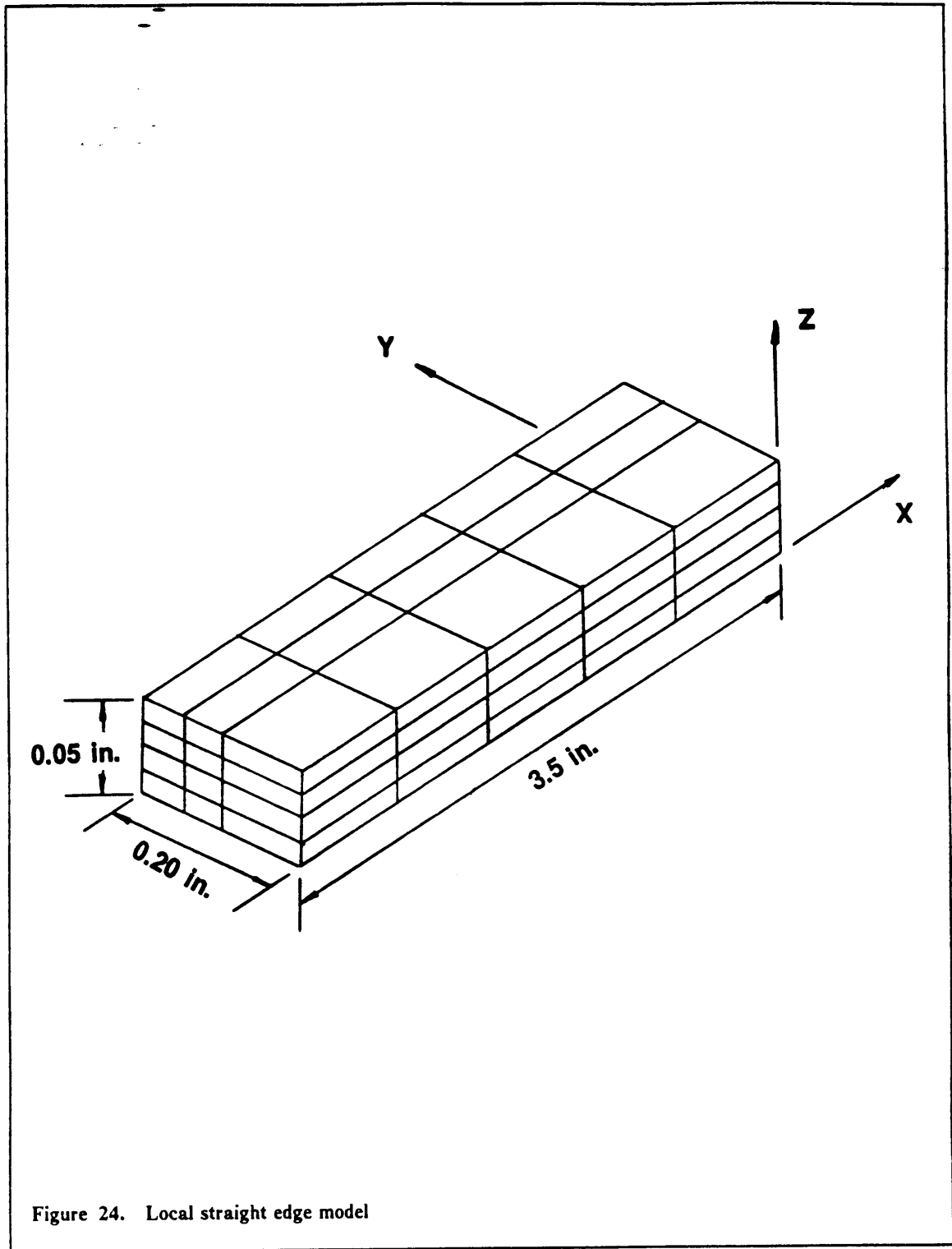


Figure 24. Local straight edge model

This resulted in the model having five elements along the x-direction which resulted in a considerably smoother response. The local y-direction was modeled using only three elements, which if placed in the correct locations would result in sufficiently accurate solutions to the problem. Finally, the study which had been performed earlier suggested the use of two 20-node elements through the thickness of each layer.

The region of growth for the boundary layer is known to be of the order of the laminate thickness². This dimension was of critical importance for the position of the Local model. In order to determine the optimal location of the Global-Local interface two models were prepared, one with the interface placed 1.5 laminate thicknesses away and the second model 2.0 laminate thicknesses from the edge.

Since the stress gradients away from the edge are small and increase with their proximity to the edge, it was felt necessary to grade the mesh in a way which would allow the edge stresses to develop fully. This meant creating a finer mesh closer to the edge. The element boundaries in the y-direction were shifted to obtain the best possible response of the model. The moving of the element boundaries did not affect the imposed boundary conditions because they had been found to remain unchanged within the y-direction.

A number of meshes were prepared and analyzed by varying the width and the location of the y-direction element boundaries of the Local model. A summary of the cases which were investigated is presented in Table 6.

All the cases which were analyzed revealed the same general shape of the interlaminar normal stress, however the one which resulted in the more likely distribution was the T2.0-II shown in Figure 25. This was preferred over the other meshes because it resulted in an overall smoother stress distribution. The differences between the plots however were very small. They amounted to the location of the minimum, and the rates at which the distributions approach the minimum. However, the actual minimum and maximum values showed very small discrepancies between meshes. This

Table 6. Summary of optimal interface location for straight edge problem

Model width	element boundary location, y-direction (in.)	Plot name
1.5 t	11.85, 11.90, 11.95, 12.00	T1.5-I
1.5 t	11.85, 11.91, 11.96, 12.00	T1.5-II
2.0 t	11.80, 11.90, 11.95, 12.00	T2.0-I
2.0 t	11.80, 11.90, 11.9667, 12.00	T2.0-II
2.0 t	11.80, 11.91, 11.96, 12.00	T2.0-III

would suggest that as long as the Local region is chosen fairly successfully, the response would be to a large extent insensitive of the specific mesh. The present study was performed only for $[0/90]_S$ laminates, but similar deductions seem plausible for any other combination of cross-ply laminates.

5.3.2. Free edge stresses

The purpose of this study was to determine the distribution of straight edge interlaminar stresses in the presence of a circular hole. For this reason a number of cases were considered: first varying the diameter of the hole from 0.0", to a maximum of 6.0" in 1.0" intervals, then by considering different laminate layups all with 6.0" diameter holes. The local mesh used was the T2.0-II described in the previous section. The entire analysis schedule for this section is presented in table 7.

The length of the Local model in the x-direction was limited to 3.5" because this distance covered the entire region of maximum deformation at the edge and thus captured all the highest stresses.

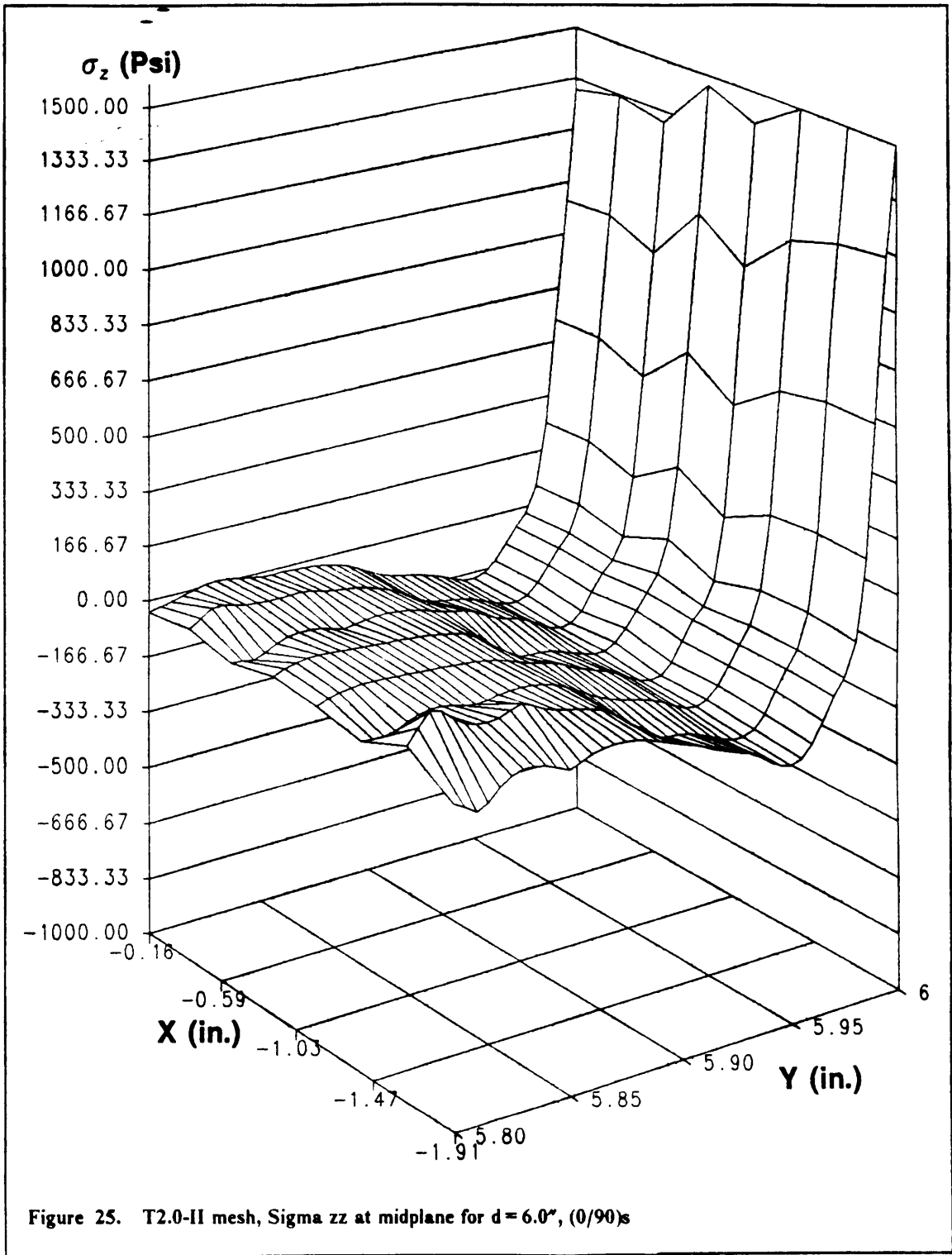
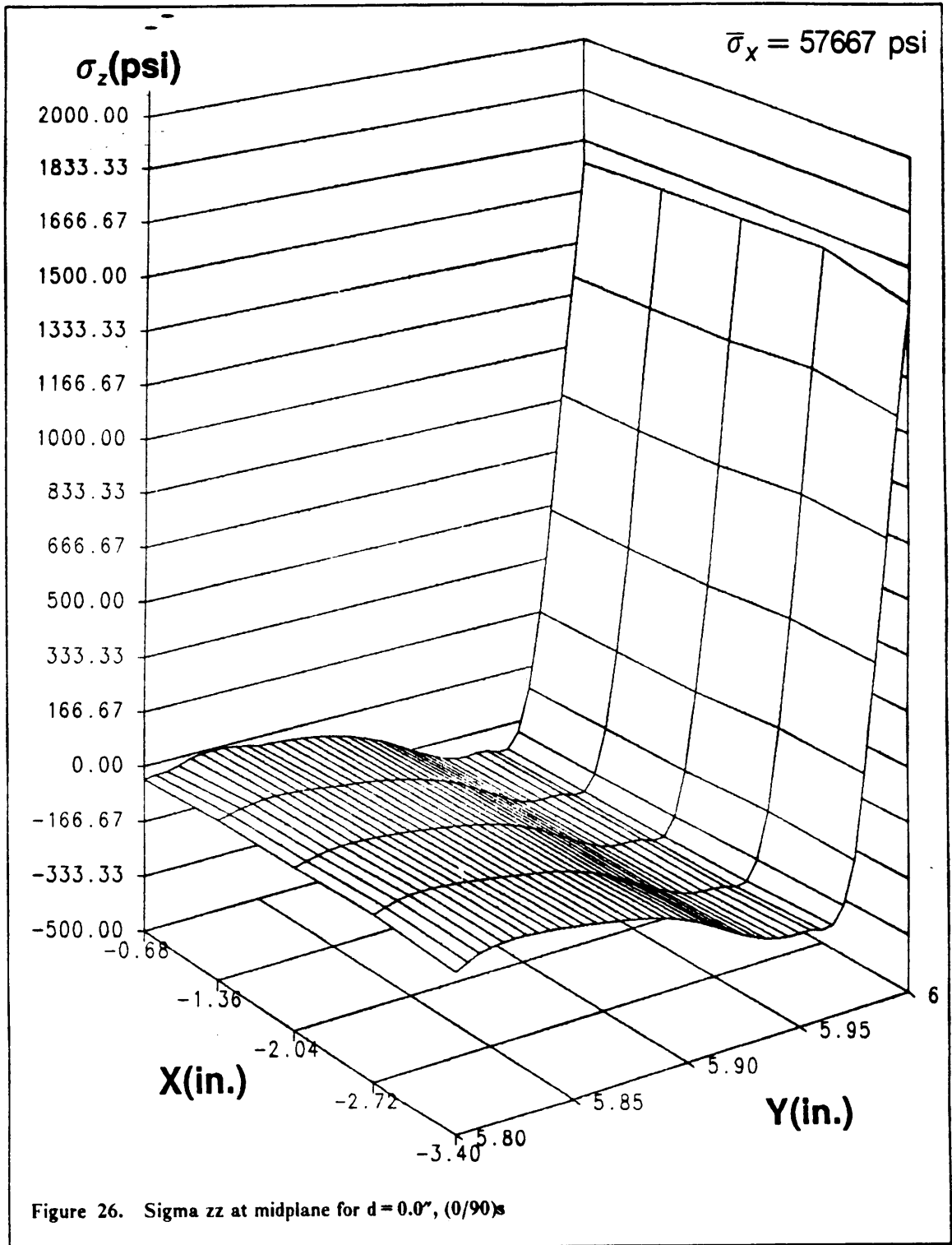


Table 7. Summary of analyses performed on the straight free edge

Hole diameter	$[0/90]_s$	$[90/0]_s$	$[0/90/0/90]_s$
No Hole	Yes	No	No
1"	Yes	No	No
2"	Yes	No	No
3"	Yes	No	No
4"	Yes	No	No
5"	Yes	No	No
6"	Yes	Yes	Yes

The first set of plots to be discussed pertains to the $[0/90]_s$ laminate. The local three-dimensional model consisted of a total of sixty 20 node elements, as shown in Figure 24. The far field average applied stress was maintained at 57667 psi.

Figure 26 shows the results of the analysis performed on the laminate with no hole ($d = 0.0$). The response displayed a very uniform stress distribution in the x-direction. The maximum value of stress was found to occur at the edge with a magnitude of 1600 psi. The minimum was found to reach a value of -250 psi. The presence of a small disturbance close to the minimum was attributable to the location of the Gauss points. The value of the maximum has a slight tendency to increase away from the plane of symmetry (local $x = 0$), and then decrease sharply. This behavior could be promoted either by the closeness to the point of load introduction, or otherwise by a peculiarity of the two-dimensional model which even in the absence of the hole, still analyzes a model with radially distributed elements about the center of the plate, as shown in Figure 27. This variation, however, is extremely small at 40 psi (2.5% of the maximum).



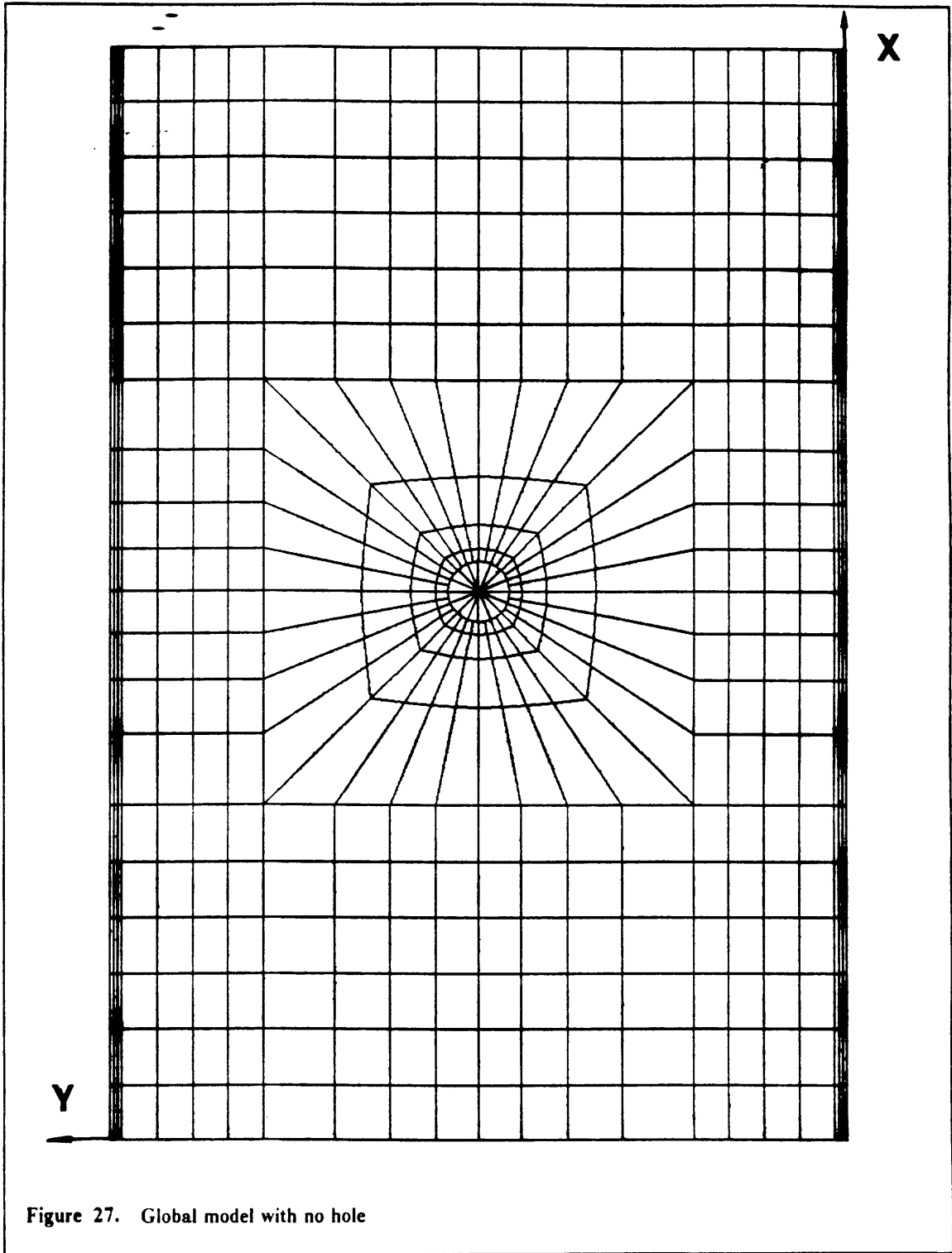
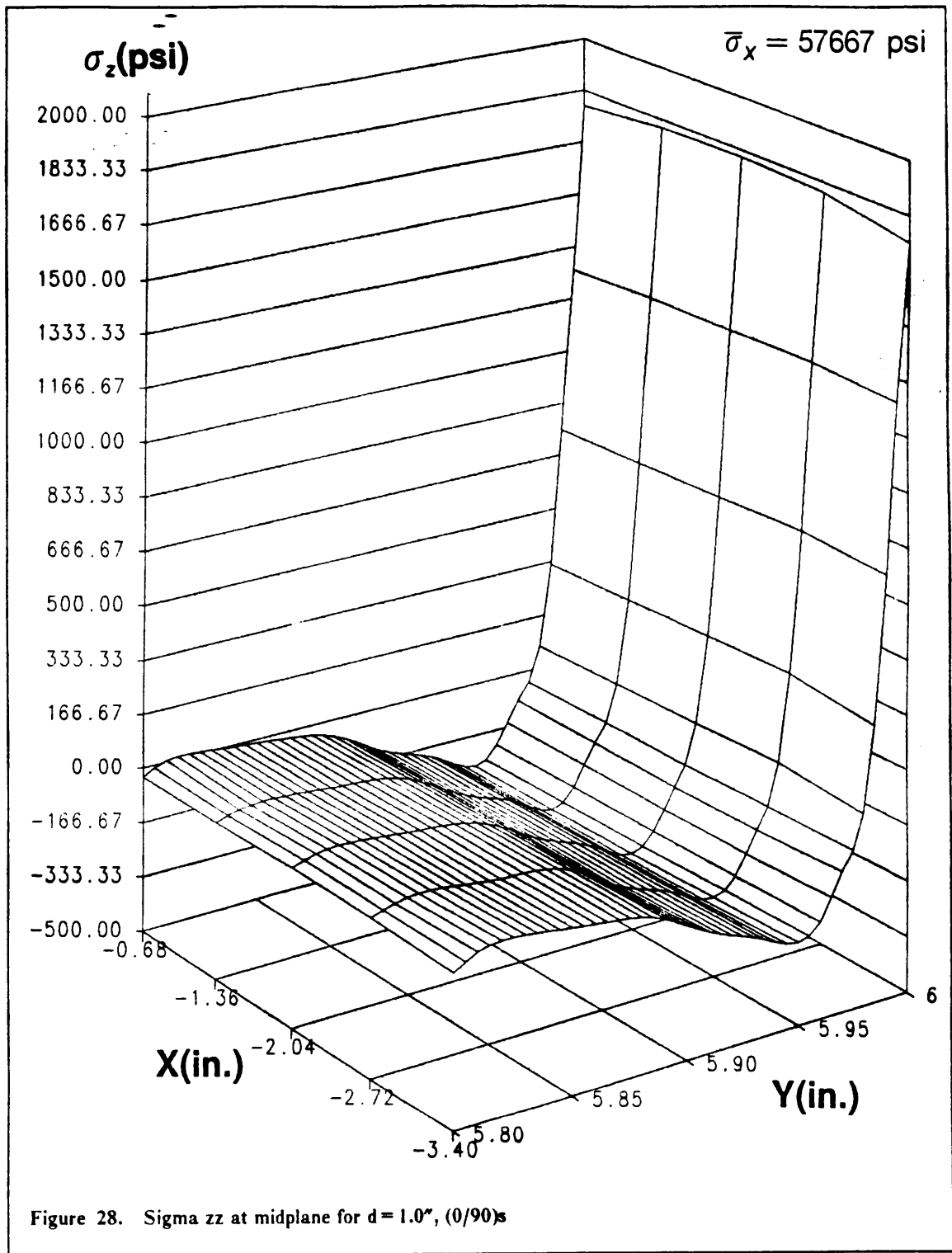


Figure 27. Global model with no hole

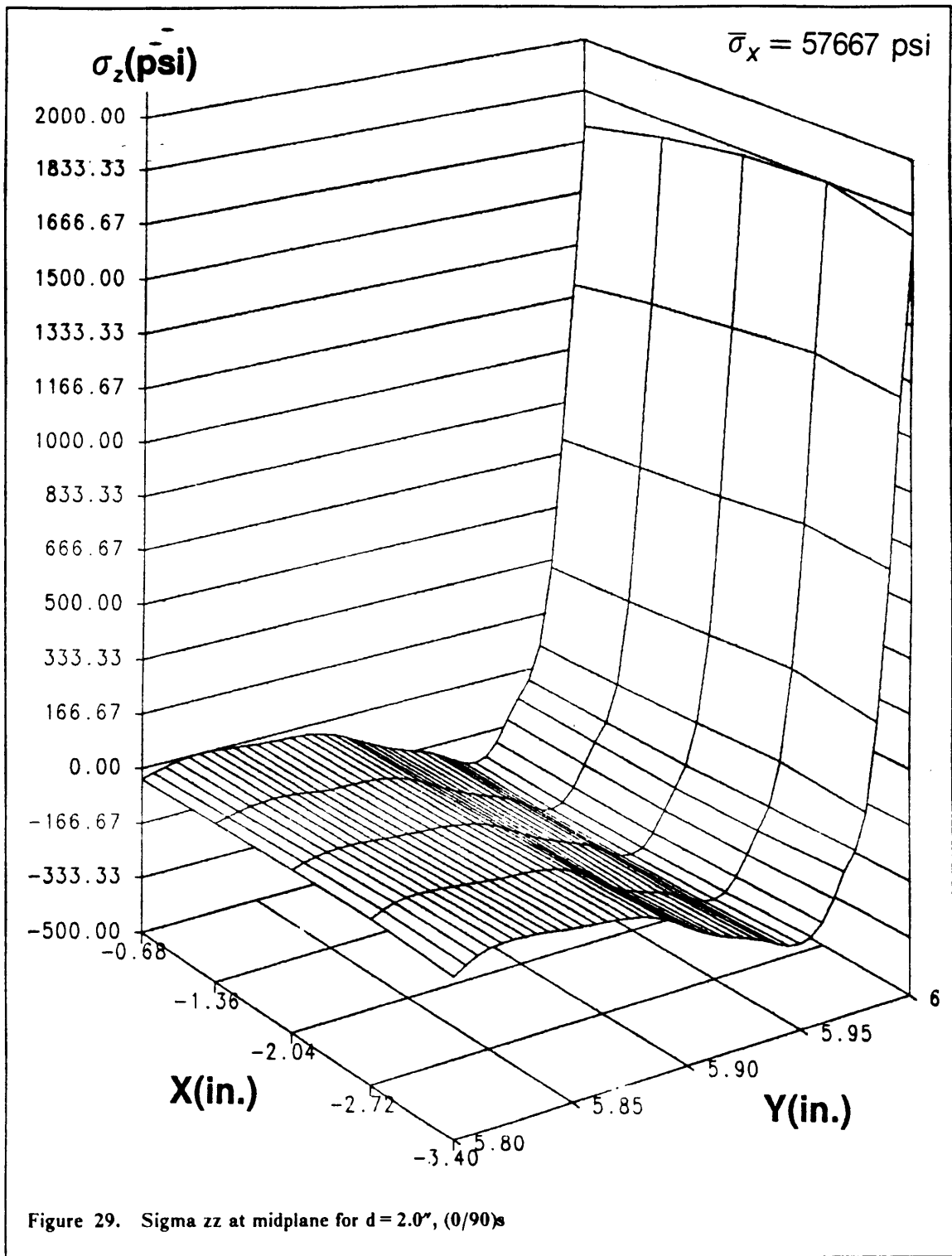


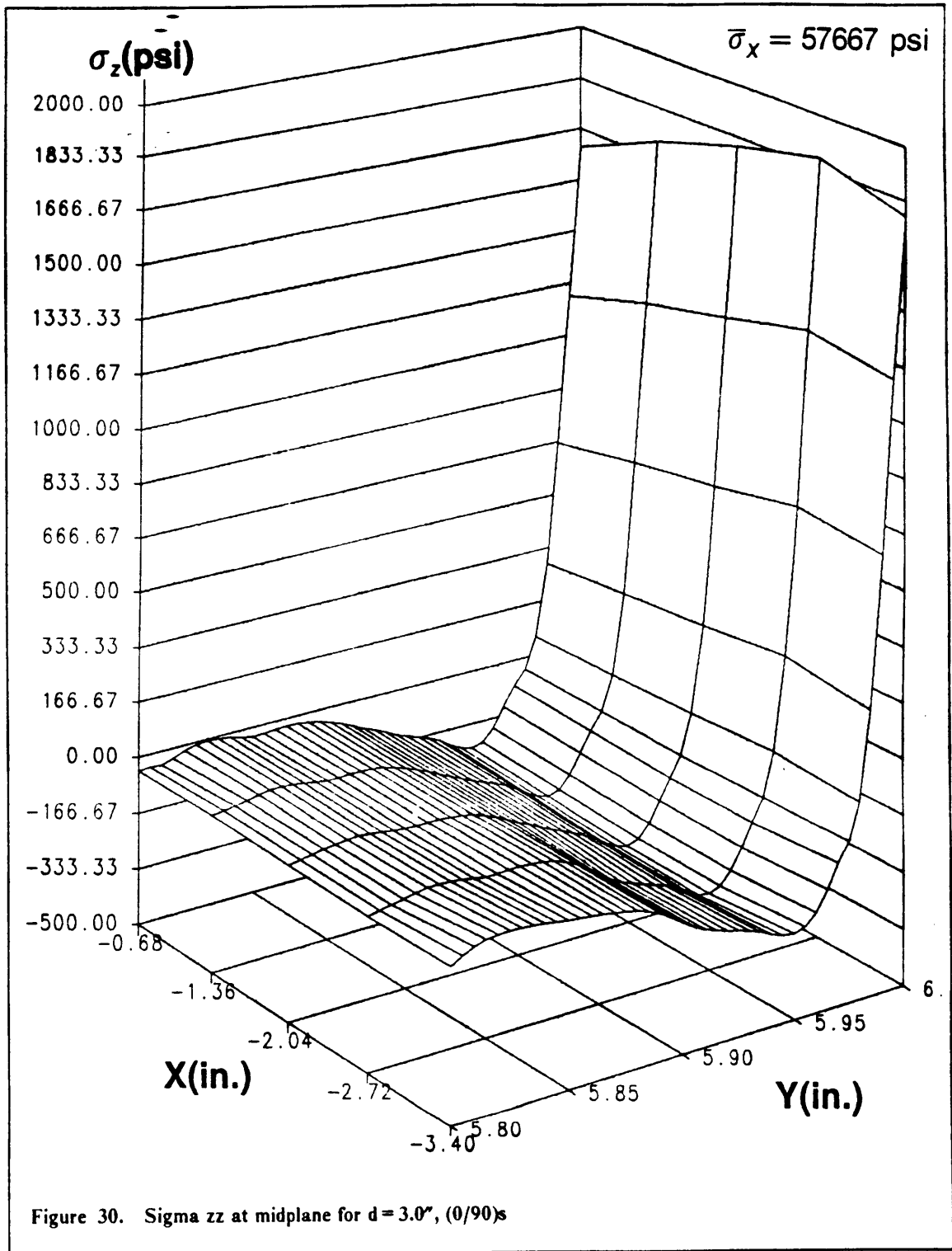
Inspection of the results provided for $d = 1.0''$ (fig. 28), displays the presence of a much higher edge stress, 1800 psi (15% increase). The magnitude of the minimum was maintained constant to that predicted in the previous case, however the location of the minimum was found to be shifted away from the edge from 5.96" to 5.95". This movement of the local minimum could lead to a loss of force equilibrium, since the integral of the interlaminar normal stress over a line of constant y must always be zero. An approximate graphical integration was performed and the error was found to be 6% of the maximum force at the edge. This shift could also be attributed to the curve fitting routine, but an increase in the maximum edge stress can only be balanced by either an increase in the magnitude of the minimum or by a relocation of such a minimum.

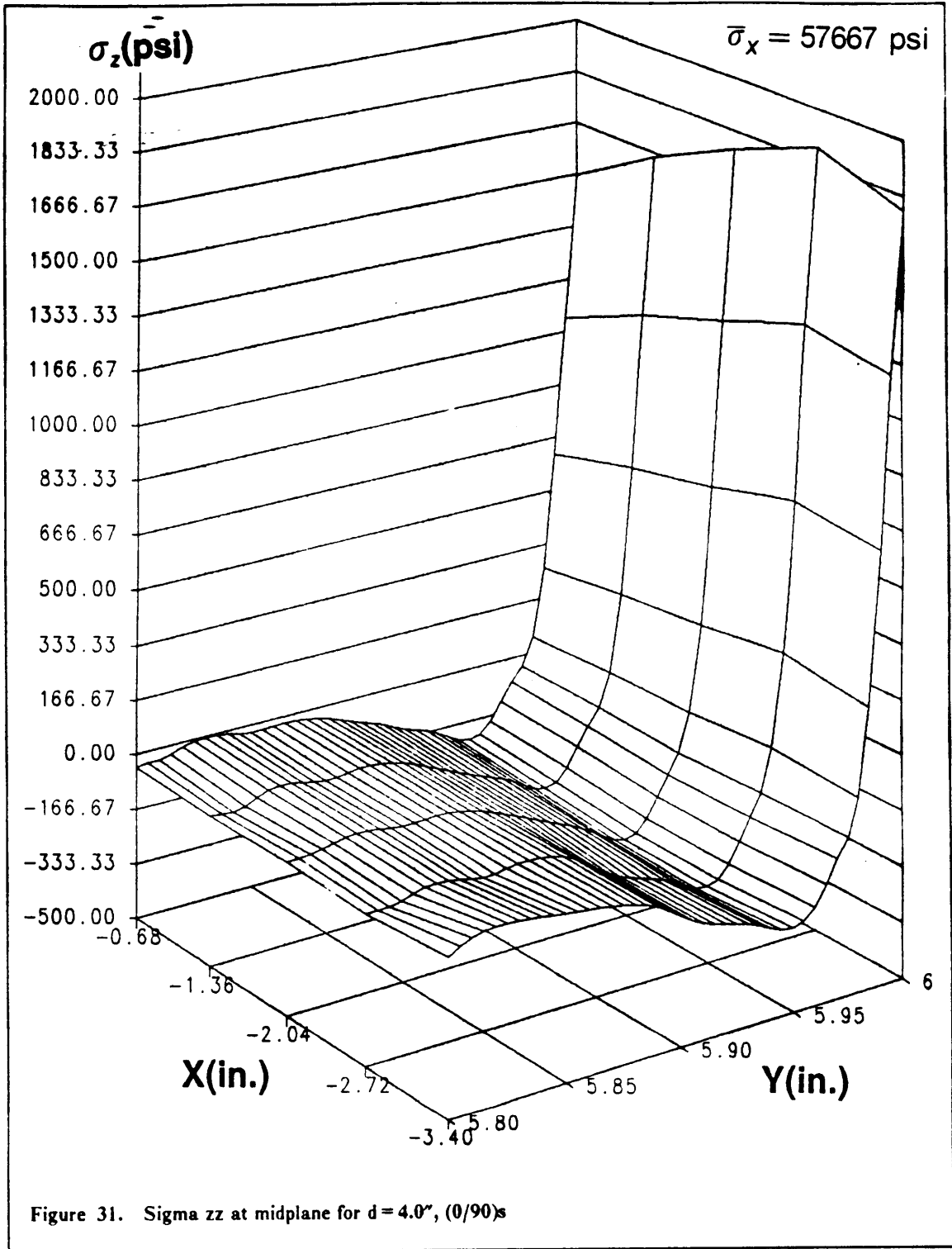
When the diameter of the aperture was increased to 2" (fig. 29), the stresses at the edge were found to vary from a maximum of 1833 psi down to 1700 psi, along the free edge. The lower value coincided with the axis of symmetry at $x = 0.0''$ (local coordinates). The magnitude of the minimum stress remained constant throughout at a value of -230 psi. The location of the minimum remained unchanged from the previous case.

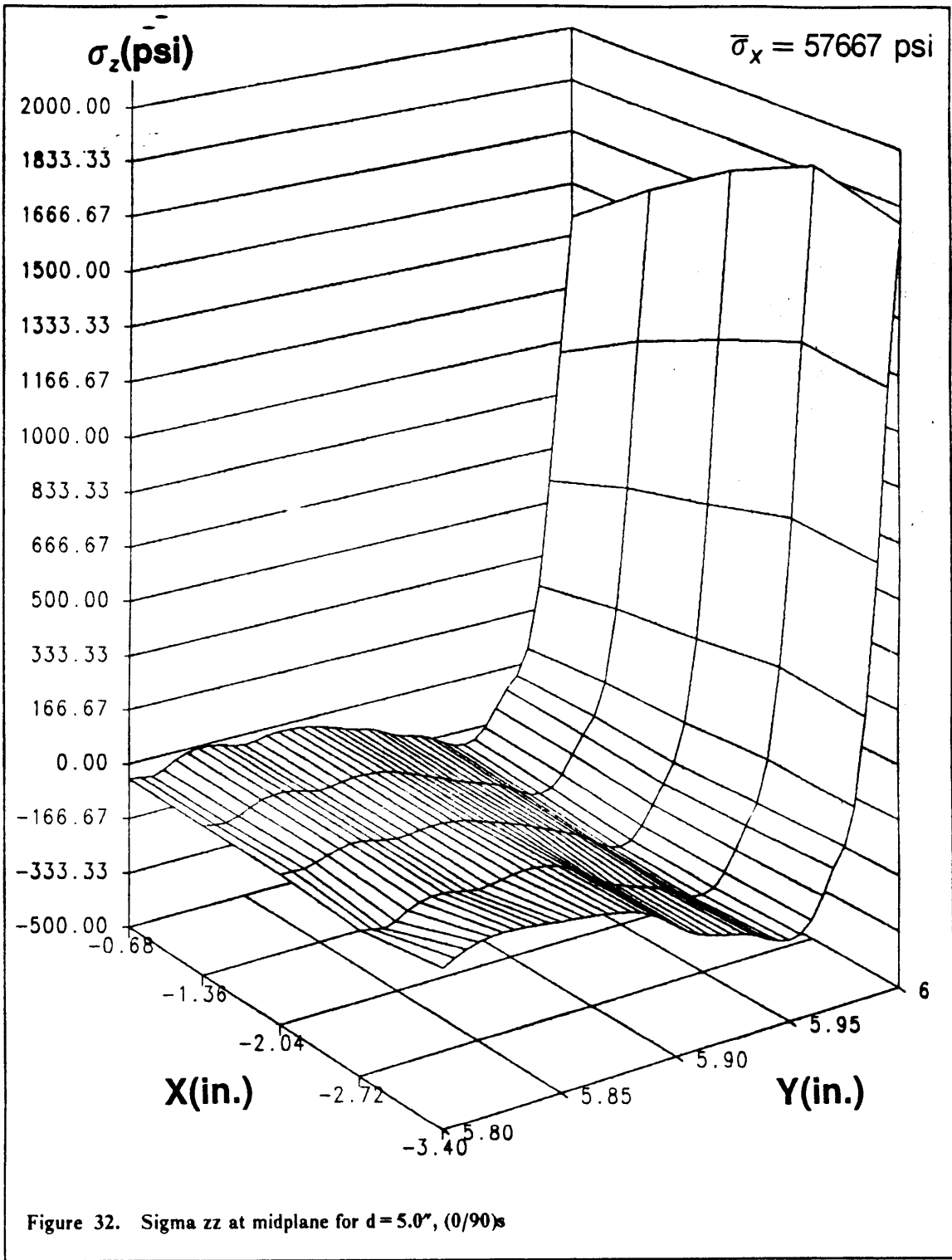
Once the hole diameter was increased to 3.0", the stress at the edge varied considerably from a maximum of 1870 psi to a lower value of 1600 psi (fig. 30). Again the lower value occurred at the axis of symmetry, also the location and magnitude of the minimum remained unchanged. Coinciding with the element boundaries along the interface, some stress fluctuations came into evidence, although hardly significant (30 psi).

Figure 31 shows the response of the model with a 4" diameter hole, again the trend which was created in the previous cases appeared more marked. The stress at the edge showed a variation of 20% from 1890 psi down to 1500 psi. The location of the minimum remained unchanged, but the magnitude showed a small increase to -200 psi. The unevenness in response seemed to become more noticeable as the size of the hole was increased, although the presence of such disturbances did not seem to affect the results otherwise.





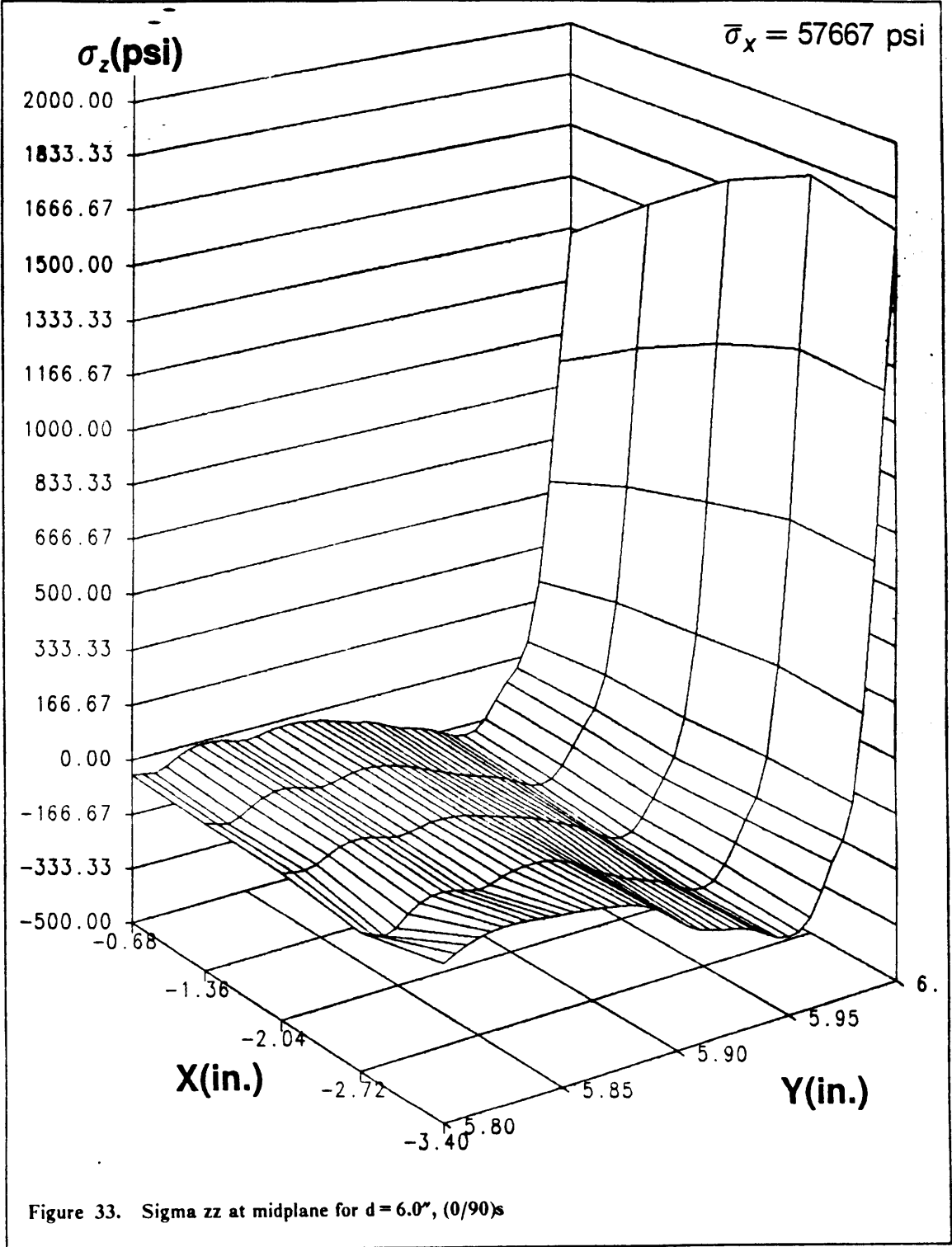


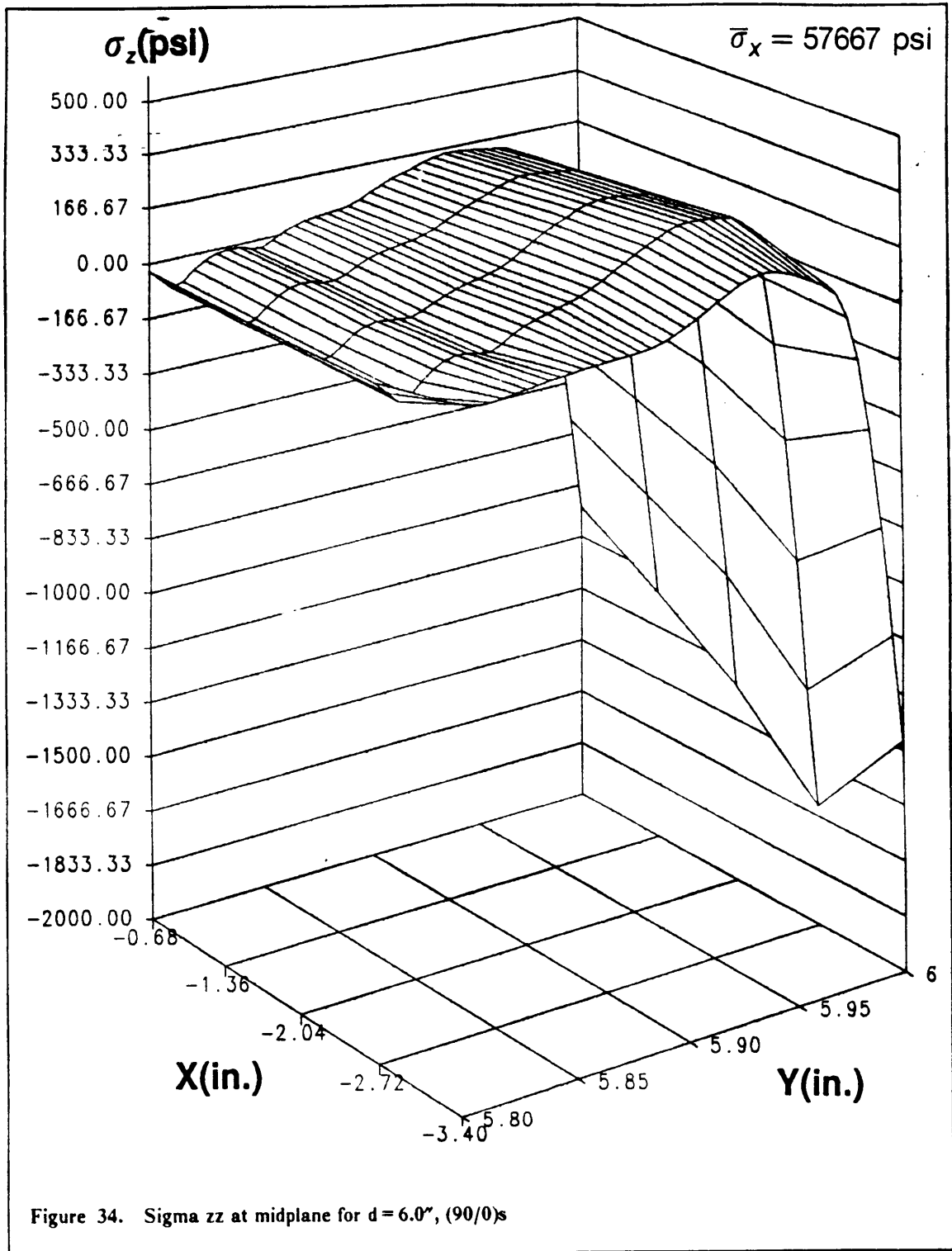


The 5.0" diameter hole did not disprove the trends set up by the earlier cases. The edge stresses were predicted to vary from 1850 psi to 1400 psi (fig. 32). The location of the minimum was found not to change in any way, although a further increase in the size of the minimum was recorded at -180 psi. The unevenness in the distribution seems to suggest that the solution to the Local model was beginning to accumulate inaccuracies.

Lastly the response for the largest hole diameter was considered (fig.33). The stresses showed a drastic variation at the free edge. The values ranged from 1320 psi at the plane of symmetry to 1800 psi at the maximum (27% variation). It is interesting to note that the average stress at the edge has the same value as for the plate with no hole (1600 psi), but the relative variations in stress distributions at the edge bear little resemblance between the two cases. Contrary to intuitive thought, the presence of a large size hole for the most part reduces the size the the stresses at the edge. In order to maintain force equilibrium in the y-direction, if the magnitude of the edge stress is reduced then the location of the minimum must be moved away from the edge, which was noticed during the course of this study (a shift from $y = 5.96''$ to $y = 5.95''$). For the $[0/90]_5$ laminate the average stress at the edge was approximately 100 psi. Wang and Crossman³ predicted a maximum σ_z stress of $0.3 \times 10^6 \chi_{e_0}$ psi. Expressing the edge stress in a similar form transforms into $0.29 \times 10^6 \chi_{e_0}$, which results in a very good correlation.

The results discussed so far indicated larger stress distribution differences along the free edge. These seemed to increase and become more marked with increasing hole diameter. When dealing with larger hole sizes the edge stresses were found to fall below the value measured for the model with no hole. This could only be explained if a stress redistribution occurred around the hole, thus unloading the straight edge. The results which have been obtained thus far are of a satisfactory quality, since even for the most critical case the response was sufficiently clear. The comparison of the responses for the various laminates should provide only very general guidelines about the possible behavior of cross-ply laminates. Figure 34 shows the plot obtained for the $[90/0]_5$ laminate. The edge stresses are somewhat smaller in absolute terms than those measured for the $[0/90]_5$ laminate.





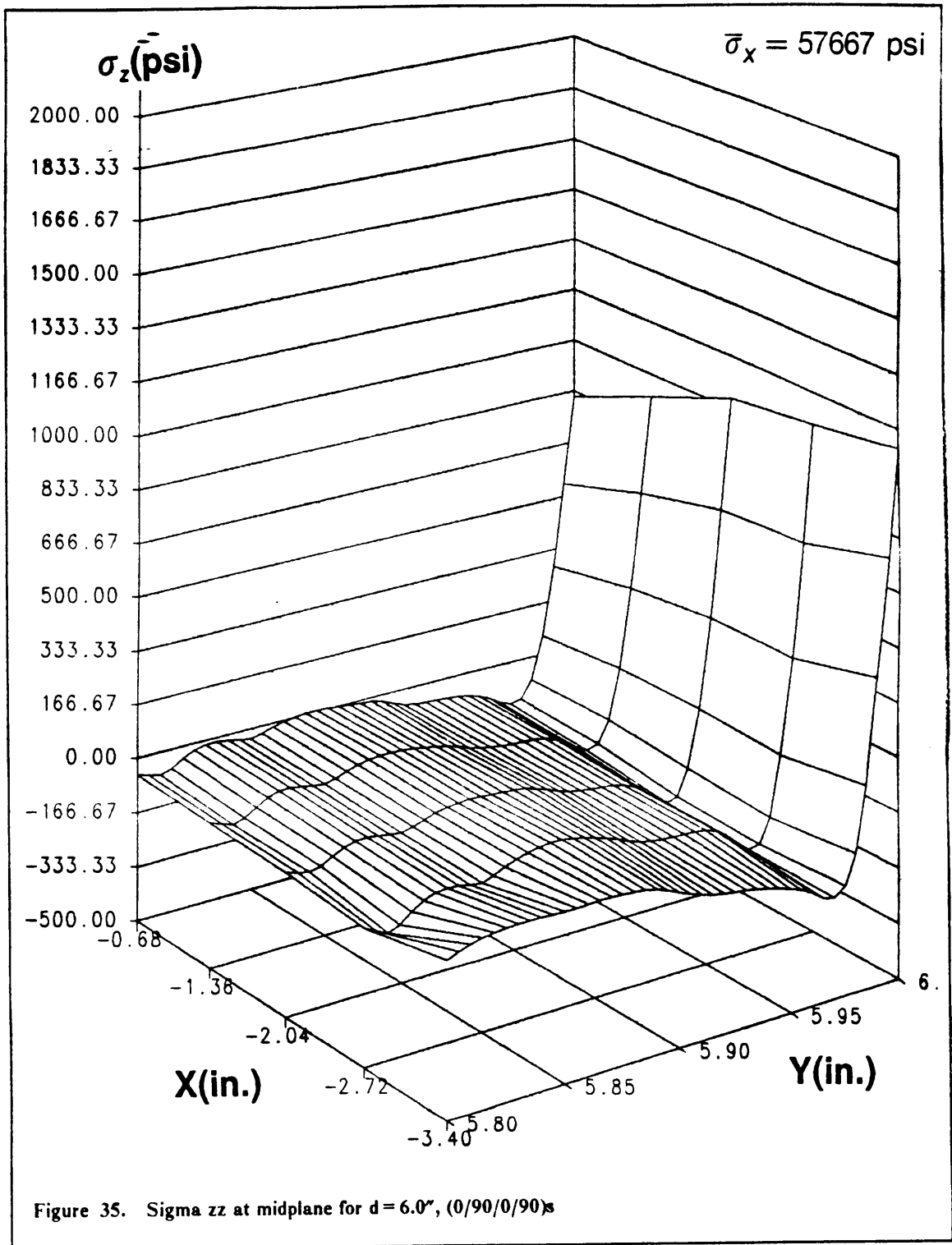
However, the variations at the edge are still large, with a minimum of -1600 psi increasing to -1080 psi at the edge (33% variation). Also the location of the maximum is extremely close to that for the $[0/90]_5$ laminate (5.96"), the magnitude is slightly lower at 150 psi. All of these similarities with the previous laminate could lead one to believe that all of the comments previously made for the $[0/90]_5$ laminate were applicable. It is reassuring also, to see how the stress fluctuations at the interface smooth out when approaching the free edge. Wang and Crossman again report an edge stress of $-0.35 \times 10^6 \times \epsilon_0$, whereas for the case at hand the edge stress was calculated to be $-0.24 \times 10^6 \times \epsilon_0$. The differences between these results are rather large and can be partly explained by the differences in the materials employed. Wang and Crossman further predict the peak away from the edge to be approximately 14% of the full edge stress. This is in complete agreement with the results obtained thus far.

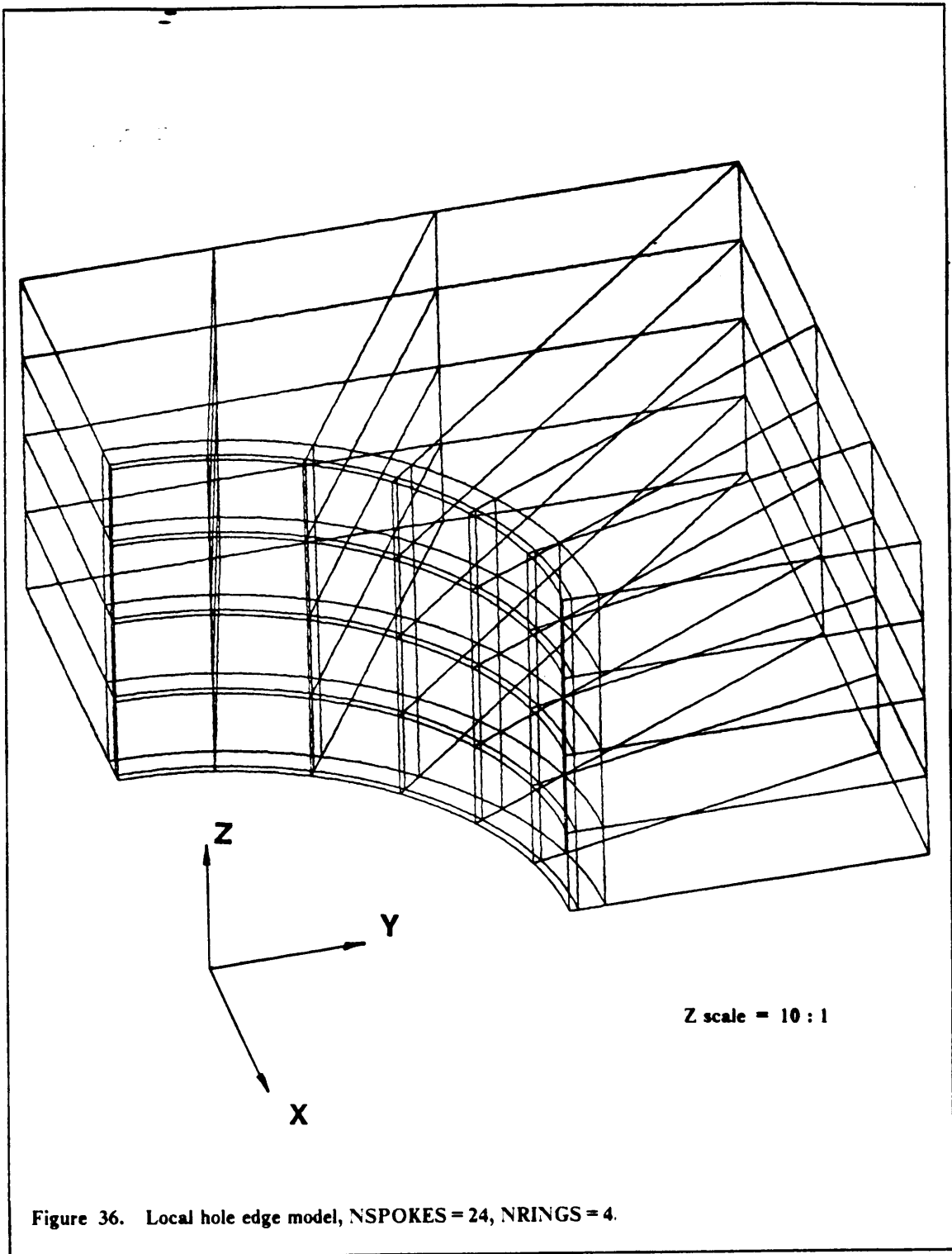
When the plies were staggered, such as for the $[0/90/0/90]_5$ laminate, the resulting stresses were found to be very much lower than when plies were clustered together. Figure 35 shows the response obtained for the staggered laminate. The edge displayed a large variation in stresses (22%), however the location of the minimum was found to be much closer to the edge (5.97") than was the case for the other two laminates. The resemblance which this plot bears to those discussed previously leads to similar comments being applicable.

Thus it appears that cross-ply laminates as a family would all display very similar responses, and would behave in the same general way in the presence of a circular aperture.

5.4. Hole Free Edge Problem

Figure 36 is a typical representation of the Local mesh used to analyze the stresses around the hole.





In order to verify the convergence of the local problem, a preliminary analysis was performed on a laminated plate with a hole diameter equal to the laminate thickness. This problem is similar in nature to the one analyzed by Dana³². Also this run created the opportunity to perform a final comparison between the results produced by the CSM Testbed and ANISAP. The Global two-dimensional analysis was performed over the entire plate, then the Local region was extracted and analyzed again to produce the final solution around the hole. The plate geometry was the same as that used in the previous section with the exceptions that the hole diameter was fixed at 0.1 inches, the characteristic local dimension 'A' was assigned a value of 0.5 inches and the number of spokes radiating from the center of the hole was selected to be 24.

When the results obtained with the CSM Testbed and ANISAP were compared, the solutions were identical. Figure 37 depicts the deformed mesh of the Local model. The main direction of loading is in the x-direction. Inspection of Figure 37 around the hole shows a large amount of deformation occurring at the first ring of elements. The top layer displays a large Poisson deformation in the z-direction. This should result in large interlaminar stresses close to the hole.

Figure 38 is a plot of σ_z versus θ , the angle is measured from the loading direction around the hole. It is of interest to note in Figure 38 that the transition from negative stress to positive occurs in the second element around the hole somewhere close to 66° , which is in agreement with Figure 37 when inspected closer. The far field stress was calculated to be 57667 psi. Figure 38 has a maximum occurring at -3500 psi at the $0^\circ/90^\circ$ interface which corresponds to a stress ratio of 0.06. The maximum stress at the midplane was predicted at 4000 psi, which resulted in a stress ratio of 0.8. The stress ratio is obtained by dividing the stress under consideration by the average applied stress. The locations of Z/h correspond to: 1. just above the midplane for $Z/h = 0.00141$, 2. Just below the interface at $Z/h = 0.002359$, and 3. just above the interface for $Z/h = 0.002641$. Dana³² reported results to a similar problem with the maximum stress ratio found to be 0.25.

Figures 39 and 40 are plots of σ_x versus θ and σ_y versus θ . It is interesting how the two plots complement each other for the stresses at particular z positions. The direct comparison of Figure

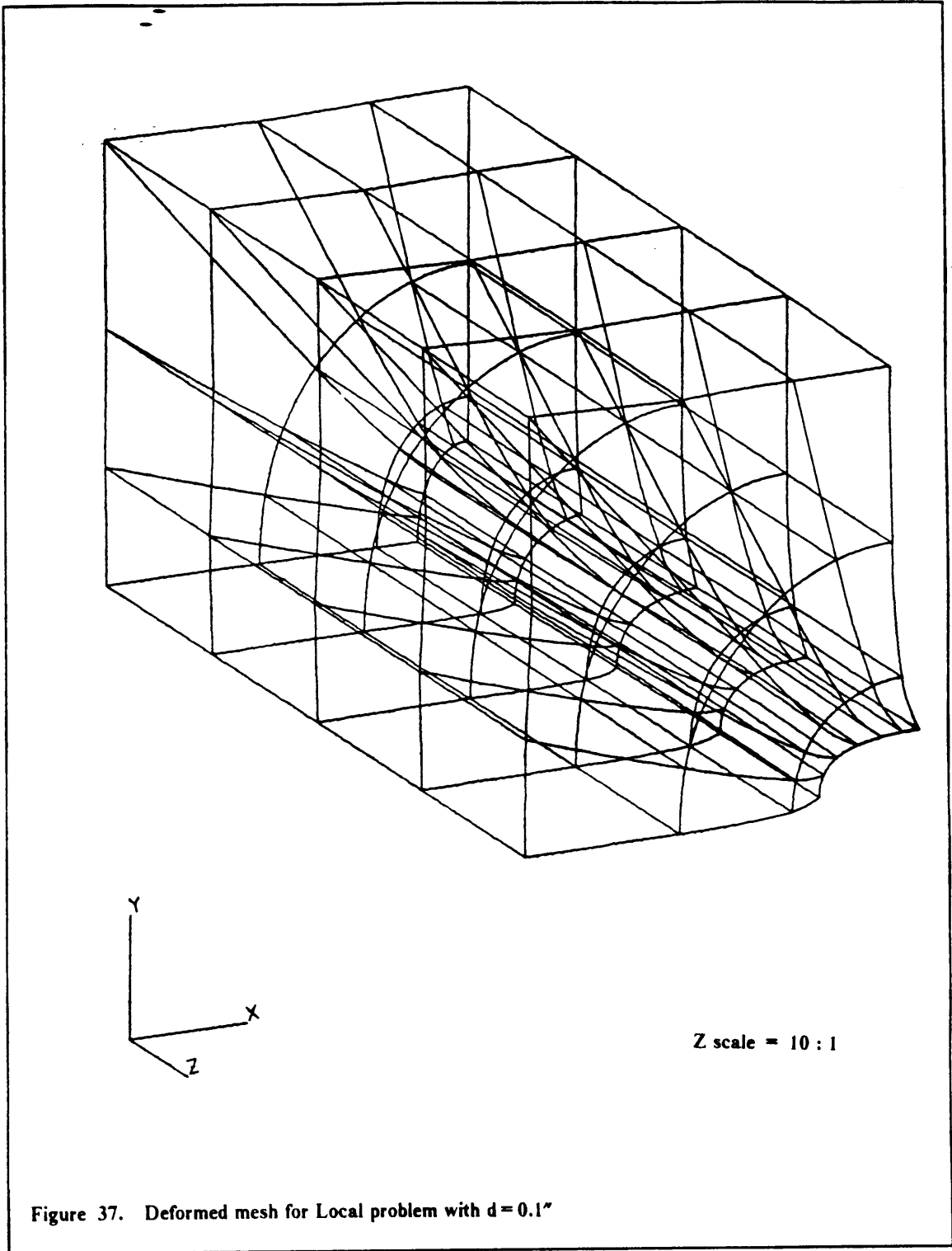
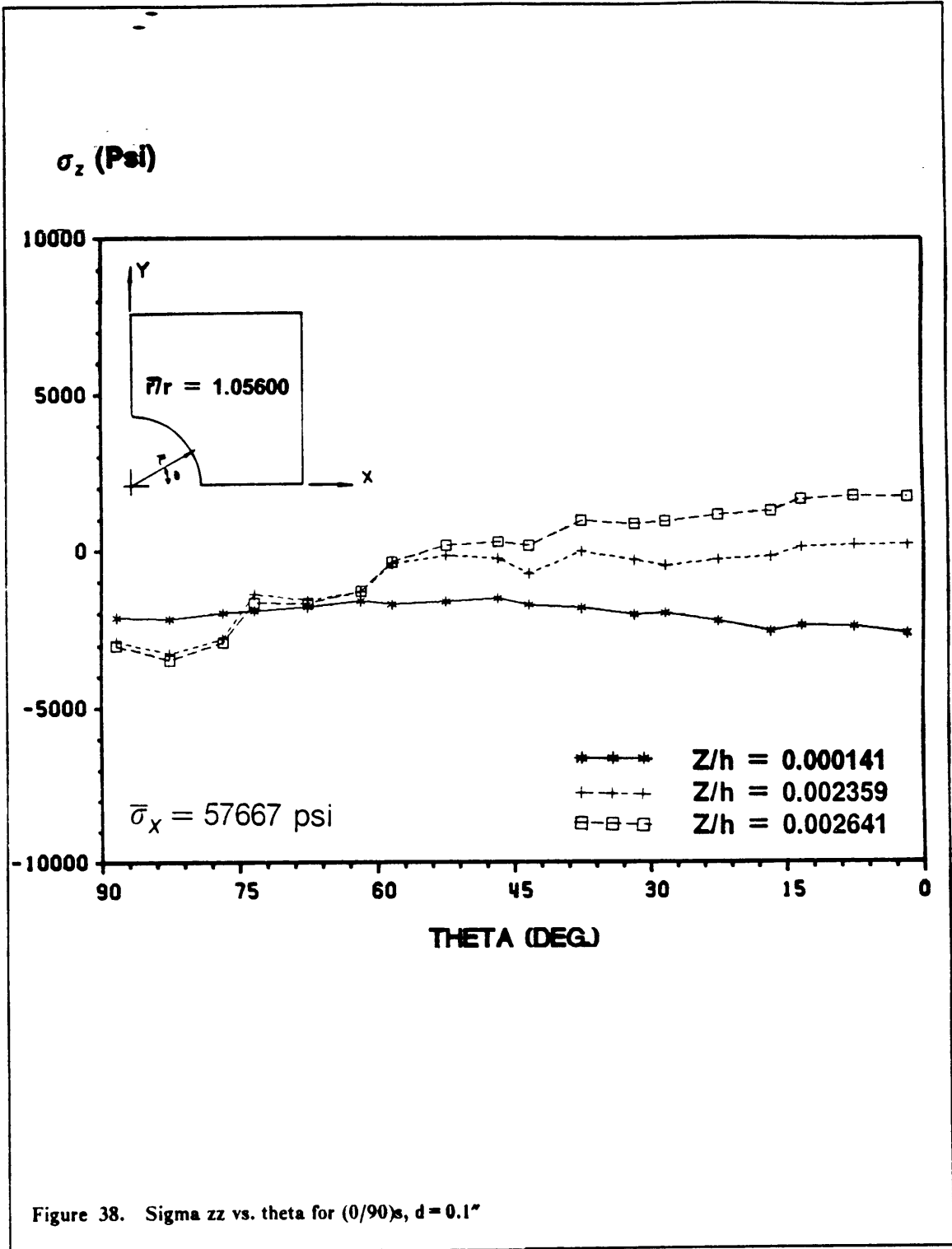


Figure 37. Deformed mesh for Local problem with $d = 0.1''$

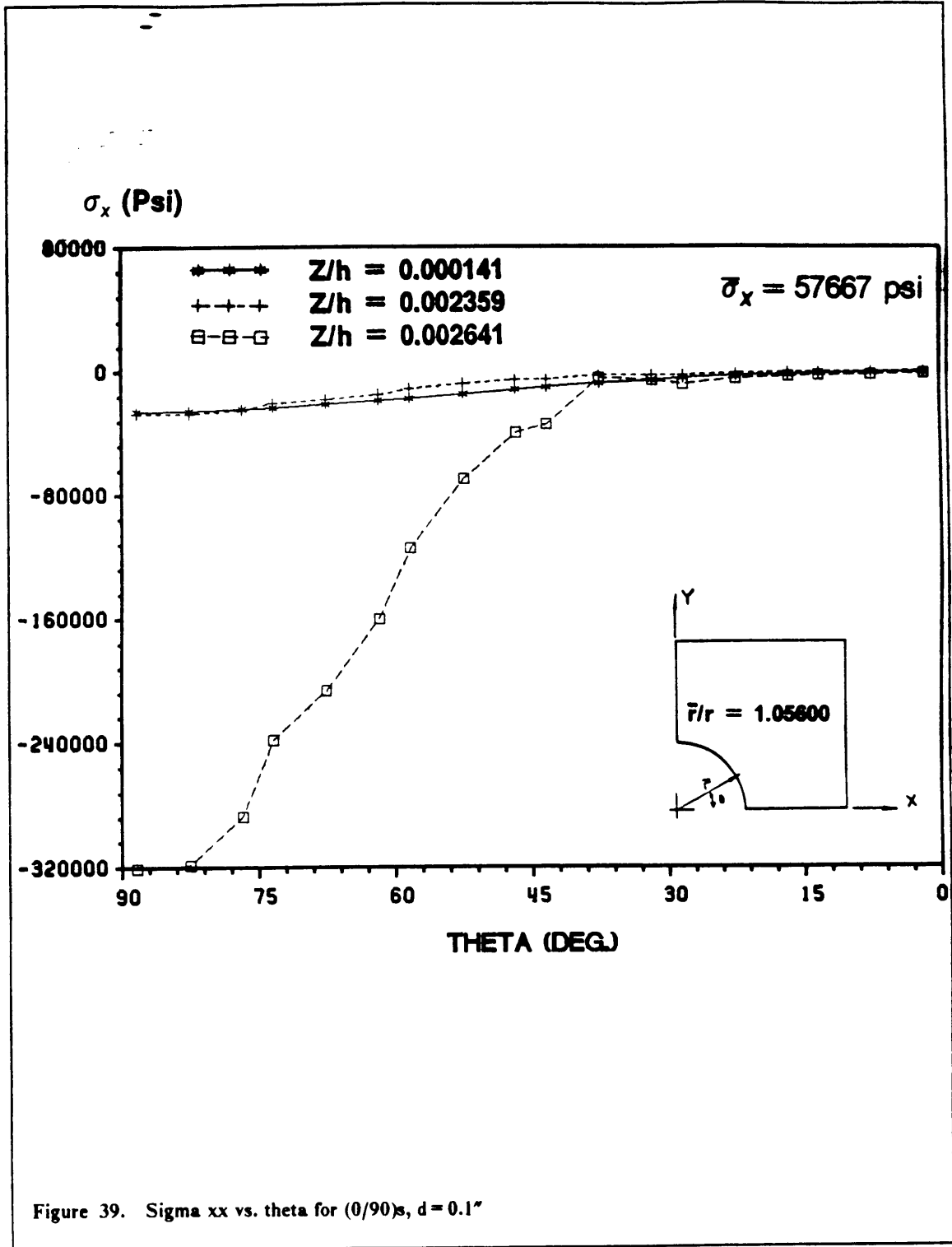


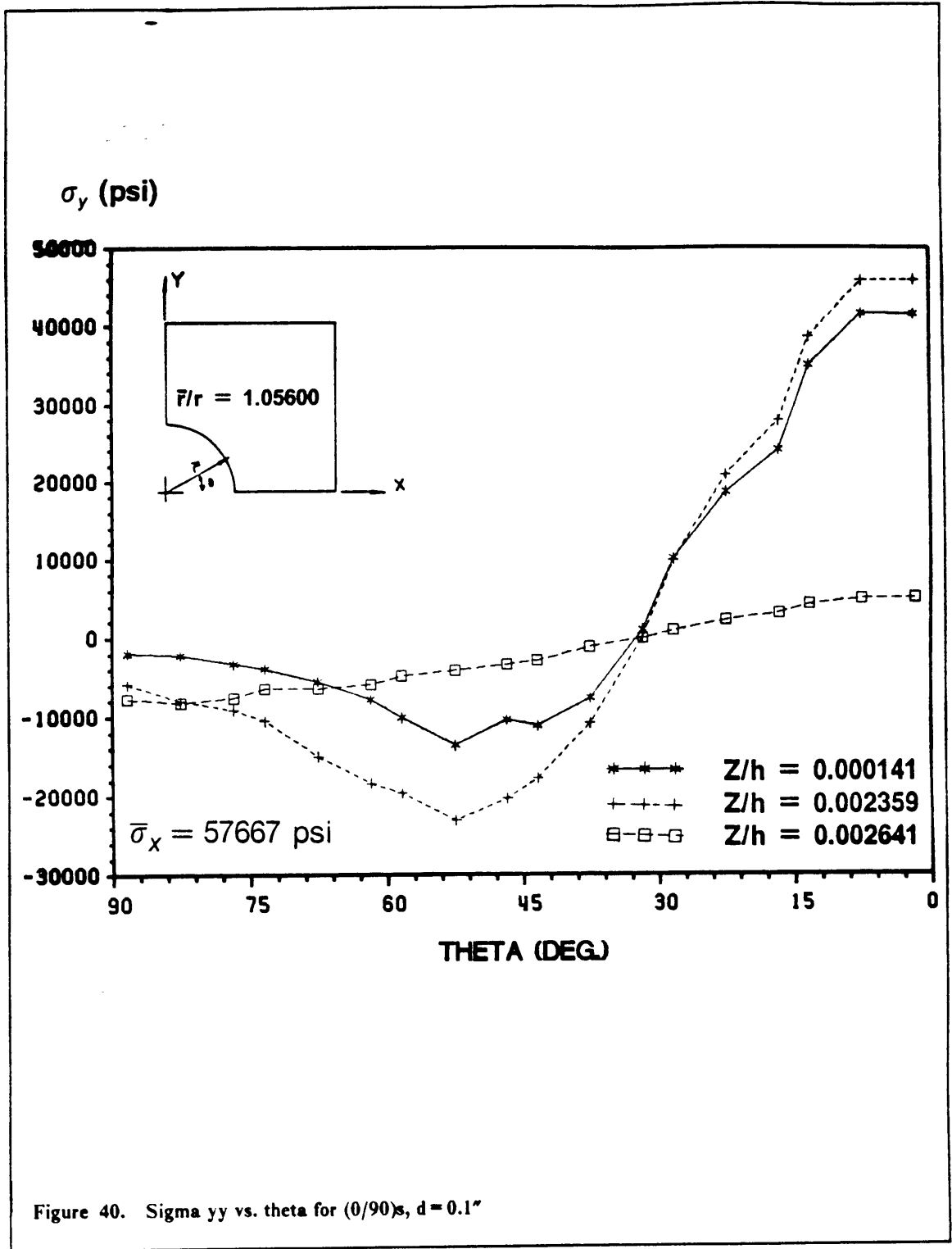
38, 39 and 40 for the analyses performed with the CSM Testbed and ANISAP gave identical curves. Thus the final verification was successful.

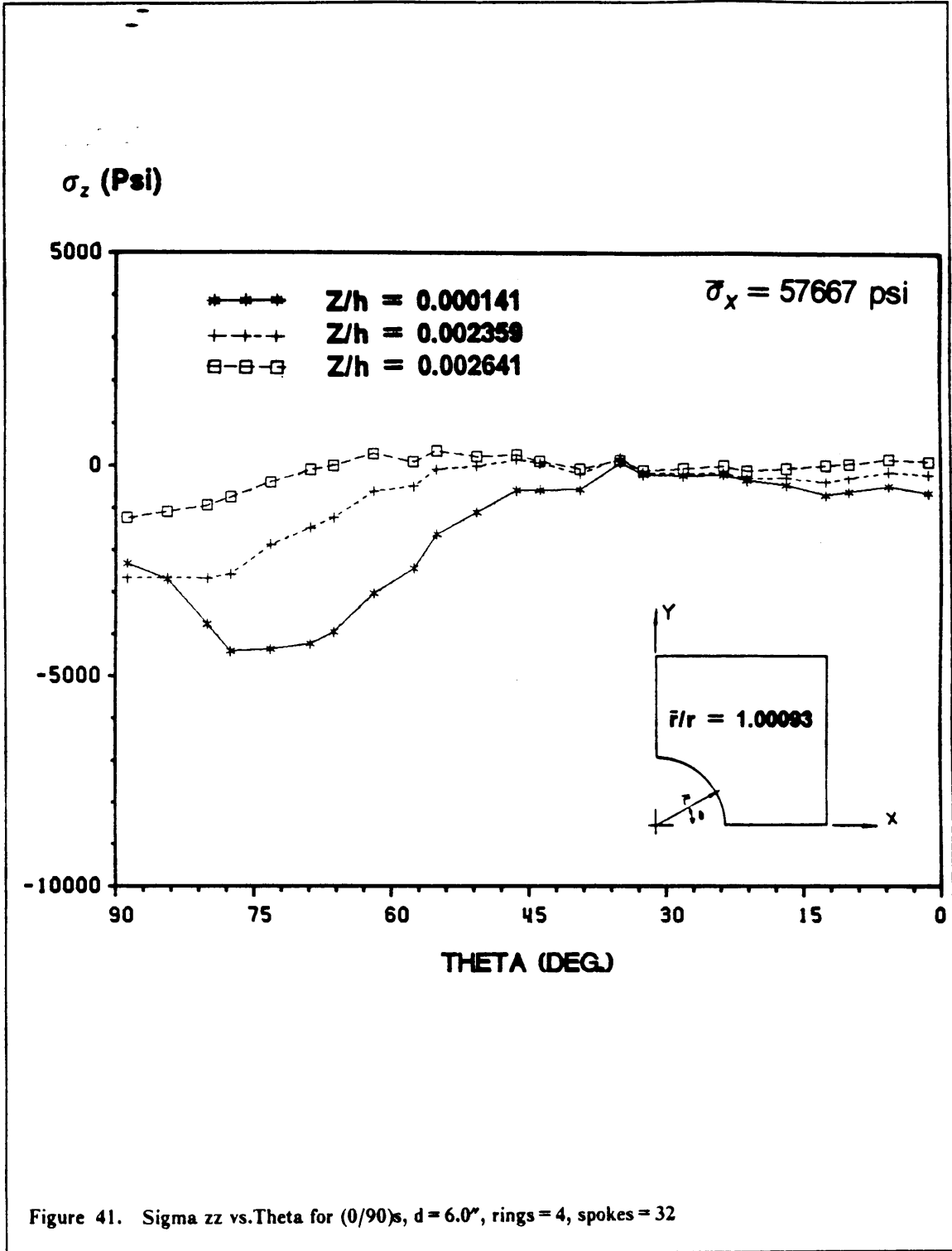
5.4.1. Location of the Global-Local interface

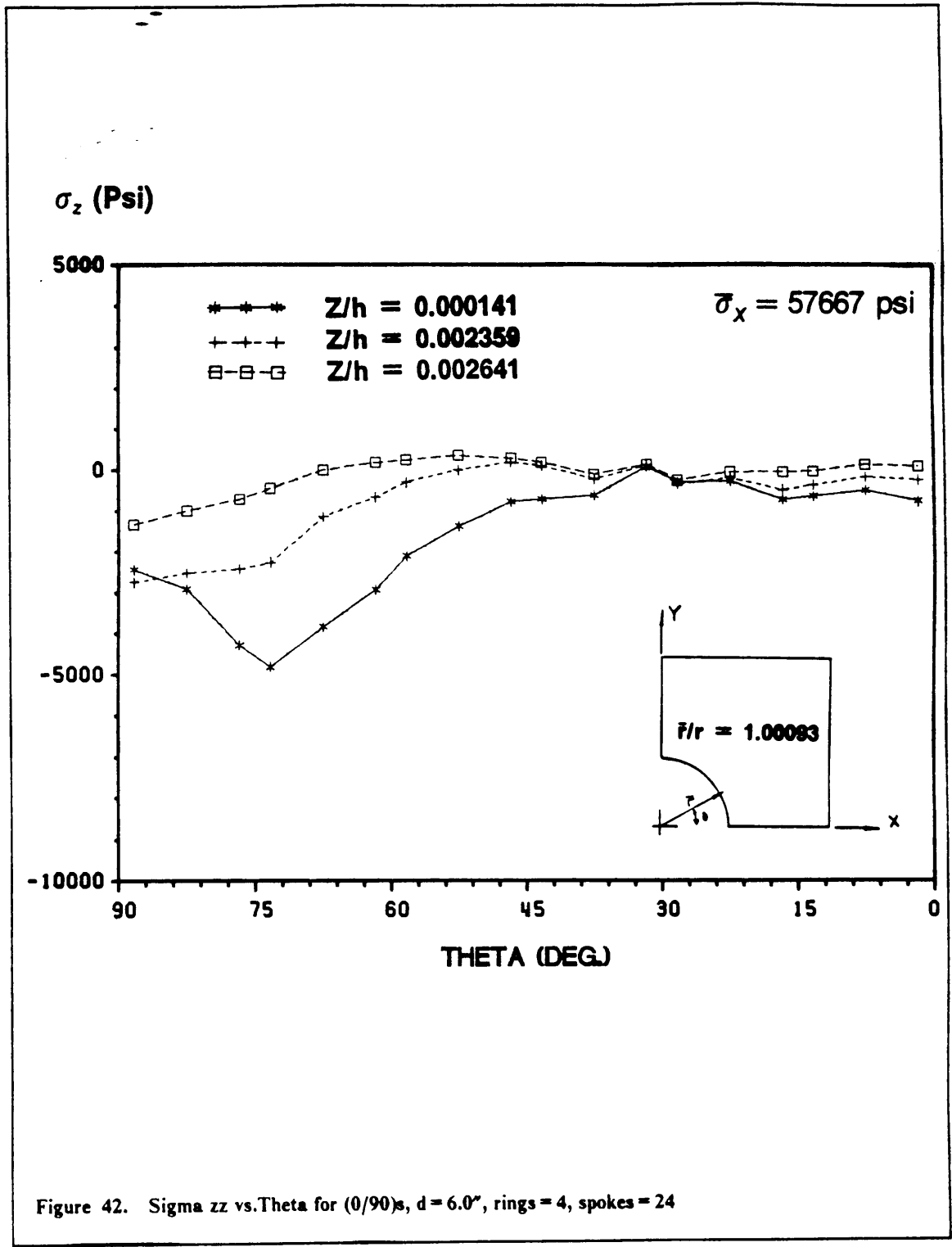
The selection for the location of the interface was made based on the largest size hole chosen. Since the maximum hole diameter analyzed was 6.0", the characteristic interface size Λ was fixed at 7.0". This would allow enough distance between the edge of the 6.0" hole and the model boundary to allow the stresses to develop completely. Also it was decided to maintain the value of Λ constant in order not to bias the results of the various runs. Initially it was decided that three rings of elements around the hole should be sufficient to model the stresses accurately. The width of the innermost ring was set to be one fourth of the laminate thickness (0.025"), the middle ring was chosen to have a width of three fourths of the laminate thickness (0.075"). By means of these two rings covering one laminate thickness away from the edge it was expected to determine the stresses around the hole accurately. Various analyses were performed on this model by increasing the number of elements around the hole. Eventually a satisfactory distribution was obtained when 48 spokes were used around the hole. The distribution of σ_z versus θ was acceptable but still very coarse, it was speculated that by using the same total number of elements or even less but with a better mesh a more accurate distribution could be obtained. For this reason the number of rings was increased to four. The third ring had a width equal to the thickness of the laminate (0.1"). A first run was performed with 32 spokes around the hole, this resulted in a distinctly more accurate and smooth distribution (fig. 41). Another computer run was performed with only 24 elements around the hole. The distribution was still smooth but a definite loss in accuracy of the results was noted (fig. 42).

When the responses for σ_x versus θ and σ_y versus θ were inspected the same characteristics became evident. Thus the final selection for the local model was made and it consisted of 4 rings and 32









spokes with the interface parameter Λ set to 7". Only one eighth of the hole was actually modeled by observing symmetry about all three planes.

5.4.2. Hole edge stresses

In order to draw a parallel between the interlaminar normal stress distribution at the straight free edge and at the hole edge it was necessary to perform the analysis on problems similar to those investigated in section 5.3.2.

Table 8. Summary of analyses performed on the hole free edge

Hole diameter	$[0/90]_s$	$[90/0]_s$	$[0/90/0/90]_s$
1"	Yes	No	No
2"	Yes	No	No
3"	Yes	No	No
4"	Yes	No	No
5"	Yes	No	No
6"	Yes	Yes	Yes

Table 8 is very similar to Table 7 with the exception of the "no hole" case which would have no meaning in this context. Due to the choice of the Local mesh made in the previous section the analysis had to solve a 128 element model. This required approximately 42 CPU minutes on a VAX 11/785, on the other hand the straight edge problem consisted of only 60 elements and required 26 CPU minutes to execute on the same machine.

The results were plotted to show the stresses around the hole at the laminate midplane as well as at the Gauss points just below and just above the 0° - 90° interface. Plots were produced for the

interlaminar normal stress versus the angle θ , but also for the normal inplane components versus the angle θ .

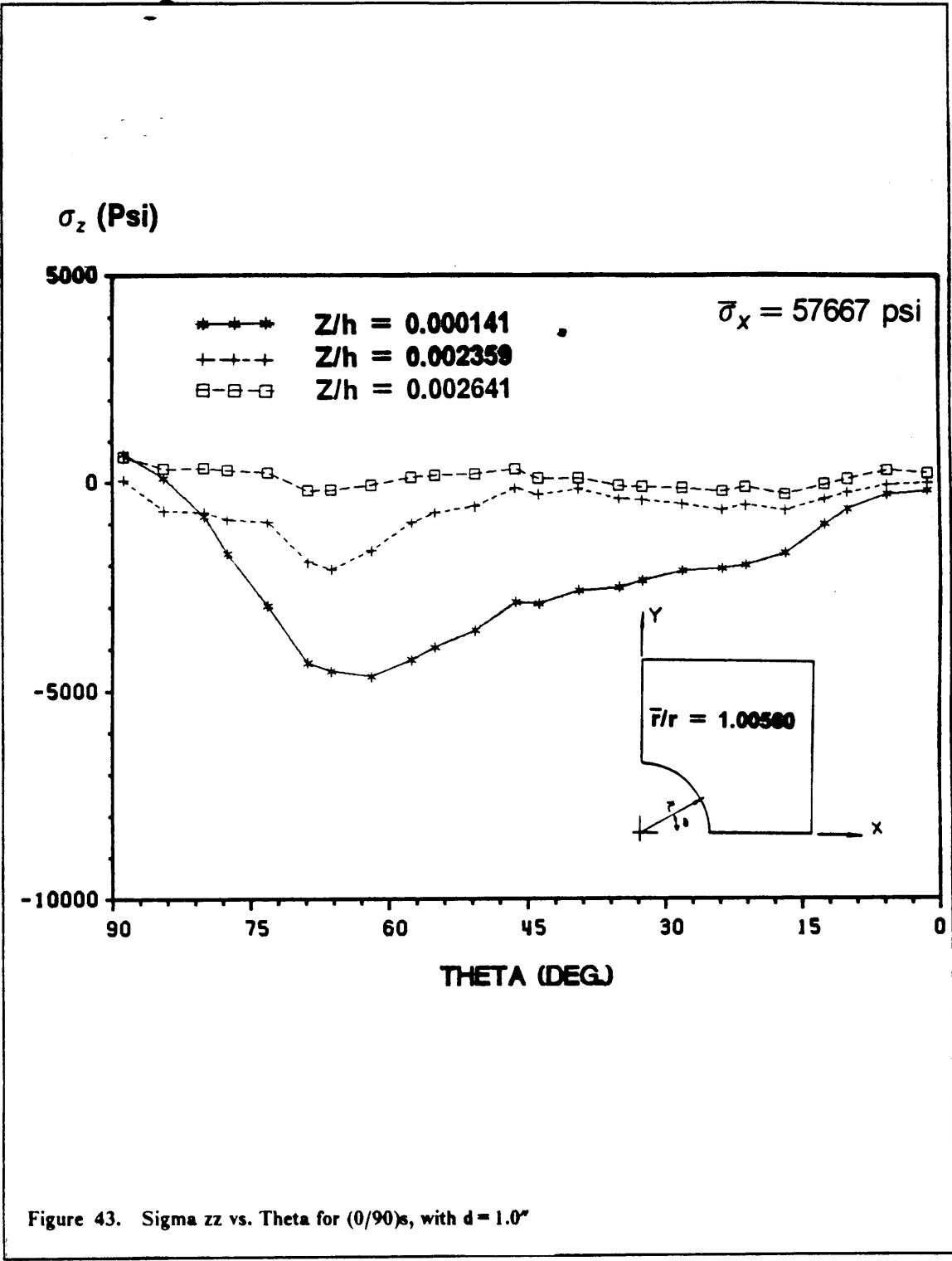
Again the discussion will first consider the results for the $[0/90]_5$ laminate. Figure 43 is a plot of σ_z versus θ for a hole diameter of 1.0". The plot displays a large trough at -63° reaching a value of -5000 psi at the midplane. The interface stresses are relatively small barely reaching -2000 psi. All the curves are smooth within acceptable limits.

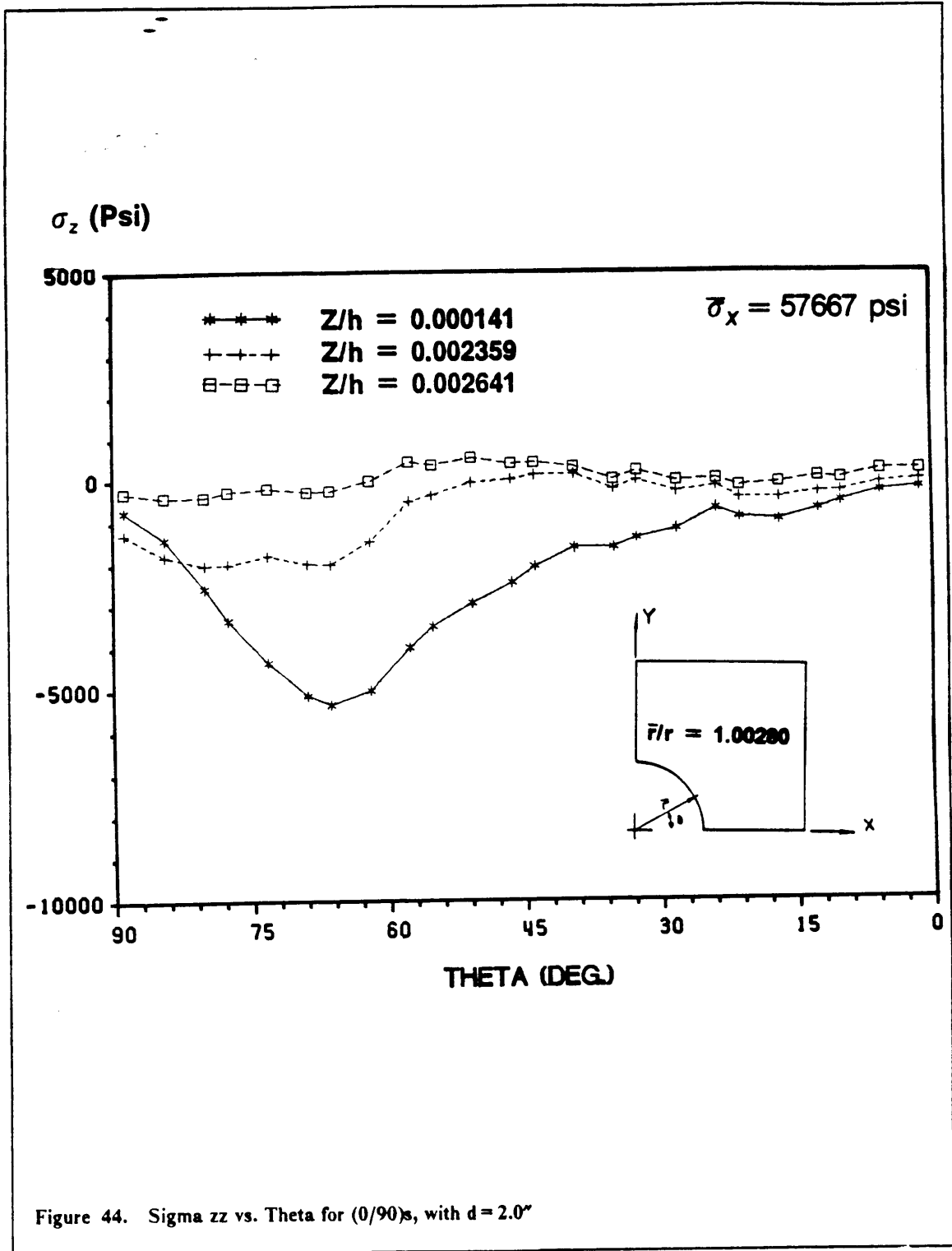
The 2.0" diameter hole causes the midplane σ_z around the aperture to vary more sharply at -66° , attaining a minimum at -5500 psi (fig. 44). The distribution at the interface remained extremely similar to the one obtained from the previous case.

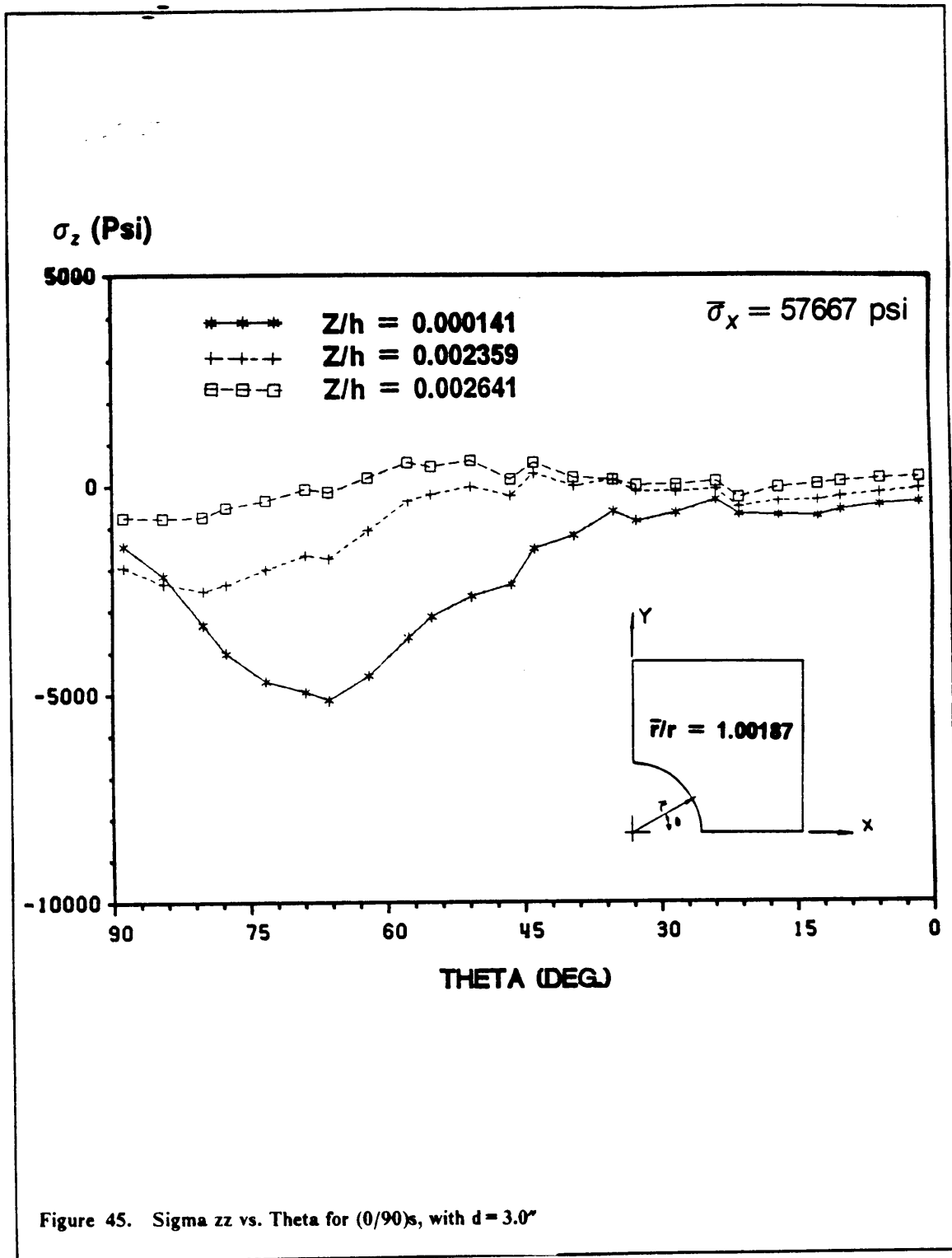
The 3.0" aperture promotes a response which is nearly identical to that caused by the 2.0" hole (fig. 45). The only significant difference is the somewhat faster growth of σ_z close to -90° . Also the interface stresses displayed a slight increase in absolute magnitude. Figure 46 shows σ_z versus θ for the 4.0" hole. The maximum stress at the midplane displays a small decrease to -5000 psi occurring at -69° . The interface stresses are virtually unchanged from the previous case.

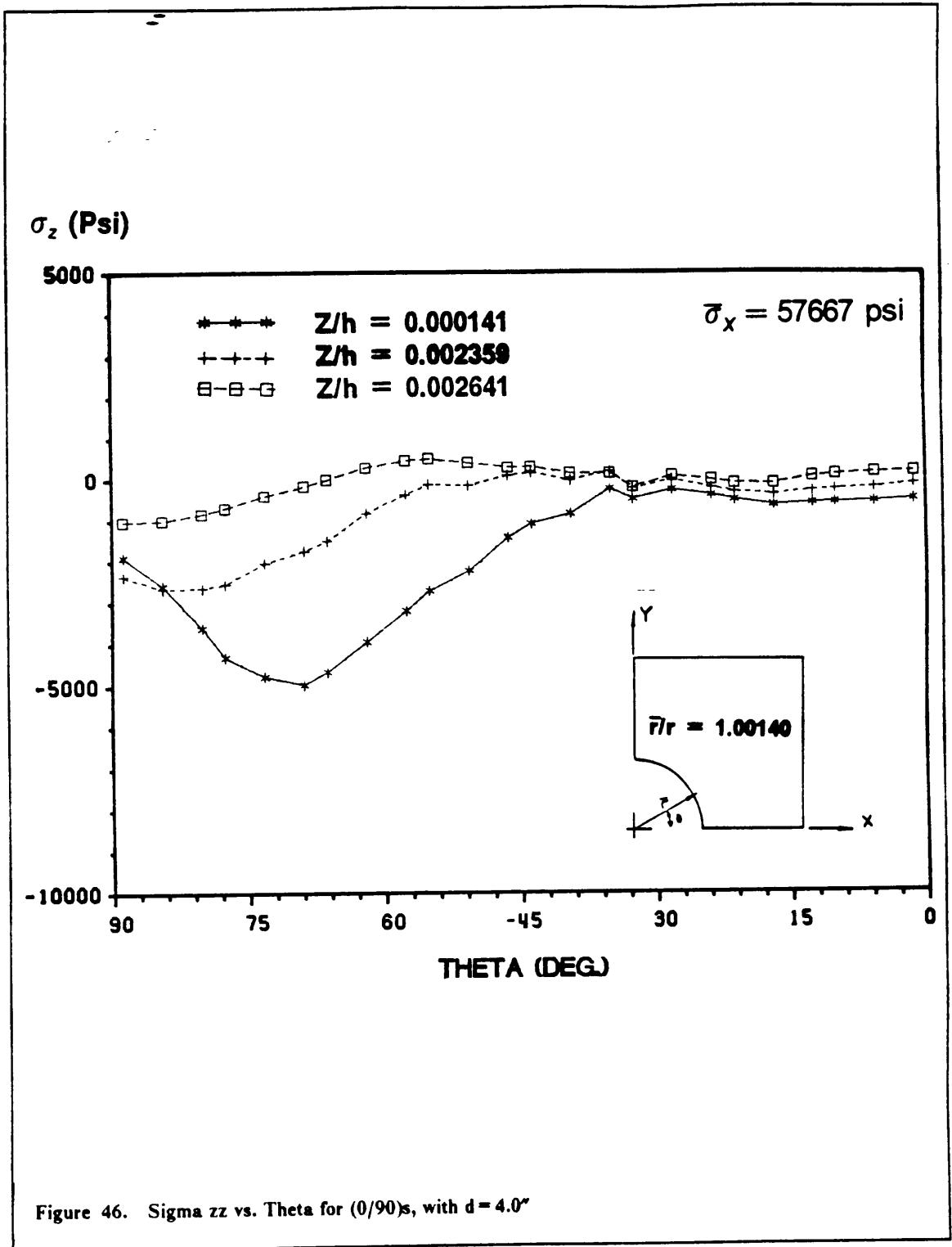
When the hole diameter is increased to 5.0" the midplane stress distribution remains virtually unchanged (fig. 47). Some small variations can be detected for the interface. The maximum has increased to -3000 psi with a location of -84° . Finally Figure 48 shows the interlaminar normal stress distribution for the 6.0" diameter hole. The midplane stress shows a slight loss, with the peak decreasing to -4500 Psi and the location shifting to -78° . The interface stresses remained very similar to those obtained from the previous analysis.

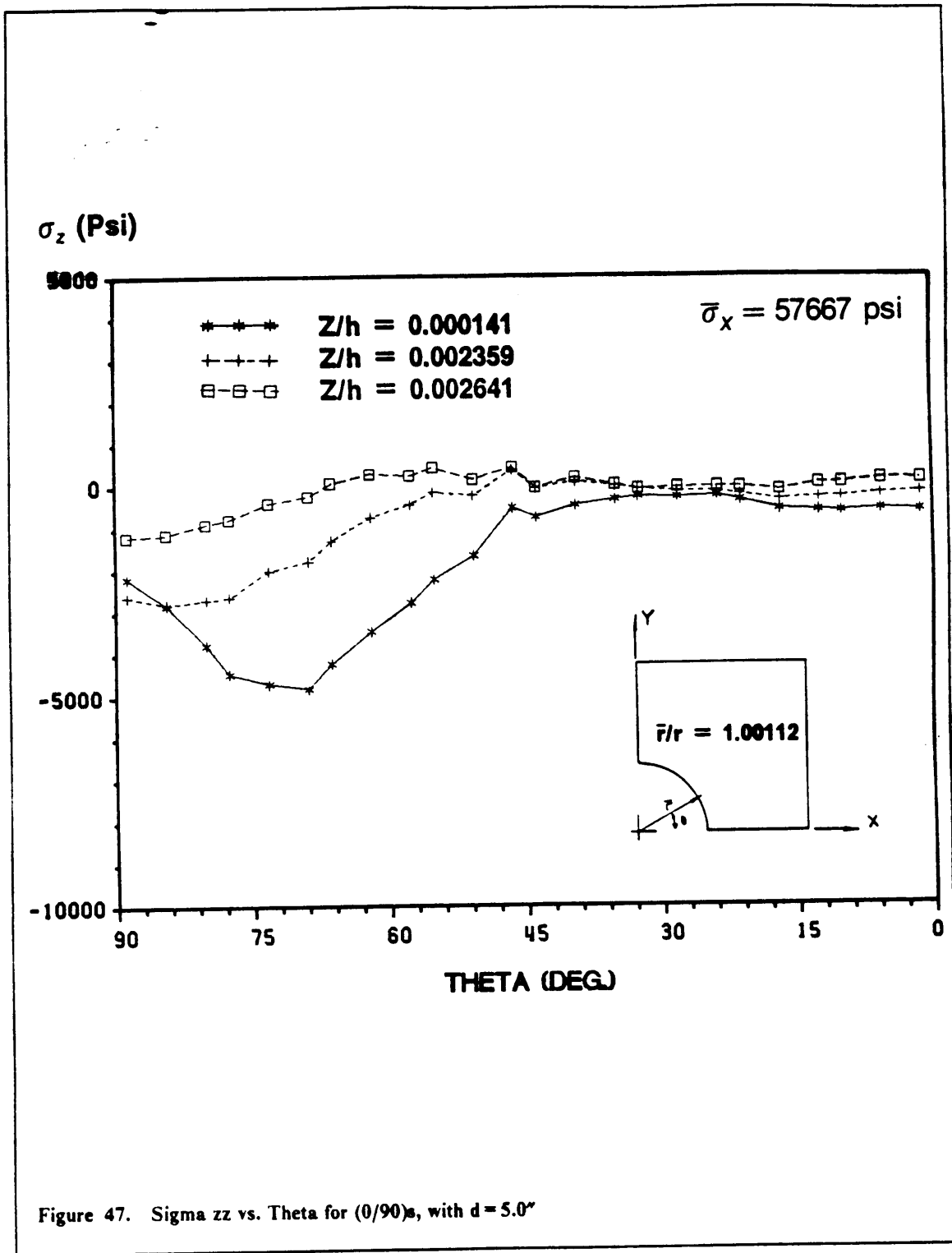
Tang³⁵ performed analyses on Boron/Epoxy laminated plates with a hole. The hole diameter to laminate thickness ratio was 16.0. The results published quoted the maximum σ_z to occur at 75° with a stress ratio of 0.25 at the midplane. The shape of the distribution was in many ways similar to that obtained in the present study, one large peak close to 90° decreasing slowly towards 0° . Rybicki³¹ as well analyzed a Boron/Epoxy $[0/90]_5$ plate with a hole, the hole diameter to laminate

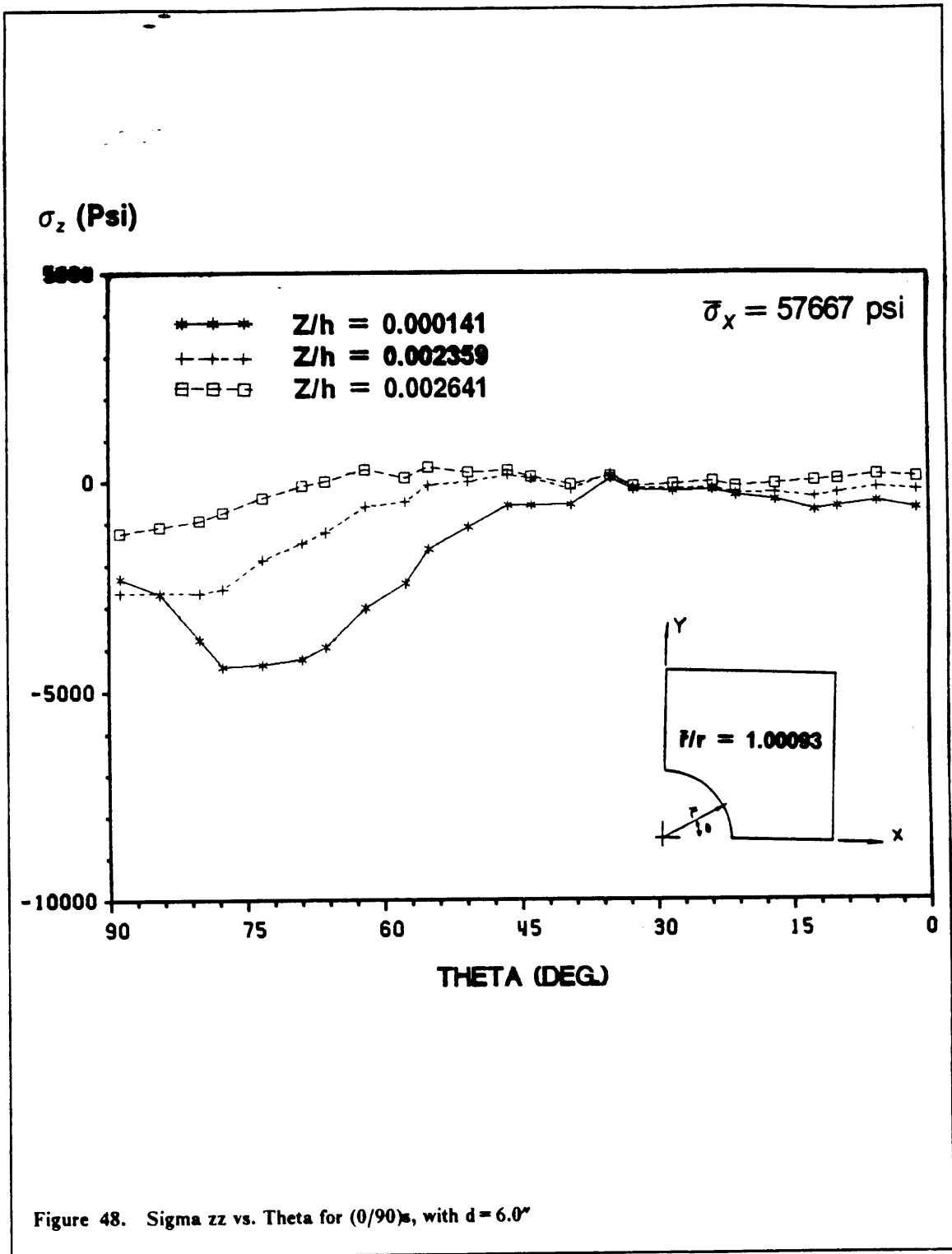












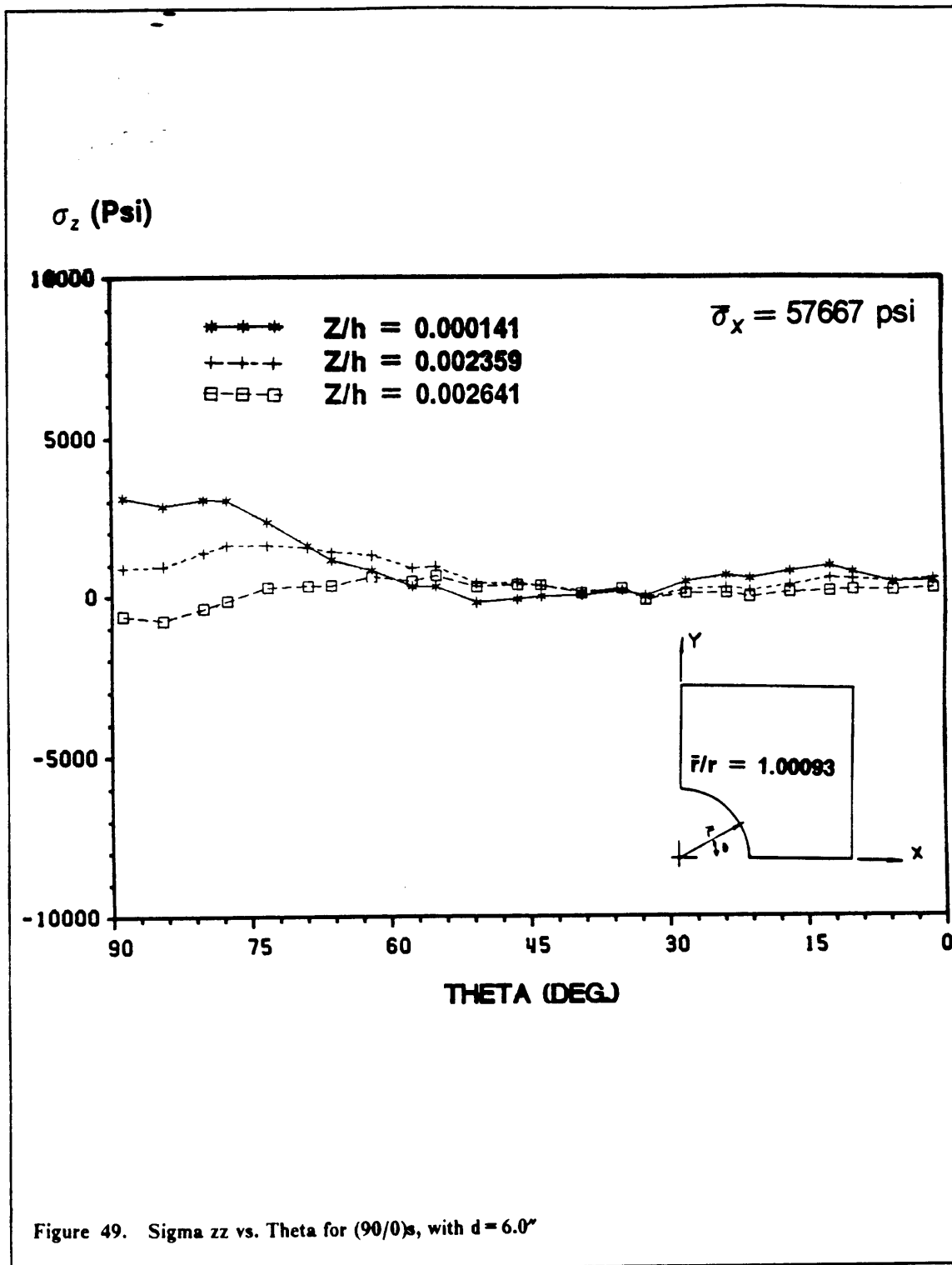
thickness ratio in this case was 0.8224. The maximum was noted to occur close to 50° with a stress ratio of 0.15. The stress ratio obtained during the course of the present investigation was calculated to be 0.08 for the 6.0" hole. A close comparison of the results provided by Tang³⁵ and Rybicki³³ show very little resemblance in the stress distributions even with material systems which should be similar. In other words a comparison of the stress fields around a hole can only be compared to the extent of the relative orders of magnitude and possibly the general shape of the distribution.

The interlaminar normal stress distributions obtained for the $[0/90]_5$ laminate show little variation with increasing hole size, this could suggest that within the limits of this investigation the response is relatively insensitive to the hole diameter if such diameter falls within a range of 10 to 60 laminate thicknesses.

The results obtained for the $[90/0]_5$ laminate with a 6.0" diameter hole presented smaller stresses (fig. 49). The midplane distribution peaked at 3200 psi at 90° , the interface stresses reached a maximum of 1500 psi at 75° .

Tang⁵, and Schmueser²⁶ published results pertaining to a $[90/0]_5$ Boron/Epoxy laminate with a hole. Tang predicted a maximum midplane stress at 90° with a stress ratio of 0.3, Schmueser also predicted a maximum at 90° with a stress ratio of 0.26, the stress ratio for the present study was found to be 0.06. Considering that the material systems used by Tang and Schmueser were very different from the one employed in this investigation, the correlation of the results was very encouraging.

Dana³² analyzed thick laminated plates with holes. The laminates were considered thick because the hole diameter was of the same order of magnitude as the laminate thickness. Also Dana used Boron/Epoxy as a material system. The results published included the analysis of a $[90/0]_5$ laminate with hole diameter 10 times the laminate thickness. If the assertion of the indifference of hole diameter to stress distribution is correct, then the results presented by Dana for this particular case should be comparable to those obtained in the study. The σ_z distribution presented by Dana



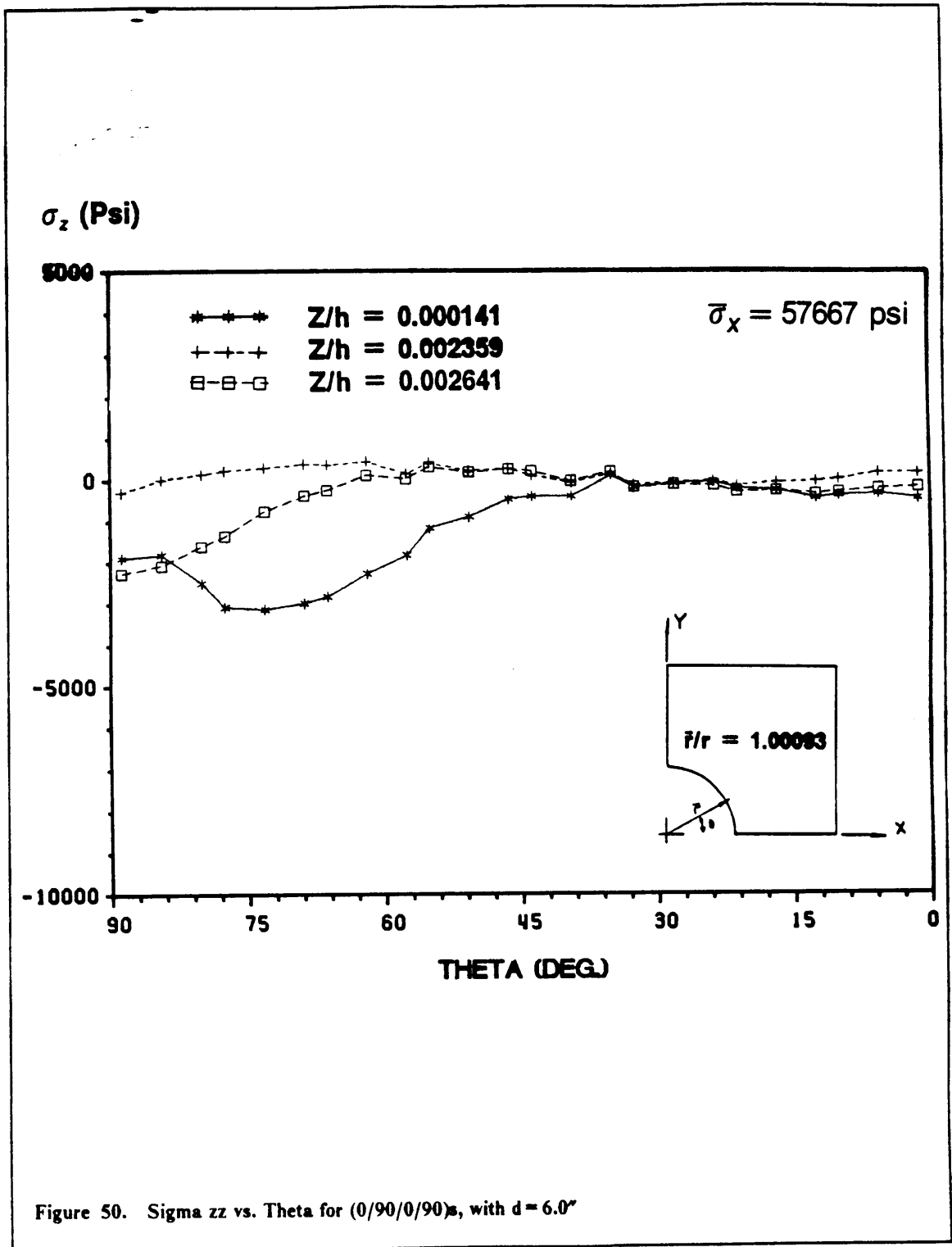
reached a maximum at 0° with a stress ratio of 0.15. The shape of the distribution was in complete disagreement with the one obtained in the study, as well as the location of the maximum (90°). The magnitude (0.06) was certainly comparable and represented the best correlation obtained thus far. However there is a large disagreement in the distribution between the results obtained by Dana and those of Tang. There is reason to find Tang's results more probable due to a number of deficiencies found in Dana's investigation. The use of three elements through the thickness with the 24 node element provided a modelling of the edge effects which was not as accurate as it could have been by using four elements per lamina thickness, as was concluded in Chapter 4. Also, the model Dana used produced only 7 data points to plot the results over 90° .

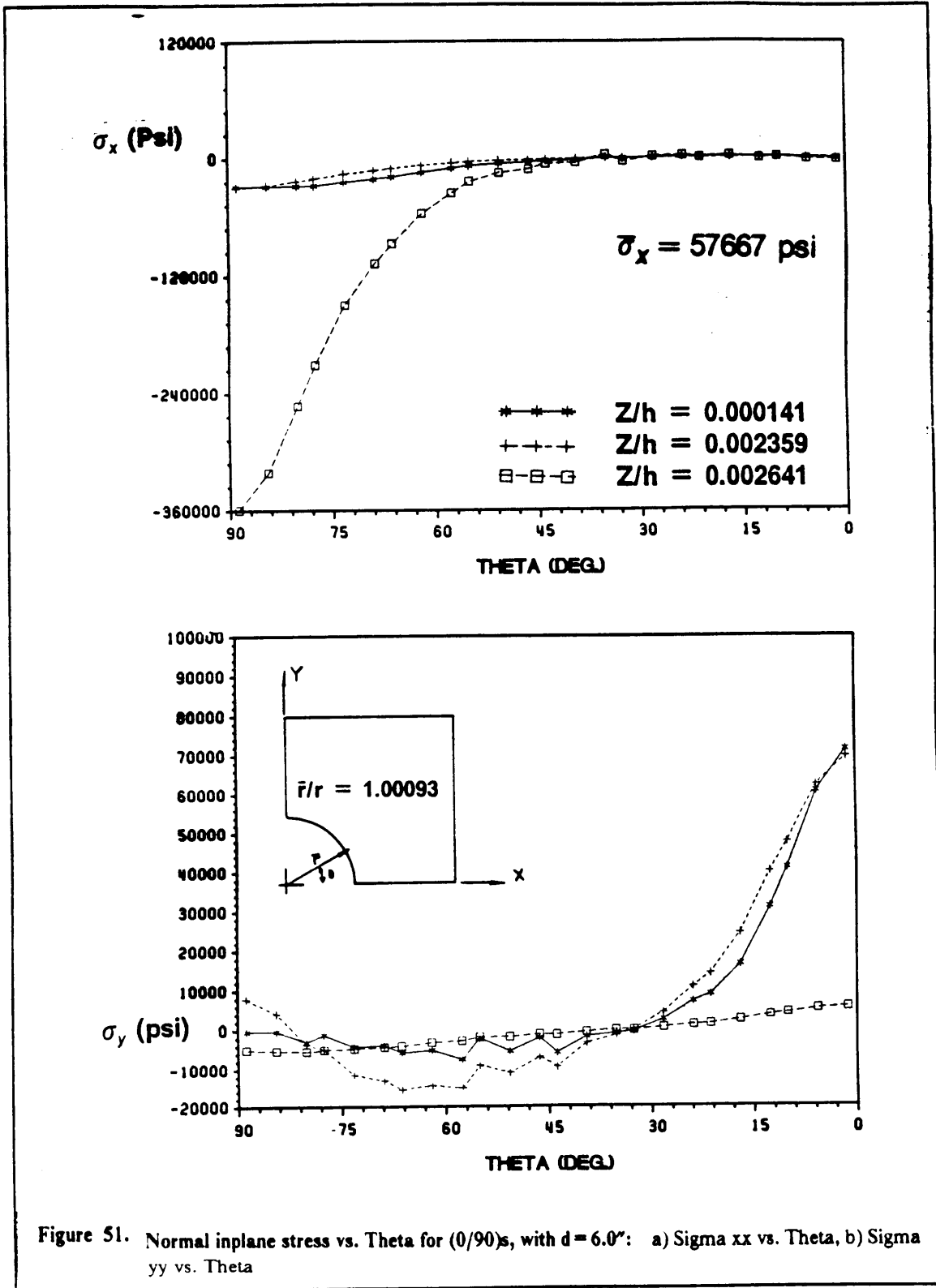
Figure 50 shows the interlaminar normal stress distribution for the $[0/90/0/90]_S$ laminate with a 6.0" diameter hole. The effect of staggering the plies becomes evident. The maximum at the midplane shows a decrease from -4500 psi to -3200 Psi when compared to the results for the $[0/90]_S$. The interface stresses are very nearly 0 psi everywhere except for a peak at -90° which reaches -2300 psi.

Inspection of the plots obtained for the normal inplane stresses around the hole tend to support the insensitivity of the response to the hole size. Figure 51 shows typical plots for both components of stress. The plots obtained at various hole sizes are extremely similar for the $[0/90]_S$ laminate as well as for the $[90/0]_S$ and the $[0/90/0/90]_S$.

5.5. Discussion

By inspecting Figure 52, the deformed global model, it is possible to notice that the necessary symmetry of displacements about the lines $x = 9.0$ in. and $y = 6.0$ in. (global coordinates) are satisfied as well as the intuitive deformed shape of the model.





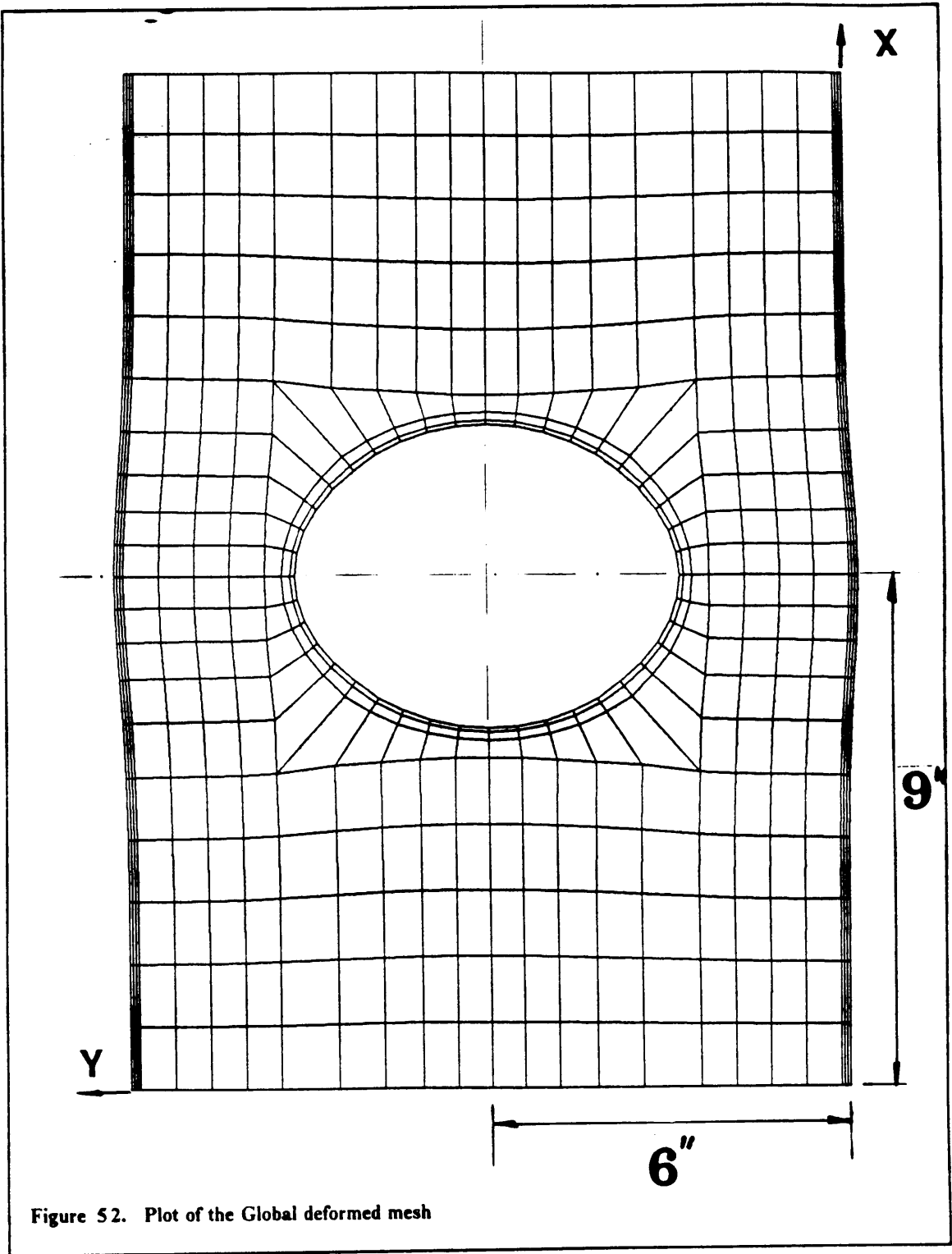


Figure 52. Plot of the Global deformed mesh

Although this would seem the least to be expected, when the model was analyzed with the E43⁸ two-dimensional hybrid formulation element, the resulting deformed mesh was found to be unsymmetrical and the results were completely unsatisfactory. This brought to evidence the limitations of the E43 element which operated satisfactorily for regular slightly deformed models, but could not model the correct behavior of highly distorted element geometries. For this reason the EX41 experimental element³⁷ was employed.

The two ~~local~~^{local} regions under consideration could possibly exercise a large influence over each other. For this reason the results obtained for each model need to be discussed as a "local pair", instead of restricting the results to each specific region. Thus it is necessary to look at the results obtained from both regions simultaneously, in order to give a valid representation of the effects noted during the course of the investigation.

When inspecting the stress state around the hole it is necessary to consider the midplane distribution only, since all the straight edge results are presented for the midplane only. The value of $\theta = -90^\circ$ coincides with the global line $x = 9.0''$ which is the plane of symmetry used by the straight edge model (local $x = 0.0''$) (fig. 22).

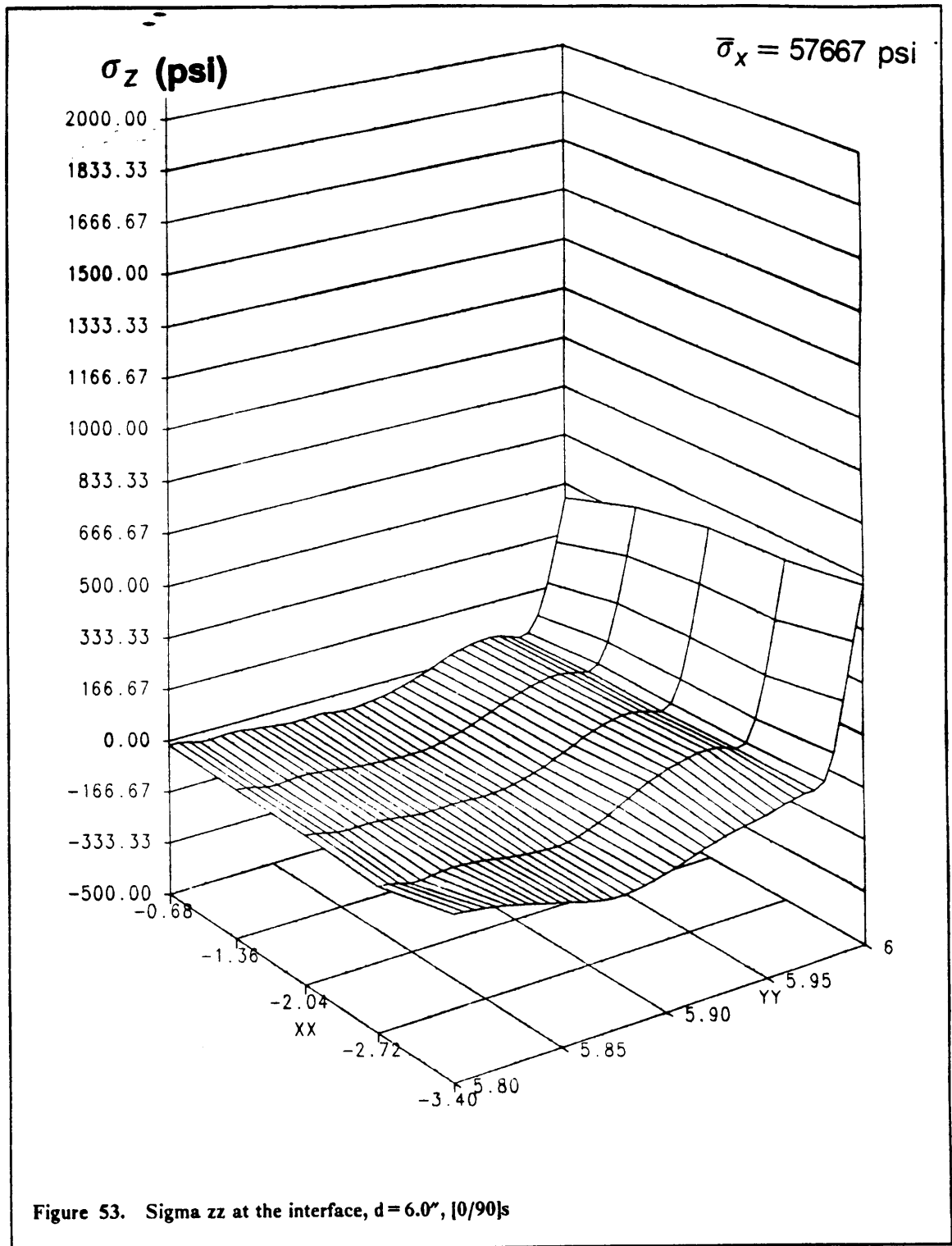
A close inspection of the results revealed certain trends when the diameter of the hole in the plate was increased. First at the straight edge the stresses displayed an increasing disparity at the edge with increasing hole size. The decrease in stresses was noticed to increase with closeness to the plane of symmetry (local $x = 0.0''$). Second, the hole edge stresses displayed a curve covering more area for small hole diameters, peaking at -63° . The stresses were negligible only at 0° and -90° . With larger hole diameters a shift of the curve towards -90° was noticed, also the distribution was found to enclose less area than for smaller holes. At maximum diameter the curve was essentially zero from -40° to 0° , peaking at approximately -80° . These comments were found to be applicable for all the laminates under consideration.

It was not feasible to infer if the stresses at the straight edge and at the hole exercised influence over each other. To possibly get an indication of such behavior it would be necessary to analyze a case where the hole diameter was smaller than the plate width only by a few laminate thicknesses. In this manner it would be possible to investigate the interaction between the edge stresses and the hole stresses. All the cases analyzed in this study had at least 30 laminate thicknesses distance between the straight and hole edges. It would seem unlikely that any stress interaction could possibly occur at such a large distance.

An important note must be made to the effect that the laminates considered in this study are all thin, as opposed to thick laminates. All the investigations which have been performed with finite elements up to date have considered thick laminates (Lin³⁸, Wang et al.³ and Griffin²⁹). This assumption results in simpler models because by using a thick laminate a much less fine mesh needs to be used in order to satisfy the side-to-thickness element ratio limitation. However the use of laminates with thicknesses of 0.5" is unrealistic, whereas laminate thicknesses of 0.1" are the correct order of magnitude for everyday applications. The other factor which makes the present study unique in finite elements is the analysis of laminated plates with a hole diameter many times larger than the total laminate thickness, all of the research performed earlier was for hole diameters close to the laminate thickness (Dana³², Rybicki et al.³³), which again have very limited applications.

Figure 53 is a plot of σ_z at the 90°/0° interface close to the straight edge. This plot represents the response of the $[0/90]_5$ laminate with a 6" diameter hole. The maximum (650 psi) was found to be much lower than all the maxima predicted at the midplane. The shape of the distribution was similar to that obtained at the midplane but some disturbances were much more evident.

The distribution of the interlaminar normal stress through the half thickness of the $[0/90]_5$ laminate is shown in Figure 54. It is plotted at the straight edge. It is reassuring to see how the σ_z stresses are smaller in the 0° layer than in the 90° layer. This is in accordance with the results predicted by the plot shown in Figure 53. It is noteworthy also the fact that the interlaminar normal stress ap-



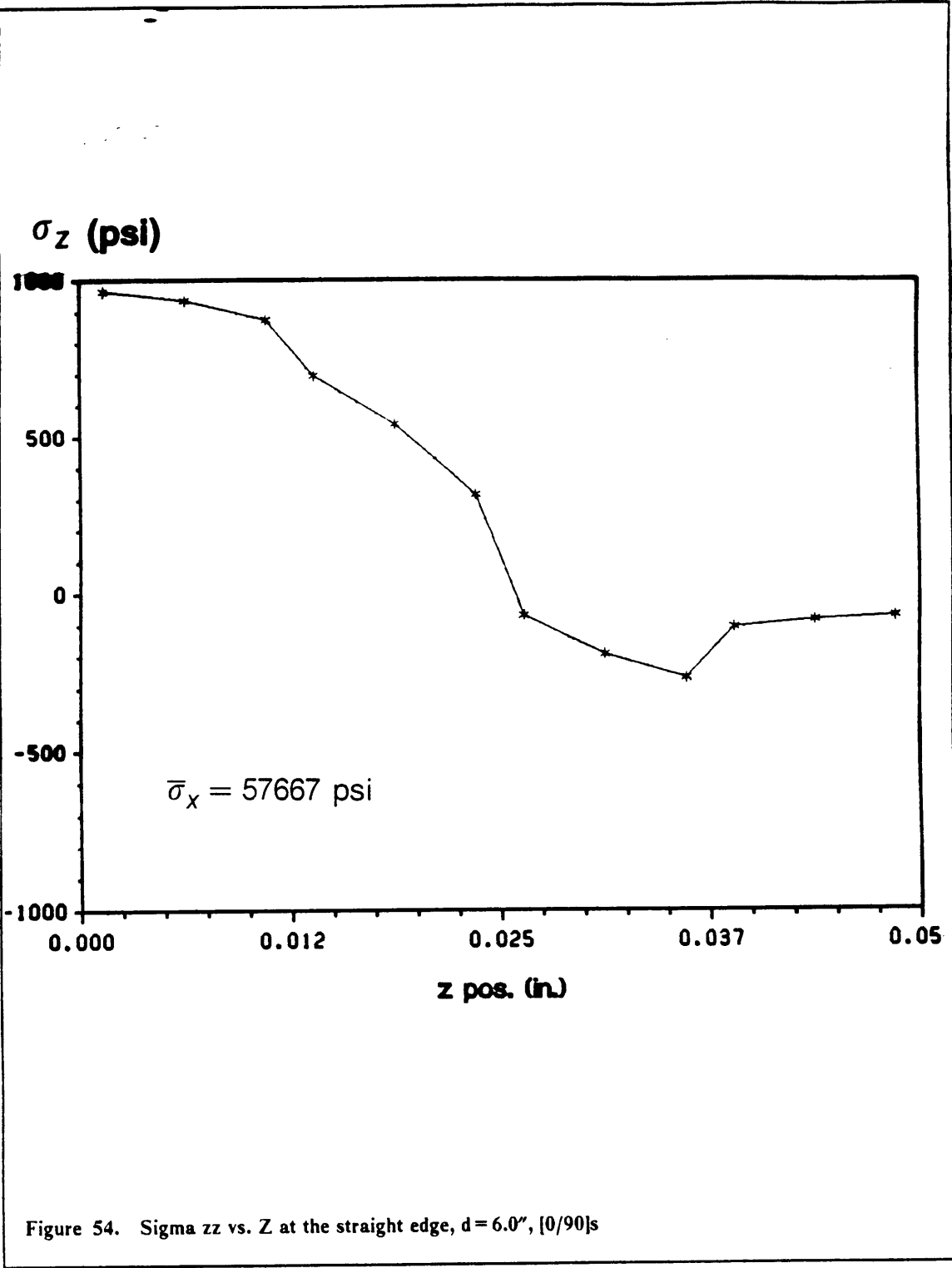


Figure 54. Sigma zz vs. Z at the straight edge, d = 6.0", [0/90]s

proaches 0 psi close to the top surface of the laminate. This is an essential condition for maintaining equilibrium.

5.6. Conclusion

The interlaminar normal stress distribution around the hole was found to be insensitive to a large extent to changes in hole diameter within the constraints of the cases analyzed. The interlaminar normal stress at the straight edge was also fairly insensitive to the presence of a hole in the plate. This conclusion is supported by previous work performed by Griffin et al.³⁸. No indication was found to support the possibility of the stresses at the edge and hole influencing each other. The maximum interlaminar normal stress at the edge was found to occur at the midplane and not at the interface. Also, the equilibrium condition of $\sigma_z = 0.0$ psi at the top surface seemed to be satisfied.

When modeling the edge of the hole, the innermost ring of elements had a very distorted and extreme geometry. These elements had a thickness of 0.0125" a width of 0.025" and a maximum length of approximately 1.6" for the case of 24 elements around the hole. The elements have a rather large curvature which causes to the interpolating functions difficulties in accommodating the inherent displacements. To solve the problem it was necessary to increase the parameter NSPOKES in the CSM1 processor.

Chapter 6: Conclusion to the study

The purpose of this study was to obtain some first hand experience at applying the Global-Local technique to laminated plates. The accuracy of the results was not considered a critical issue since the results could be improved drastically by considering finer meshes, but this would have resulted in a much more expensive investigation, with questionable cost-effectiveness of the results.

The application of the Global-Local technique proved to be very successful once basic rules are followed. These are:

1. The Global analysis needs to be acceptably accurate although there is no need for a very fine mesh since the boundary conditions which will be applied at the interface will be taken from regions with relatively uniform stress fields.
2. The location of the interface is not extremely critical as long as some a priori knowledge of the stress distribution in the area of interest exists.
3. The Local model can be made as large as the accuracy of the results demand. However with proper mesh design the size of the model can be kept to a minimum. It is in the best interest of the user to specify as many boundary conditions as possible in order to prevent the the finite element code from

having to recalculate those quantities. This is most important especially when performing three-dimensional analyses.

Global-Local analyses, if performed correctly, can drastically improve the efficiency of structural computer analysis as well as providing sizeable savings by preventing expensive analyses from being performed on non-critical regions.

The specific model analyzed in this study provided significant results without the need to perform a full three-dimensional analysis over the entire plate. It should be noted that use of the Global-Local methodology made the analysis of a thin laminated plate possible. The three-dimensional finite element analysis of laminated plates had always been restricted to thick laminates because the limitations in resources always forced the analysts to solve the unrealistic problem of a thick laminated plate. However, by the use of the Global-Local method it was possible to tailor the problem size in relation to the accuracy required, and more specifically to model thin laminated plates.

During the investigation it was found that the S81 and E43 elements from the CSM Testbed performed very poorly. Experimental elements were used to substitute these elements during the analysis.

References

- [1] - J. M. Whitney, **Structural Analysis of Laminated Anisotropic Plates**, Technomic Publishing Co., 1987, pp. 17-26.
- [2] - R. B. Pipes and N. J. Pagano, "Interlaminar Stresses in Composite Laminates - An Approximate Elasticity Solution," **J. Applied Mechanics**, Vol. 41, 1974, pp. 668-672.
- [3] - A. S. D. Wang and F. W. Crossman, "Some New Results on Edge Effects in Symmetric Composite Laminates," **J. Composite Materials**, Vol.11, 1977, pp.92-106.
- [4] - R. B. Pipes and N. J. Pagano, "Interlaminar Stresses in Composite Laminates Under Uniform Axial Extension," **J. Composite Materials**, Vol. 4, 1970, pp. 538-548.
- [5] - S. Tang, "A variational approach to edge stresses of circular cutouts in composites," 20th AIAA/ASME/ASCE/AHS, SDM Conference, St. Louis, Missouri, April 4-6, 1979.
- [6] - C. G. Lotts, W. H. Greene, S. L. McCleary, N. F. Knight, S. S. Paulson, and R. E. Gillian, "Introduction to the Computational Structural Mechanics Testbed," NASA-TM 89096, September 1987.
- [7] - S. W. Burns, C. T. Herakovich and J. G. Williams, "Compressive Failure of Notched Angle-Ply Composite Laminates: Three-Dimensional Finite Element Analysis and Experiment," CCMS-85-11, VPI-85-22, Virginia Polytechnic Institute and State University
- [8] - W. D. Whetstone, "SPAR Structural Analysis System Reference Manual- Volume 2: Theory," NASA CR 158970-1, December 1978.
- [9] - C. A. Felippa, "A Command Language for Applied Mechanics Processors: Volume I - The Language," IMSC-D878511, Lockheed Palo Alto Research Laboratory, May 1985.
- [10] - C. E. Jones, R. A. Moore, C. L. Yen and W. D. Whetstone, "SPAR Structural Analysis System, Reference Manual," Volume 1, NASA CR 158970-1, December 1978.
- [11] - K. J. Bathe and E. L. Wilson, **Numerical Methods in Finite Element Analysis**, Prentice-Hall Inc., New Jersey, 1976, pp. 132-133

- [12] - W. D. Whetstone and R. A. Moore, "SPAR Experimental Element Capability," EISI/TR4007.5, Engineering Information Systems Inc., San Jose, California, CA 95130, March 1979.
- [13] - O. C. Zienkiewicz, **The Finite Element Method in Engineering Science**, 2nd Ed., McGraw-Hill Book Company, 1971, pp.169-170.
- [14] - N. F. Knight, W. H. Greene Jr. and W. J. Stroud, "Nonlinear Response of a Blade-Stiffened Graphite-Epoxy Panel with a Discontinuous Stiffener: Work in Progress," NASA Workshop on Structural Analysis Methods, NASA Langley Research Center, June 19-21, 1985.
- [15] - J. N. Reddy, "On Computational Schemes for Global-Local Stress Analysis," NASA Workshop on Structural Analysis Methods, NASA Langley Research Center, June 19-21, 1985.
- [16] - S. B. Dong, "Global Functions in Global-Local Finite Element Analysis of Localized Stresses in Prismatic Structures," NASA Workshop on Structural Analysis Methods, NASA Langley Research Center, June 19-21, 1985.
- [17] - S. B. Dong, "Global-Local Finite Element Methods," **State-of-the-Art surveys on Finite Element Technology**, Edited by A. K. Noor, W. D. Pilkey, ASME 1983.
- [18] - R. B. Nelson, "A Review of Some Problems in Global-Local Stress Analysis," NASA Workshop on Structural Analysis Methods, NASA Langley Research Center, June 19-21, 1985.
- [19] - A. K. Noor, "Global-Local Methodologies and Their Application to Nonlinear and Postbuckling Analyses," NASA Workshop on Structural Analysis Methods, NASA Langley Research Center, June 19-21, 1985.
- [20] - J. B. Ransom, **Summary of 2-D Global/Local Stress Analysis**, Personal Notes, 1987.
- [21] - J. M. Whitney and R. J. Nuismer "Stress Fracture Criteria for Laminated Composites Containing Stress Concentrations," **J. Composite Materials**, Vol.8, July 1974, pp.253.
- [22] - C. T. Herakovich, **Free edge effects in laminated composites**, Personal Notes, 1987.
- [23] - N. J. Salamon, "An Assessment of the Interlaminar Stress Problem in Laminated Composites," **J. Composite Materials**, Vol. 14, 1980, pp. 177-194.
- [24] - G. D. Renieri and C. T. Herakovich, "Nonlinear Analysis of Laminated Fibrous Composites," VPI-E-76-10, Virginia Polytechnic Institute and State University, 1976.
- [25] - N. J. Pagano, "Stress Fields in Composite Laminates," **Inter. J. Solids and Structures**, Vol. 14, 1978, pp. 385-400.
- [26] - E. F. Rybicki, "Approximate Three-Dimensional Solutions for Symmetric Laminates Under Inplane Loading," **J. Composite Materials**, Vol. 5, 1971, pp. 354-360.
- [27] - E. L. Stanton, L. M. Crain and T. F. Neu, "A parametric Cubic Modelling System for General Solids of Composite Materials," **Inter. J. Numerical Methods in Engineering**, Vol. 11, 1977, pp. 653-670.
- [28] - C. T. Herakovich, A. Nagarkar and D. A. O'Brien, "Failure Analysis of Composite Laminates with Free Edges," **Modern Developments in Composite Materials and Structures**, J. R. Vinson Ed., ASME, N.Y., 1979, pp. 53-66.

- [29] - O. H. Griffin Jr., M. P. Kamat and C. T. Herakovich, "Three Dimensional Inelastic Finite Element Analysis of Laminated composites," VPI-E-80-28, Virginia Polytechnic Institute and State University, Blacksburg, Virginia, November 1980.
- [30] - R. M. Barker, J. R. Dana and C. W. Pryor, "Stress concentrations near holes in laminates," **J. of the Engineering Mechanics Division, ASCE**, Vol. 100, June 1974, pp. 477-488.
- [31] - E. F. Rybicki and D. W. Schmueser, "Effect of stacking sequence and layup angle on free edge stresses around a hole in a laminated plate under tension," **J. Composite Materials**, Vol.12, July 1978, PP. 300-313.
- [32] - J. Dana, "Three dimensional finite element analysis of thick laminated composites - including interlaminar and boundary effects near circular holes," VPI-E-18-74, Virginia Polytechnic Institute and State University, Blacksburg, Virginia, 1974.
- [33] - E. F. Rybicki and D. W. Schmueser, "Three dimensional finite element stress analysis of laminated plates containing a circular hole," AFML-TR-76-92, 1976.
- [34] - O. H. Griffin, Jr and M. A. Vidussoni "Global/Local Analysis of Composite Materials," Computer Aided Design in Composite Materials Technology, Proceedings of the International Symposium, Southampton, UK, April 3-15, 1988, C.A. Brebbia, W.P. de Wilde, W.R. Blain Editors, Springer-Verlag, 1988, pp. 513-524.
- [35] - S. Tang, "Interlaminar stresses around circular cutouts in composite plates under tension," **AIAA J.**, Vol.15, No.11, 1977, pp. 1631-1637.
- [36] - O. H. Griffin Jr "Mechanics of Composite Materials", Class Notes, ESM4040, Fall Quarter 1986.
- [37] - G. M. Stanley and C. A. Felippa, "Preliminary Development of a Testbed for Computational Structural Mechanics, Part 1: The NICE/SPAR Prototype", LMSC-D067201, Lockheed, June 1986.
- [38] - F. T. Lin, "The Finite Element Analysis of Laminated Composites," Ph.D. Dissertation, Virginia Polytechnic Institute and State University, Blacksburg, December 1972.
- [39] - H. J. Konish and J. M. Whitney, "Approximate stresses in an orthotropic plate containing a circular hole," **J. Composite Materials**, Vol. 9, April 1975, pp. 157-166.

Appendix A. FORTRAN Listing for Element Routines

```

C=DECK KEXPE
C= PURPOSE   NICE/SPAR Experimental-Element processor for
C= PURPOSE   16,20, 24 and 32 node VPI-3d elemnts
C= AUTHOR    M. A. Vidussoni
C= VERSION   sept 1987
C= BLOCK USAGE
C
C   CALL KEXPE ( MAJOR, MINOR, NEN, NDOF, P, X, TEG, IM, K, R, C, D
C
C   I N P U T
C
C   MAJOR      First part of element type code (NEN = 4,9,16)
C   MINOR     Second part of element type code (OPT = 1--9)
C   NEN       Number of element nodes (4,9,16)
C   NDOF      Number of degrees-of-freedom per node (6)
C   P(15)     Element material properties and integration lev
C   X(3,NEN)  Element nodal coordinates (in "E" basis)
C   TEG(3,3)  Transformation from global to element basis
C   IM        Material reference frame index:
C             0 => x_matl is parallel to x_l (lamina basis)
C             1 => x_matl is parallel to x_g
C             2 => x_matl is parallel to y_g
C             3 => x_matl is parallel to z_g
C
C   O U T P U T
C
C   K(NDOF,NDOF,NSM) Element material stiffness matrix ("E" basis
C                   ( NSM = NEN * (NEN + 1) / 2 )
C   R(NS,NEE)     Mechan. stress recovery matrix
C   C(NEE,NQ)     Thermal force influence matrix (not implem.)
C   D(NS,NQ)      Thermal stress recovery matrix (not implem.)

```

```

C
C= END USAGE
C= BLOCK FORTRAN
C$FORTRAN
C
C
SUBROUTINE KEXPE (MAJOR,MINOR,NND,NDF,P,X,teg,SREF,AK,R,A1,A2)
IMPLICIT DOUBLE PRECISION(A-H,O-Z)
INTEGER MAJOR,MINOR,NND,ND,NDF,SREF
DOUBLE PRECISION COORD(6),WEIGHT(6),C(3,32,80),D(6,6)
DOUBLE PRECISION ELXYZ(32,3)
COMMON/GPN1/H(48),WXSI(6),WETA(6),WRHO(6),XSI(6),ETA(6),RHIO(6)
COMMON/GPN2/EN(48,32),INTXSI,INTETA,INTRHO
COMMON/IDAT/NNOD,NDOF,NGAUSS
real R(162,60),A1(96,1),A2(6,1)
double precision AK(3,3,528)
REAL P(15),X(3,*),TEG(3,3),teta,dteta,dphi
INTEG1 = IFIX(P(14))
INTEG2 = IFIX(P(15))
INTXSI = INTEG1
INTETA = INTEG1
INTRHO = INTEG2
IF (NDF.NE.3) STOP 1
IF (MINOR.NE.NND) STOP 2
IF (MINOR.EQ.16) NNOD = 16
IF (MINOR.EQ.20) NNOD = 20
IF (MINOR.EQ.24) NNOD = 24
IF (MINOR.EQ.32) NNOD = 32
NDOF = 3*NNOD
NGAUSS = INTEG1*INTEG1*INTEG2
XX = X(1,7)/2.0
YY = X(2,7)/2.0
ZZ = X(3,7)/2.0
DO 50 I = 1,MINOR
  ELXYZ(I,1) = dble(X(1,i))
  ELXYZ(I,2) = dble(X(2,i))
  ELXYZ(I,3) = dble(X(3,i))
50 CONTINUE
pi = 3.141592654
teta = acos(teg(1,1))
if((teg(1,1).ge.0.0).and.(teg(1,2).ge.0.0)) flag = 1.0
if((teg(1,1).lt.0.0).and.(teg(1,2).ge.0.0)) flag = 1.0
if((teg(1,1).ge.0.0).and.(teg(1,2).lt.0.0)) flag = -1.0
if((teg(1,1).lt.0.0).and.(teg(1,2).lt.0.0)) flag = -1.0
teta = teta*flag
dteta = teta*180/pi
c   this is the geometric value of phi different from p(11) fiber
c   value of phi
phi = sngl(p(12))
dphi = sngl(p(12))*180/pi
write(6,198) dteta,dphi
198 format(t10,f10.4)
c
CALL GCOORD(COORD,WEIGHT,1,INTEG1)
DO 11 I = 1,INTEG1
  XSI(I) = COORD(I)

```

```

      ETA(I) = COORD(I)
      WXS(I) = WEIGHT(I)
      WETA(I) = WEIGHT(I)
11  CONTINUE
      CALL GCOORD(COORD,WEIGHT,1,INTEG2)
      DO 12 I= 1,INTEG2
         RHO(I) = COORD(I)
         WRHO(I) = WEIGHT(I)
12  CONTINUE
C
      IF(NNOD.EQ.16) CALL GPN16
      IF(NNOD.EQ.20) CALL GPN20
      IF(NNOD.EQ.24) CALL GPN24
      IF(NNOD.EQ.32) CALL GPN32
C
      IF(NNOD.EQ.16) CALL DN16 (C)
      IF(NNOD.EQ.20) CALL DN20 (C)
      IF(NNOD.EQ.24) CALL DN24 (C)
      IF(NNOD.EQ.32) CALL DN32 (C)
C
      CALL DMAT (P,D,teta)
      CALL ELKAY (D,ELXYZ,ak,C,R,teta,phi)
      RETURN
      END
C
C      CALCULATES WEIGHTS AND GAUSS POINT COORDINATES
C      IN XSI - ETA - RHO SPACE CORRESPONDING TO THE CHOSEN
C      ORDER OF INTEGRATION
C
SUBROUTINE GCOORD(COORD,WEIGHT,NCALL,INTEG)
IMPLICIT DOUBLE PRECISION(A-H,O-Z)
DOUBLE PRECISION COORD(6),WEIGHT(6)
IF(INTEG.EQ.2) GO TO 20
IF(INTEG.EQ.3) GO TO 30
IF(INTEG.EQ.4) GO TO 40
IF(INTEG.EQ.5) GO TO 50
IF(INTEG.EQ.6) GO TO 60
C
      COORD(1) = 0.0
      WEIGHT(1) = 2.0
      GO TO 10
20  CONTINUE
C
      IF(NCALL.EQ.2) GO TO 35
      COORD(1) = -.577350269189626
      COORD(2) = .577350269189626
      WEIGHT(1) = 1.0
      WEIGHT(2) = 1.0
      GO TO 10
35  CONTINUE
C
      COORD(1) = -.577350269189626
      COORD(2) = .577350269189626
      GO TO 10
30  CONTINUE
C

```

```

IF(NCALL.EQ.2) GO TO 70
  COORD(1) = -.774596669241483
  COORD(2) = 0.0
  COORD(3) = .774596669241483
  WEIGHT(1) = .555555555555556
  WEIGHT(2) = .888888888888889
  WEIGHT(3) = .555555555555556
  GO TO 10
70  CONTINUE
C
  COORD(1) = -.577350269189626
  COORD(2) = 0.
  COORD(3) = .577350269189626
  GO TO 10
40  CONTINUE
C
IF(NCALL.EQ.2) GO TO 90
  COORD(1) = -.861136311594053
  COORD(2) = -.339981043584856
  COORD(3) = .339981043584856
  COORD(4) = .861136311594053
  WEIGHT(1) = .347854845137454
  WEIGHT(2) = .652145154862546
  WEIGHT(3) = .652145154862546
  WEIGHT(4) = .347854845137454
  GO TO 10
90  CONTINUE
  COORD(1) = -1.0
  COORD(2) = -.333333333333333
  COORD(3) = .333333333333333
  COORD(4) = 1.0
  GO TO 10
50  CONTINUE
C
IF(NCALL.EQ.2) GO TO 55
  COORD(1) = -0.906179845938664
  COORD(2) = -0.538569310105683
  COORD(3) = 0.000000000000000
  COORD(4) = 0.538569310105683
  COORD(5) = 0.906179845938664
  WEIGHT(1) = 0.236926885056189
  WEIGHT(2) = 0.478628670499366
  WEIGHT(3) = 0.568888888888889
  WEIGHT(4) = 0.478628670499366
  WEIGHT(5) = 0.236926885056189
  GO TO 10
55  CONTINUE
C
  COORD(1) = -1.00
  COORD(2) = -0.50
  COORD(3) = 0.00
  COORD(4) = 0.50
  COORD(5) = 1.00
  GO TO 10
60  CONTINUE
C

```

```

IF(NCALL.EQ.2) GO TO 65
COORD(1) = -0.932469514203152
COORD(2) = -0.661209386466265
COORD(3) = -0.238619186083197
COORD(4) = 0.238619186083197
COORD(5) = 0.661209386466265
COORD(6) = 0.932469514203152
WEIGHT(1) = 0.171324492379170
WEIGHT(2) = 0.360761573048139
WEIGHT(3) = 0.467913934572691
WEIGHT(4) = 0.467913934572691
WEIGHT(5) = 0.360761573048139
WEIGHT(6) = 0.171324492379170
GO TO 10
65 CONTINUE
C
COORD(1) = -1.00
COORD(2) = -0.60
COORD(3) = -0.20
COORD(4) = 0.20
COORD(5) = 0.60
COORD(6) = 1.00
10 CONTINUE
RETURN
END
C
C
C
C
***** 16 NODE ELEMENT ****
SUBROUTINE GPN16
IMPLICIT DOUBLE PRECISION(A-H,O-Z)
COMMON/GPN1/H(48),WXS(6),WETA(6),WRHO(6),XSI(6),ETA(6),RHO(6)
COMMON/GPN2/EN(48,32),INTXSI,INTETA,INTRHO
FOR = .2500
ATE = .1250
DO 10 I = 1,INTRHO
DO 10 J = 1,INTXSI
DO 10 K = 1,INTETA
N = INTXSI*INTETA*(I-1) + INTETA*(J-1) + K
H(N) = WRHO(I)*WXS(J)*WETA(K)
RH = RH(I)
XS = XSI(J)
ET = ETA(K)
XS2 = XS*XS
ET2 = ET*ET
EN(N,1) = ATE*( RH -1)*( ET -1)*( XS -1)*( ET + XS + 1)
EN(N,12) = FOR*( RH -1)*( XS -1)*(1- ET2)
EN(N,4) = ATE*( RH -1)*( ET + 1)*( XS -1)*( ET - XS -1)
EN(N,11) = -FOR*( RH -1)*( ET + 1)*(1- XS2)
EN(N,3) = ATE*( RH -1)*( ET + 1)*( XS + 1)*( -ET - XS + 1)
EN(N,10) = -FOR*( RH -1)*( XS + 1)*(1- ET2)
EN(N,2) = ATE*( RH -1)*( ET -1)*( XS + 1)*( -ET + XS -1)
EN(N,9) = FOR*( RH -1)*( ET -1)*(1- XS2)
EN(N,5) = ATE*( RH + 1)*( ET -1)*( XS -1)*( -ET - XS -1)
EN(N,16) = -FOR*( RH + 1)*( XS -1)*(1- ET2)
EN(N,8) = ATE*( RH + 1)*( ET + 1)*( XS -1)*( -ET + XS + 1)

```

```

EN(N,15) = FOR*( RH + 1)*( ET + 1)*(1- XS2)
EN(N,7) = ATE*( RH + 1)*( XS + 1)*( ET + 1)*( ET + XS -1)
EN(N,14) = FOR*( RH + 1)*( XS + 1)*(1- ET2)
EN(N,6) = ATE*( RH + 1)*( ET -1)*( XS + 1)*( ET - XS + 1)
EN(N,13) = -FOR*( RH + 1)*( ET -1)*(1- XS2)
10 CONTINUE
RETURN
END

C
C
C          ***** 16 NODE ELEMENT *****
C
SUBROUTINE DN16 (C)
IMPLICIT DOUBLE PRECISION(A-H,O-Z)
COMMON/GPN1/H(48),WXSI(6),WETA(6),WRHO(6),XSI(6),ETA(6),RHO(6)
COMMON/GPN2/EN(48,32),INTXSI,INTETA,INTRHO
C
C DOUBLE PRECISION C(3,32,80)
C
TWO = .5000
FOR = .2500
ATE = .1250
DO 10 I = 1,INTRHO
DO 10 J = 1,INTXSI
DO 10 K = 1,INTETA
N = INTXSI*INTETA*(I-1) + INTETA*(J-1) + K
H(N) = WRHO(I)*WXSI(J)*WETA(K)
RH = RHIO(I)
XS = XSI(J)
ET = ETA(K)
XS2 = XS*XS
ET2 = ET*ET
C
C          *****
C          DERIVATIVES WITH RESPECT TO XSI:
C
C(1,1,N) = ATE*( RH -1)*( ET-1)*( ET + 2*XS )
C(1,12,N) = FOR*( RH -1)*(1- ET2)
C(1,4,N) = ATE*( RH -1)*( ET + 1)*( ET-2*XS )
C(1,11,N) = TWO*( RH -1)*( ET + 1)* XS
C(1,3,N) = ATE*( RH -1)*( ET + 1)*(-ET -2*XS )
C(1,10,N) = -FOR*( RH -1)*(1-ET2)
C(1,2,N) = ATE*( RH -1)*( ET-1)*(-ET + 2*XS )
C(1,9,N) = -TWO*( RH -1)*( ET-1)* XS
C(1,5,N) = ATE*( RH + 1)*( ET-1)*(-ET -2*XS )
C(1,16,N) = -FOR*( RH + 1)*(1- ET2)
C(1,8,N) = ATE*( RH + 1)*( ET + 1)*(-ET + 2*XS )
C(1,15,N) = -TWO*( RH + 1)*( ET + 1)* XS
C(1,7,N) = ATE*( RH + 1)*( ET + 1)*( ET + 2*XS )
C(1,14,N) = FOR*( RH + 1)*(1-ET2)
C(1,6,N) = ATE*( RH + 1)*( ET-1)*( ET-2*XS )
C(1,13,N) = TWO*( RH + 1)*( ET-1)* XS
C
C          *****
C          DERIVATIVES WITH RESPECT TO ETA:
C
C(2,1,N) = ATE*( RH -1)*( XS -1)*( XS + 2*ET )
C(2,12,N) = -TWO*( RH -1)*( XS -1)* ET
C(2,4,N) = ATE*( RH -1)*( XS -1)*(-XS + 2*ET )

```

```

C(2,11,N) = -FOR*( RH -1)*(1- XS2)
C(2,3 ,N) = ATE*( RH -1)*( XS +1)*(-XS -2*ET )
C(2,10,N) = TWO*( RH -1)*( XS +1)* ET
C(2,2 ,N) = ATE*( RH -1)*( XS +1)*( XS -2*ET )
C(2,9 ,N) = FOR*( RH -1)*(1- XS2)
C(2,5 ,N) = ATE*( RH +1)*( XS -1)*(-XS -2*ET )
C(2,16,N) = TWO*( RH +1)*( XS -1)* ET
C(2,8 ,N) = ATE*( RH +1)*( XS -1)*(XS -2*ET )
C(2,15,N) = FOR*( RH +1)*(1- XS2)
C(2,7 ,N) = ATE*( RH +1)*( XS +1)*(XS +2*ET )
C(2,14,N) = -TWO*( RH +1)*( XS +1)* ET
C(2,6 ,N) = ATE*( RH +1)*( XS +1)*(-XS +2*ET )
C(2,13,N) = -FOR*( RH +1)*(1- XS2)

```

C
C
C

DERIVATIVES WITH RESPECT TO RHO:

```

C(3,1 ,N) = ATE*( ET-1)*( XS -1)*( ET+ XS + 1 )
C(3,12,N) = FOR*( XS -1)*(1- ET2)
C(3,4 ,N) = ATE*( ET +1)*( XS -1)*( ET- XS - 1 )
C(3,11,N) = -FOR*( ET +1)*(1- XS2)
C(3,3 ,N) = ATE*( ET +1)*( XS +1)*(- ET- XS + 1 )
C(3,10,N) = -FOR*( XS +1)*(1- ET2)
C(3,2 ,N) = ATE*( ET-1)*( XS +1)*(- ET+ XS - 1 )
C(3,9 ,N) = FOR*( ET-1)*(1- XS2)
C(3,5 ,N) = ATE*( ET-1)*( XS -1)*(- ET- XS - 1 )
C(3,16,N) = -FOR*( XS -1)*(1- ET2)
C(3,8 ,N) = ATE*( ET +1)*( XS -1)*(- ET+ XS + 1 )
C(3,15,N) = FOR*( ET +1)*(1- XS2)
C(3,7 ,N) = ATE*( ET +1)*( XS +1)*( ET+ XS - 1 )
C(3,14,N) = FOR*( XS +1)*(1- ET2)
C(3,6 ,N) = ATE*( ET-1)*( XS +1)*( ET- XS + 1 )
C(3,13,N) = -FOR*( ET-1)*(1- XS2)

```

10 CONTINUE
RETURN
END

C
C
C

***** 20 NODE ELEMENT ****

```

SUBROUTINE GPN20
IMPLICIT DOUBLE PRECISION(A-H,O-Z)
COMMON/GPN1/H(48),WXSI(6),WETA(6),WRHO(6),XSI(6),FTA(6),RHIO(6)
COMMON/GPN2/FN(48,32),INTXSI,INTETA,INTRHO
FOR = .2500
ATE = .1250
DO 10 I = 1,INTRHO
DO 10 J = 1,INTXSI
DO 10 K = 1,INTETA
N = INTXSI*INTETA*(I-1) + INTETA*(J-1) + K
H(N) = WRHO(I)*WXSI(J)*WETA(K)
RH = RHIO(I)
XS = XSI(J)
ET = FTA(K)
EN(N,1) = ATE*(1-ET)*(1-XS)*(1-RH)*(-XS-ET-RH-2)
EN(N,2) = ATE*(1-ET)*(1+XS)*(1-RH)*( XS-ET-RH-2)
EN(N,3) = ATE*(1+ET)*(1+XS)*(1-RH)*( XS+ET-RH-2)
EN(N,4) = ATE*(1+ET)*(1-XS)*(1-RH)*(-XS+ET-RH-2)

```

```

EN(N,5) = ATE*(1-ET)*(1-XS)*(1+RH)*(-XS-ET+RH-2)
EN(N,6) = ATE*(1-ET)*(1+XS)*(1+RH)*( XS-ET+RH-2)
EN(N,7) = ATE*(1+ET)*(1+XS)*(1+RH)*( XS+ET+RH-2)
EN(N,8) = ATE*(1+ET)*(1-XS)*(1+RH)*(-XS+ET+RH-2)
EN(N,9) = FOR*(1-RH*RH)*(1-XS)*(1-ET)
EN(N,10) = FOR*(1-RH*RH)*(1+XS)*(1-ET)
EN(N,11) = FOR*(1-RH*RH)*(1+XS)*(1+ET)
EN(N,12) = FOR*(1-RH*RH)*(1-XS)*(1+ET)
EN(N,13) = FOR*(1-XS*XS)*(1-ET)*(1-RH)
EN(N,14) = FOR*(1-ET*ET)*(1+XS)*(1-RH)
EN(N,15) = FOR*(1-XS*XS)*(1+ET)*(1-RH)
EN(N,16) = FOR*(1-ET*ET)*(1-XS)*(1-RH)
EN(N,17) = FOR*(1-XS*XS)*(1-ET)*(1+RH)
EN(N,18) = FOR*(1-ET*ET)*(1+XS)*(1+RH)
EN(N,19) = FOR*(1-XS*XS)*(1+ET)*(1+RH)
EN(N,20) = FOR*(1-ET*ET)*(1-XS)*(1+RH)
10 CONTINUE
RETURN
END

C
C          ***** 20 NODE ELEMENT *****
C          TO CALCULATE THE C MATRIX
C
SUBROUTINE DN20 (C)
IMPLICIT DOUBLE PRECISION(A-H,O-Z)
COMMON/GPN1/H(48),WXSI(6),WETA(6),WRHO(6),XSI(6),ETA(6),RHIO(6)
COMMON/GPN2/EN(48,32),INTXSI,INTETA,INTRHO
C
DOUBLE PRECISION C(3,32,80)
C
C
FOR = .2500
ATE = .1250
DO 10 I = 1,INTRHO
DO 10 J = 1,INTXSI
DO 10 K = 1,INTETA
N = INTXSI*INTETA*(I-1) + INTETA*(J-1) + K
H(N) = WRHO(I)*WXSI(J)*WETA(K)
RH = RHIO(I)
XS = XSI(J)
ET = ETA(K)
C
C          *****
C          DERIVATIVES WITH RESPECT TO XSI:
C
C(1,1,N) = ATE*(ET + XS + RH + 2)*(ET-1)*(RH-1)
#      + ATE*(ET-1)*(XS-1)*(RH-1)
C(1,2,N) = -ATE*(ET-XS + RH + 2)*(ET-1)*(RH-1)
#      + ATE*(ET-1)*(XS + 1)*(RH-1)
C(1,3,N) = -ATE*(ET + XS-RH-2)*(ET + 1)*(RH-1)
#      - ATE*(ET + 1)*(XS + 1)*(RH-1)
C(1,4,N) = ATE*(ET-XS-RH-2)*(ET + 1)*(RH-1)
#      - ATE*(ET + 1)*(XS-1)*(RH-1)
C(1,5,N) = -ATE*(ET + XS-RH + 2)*(ET-1)*(RH + 1)
#      - ATE*(ET-1)*(XS-1)*(RH + 1)
C(1,6,N) = ATE*(ET-XS-RH + 2)*(ET-1)*(RH + 1)
#      - ATE*(ET-1)*(XS + 1)*(RH + 1)

```

```

C(1,7,N) = ATE*(ET + XS + RH-2)*(ET + 1)*(RH + 1)
#       + ATE*(ET + 1)*(XS + 1)*(RH + 1)
C(1,8,N) = -ATE*(ET-XS + RH-2)*(ET + 1)*(RH + 1)
#       + ATE*(ET + 1)*(XS-1)*(RH + 1)
C(1,9,N) = -FOR*(ET-1)*(RH**2-1)
C(1,10,N) = FOR*(ET-1)*(RH**2-1)
C(1,11,N) = -FOR*(ET + 1)*(RH**2-1)
C(1,12,N) = FOR*(ET + 1)*(RH**2-1)
C(1,13,N) = -XS*FOR*(ET-1)*(RH-1)*2
C(1,14,N) = FOR*(ET**2-1)*(RH-1)
C(1,15,N) = XS*FOR*(ET + 1)*(RH-1)*2
C(1,16,N) = -FOR*(ET**2-1)*(RH-1)
C(1,17,N) = XS*FOR*(ET-1)*(RH + 1)*2
C(1,18,N) = -FOR*(ET**2-1)*(RH + 1)
C(1,19,N) = -XS*FOR*(ET + 1)*(RH + 1)*2
C(1,20,N) = FOR*(ET**2-1)*(RH + 1)

```

C
C
C

DERIVATIVES WITH RESPECT TO ETA:

```

C(2,1,N) = ATE*(ET + XS + RH + 2)*(XS-1)*(RH-1)
#       + ATE*(ET-1)*(XS-1)*(RH-1)
C(2,2,N) = -ATE*(ET-XS + RH + 2)*(XS + 1)*(RH-1)
#       -ATE*(ET-1)*(XS + 1)*(RH-1)
C(2,3,N) = -ATE*(ET + XS-RH-2)*(XS + 1)*(RH-1)
#       -ATE*(ET + 1)*(XS + 1)*(RH-1)
C(2,4,N) = ATE*(ET-XS-RH-2)*(XS-1)*(RH-1)
#       + ATE*(ET + 1)*(XS-1)*(RH-1)
C(2,5,N) = -ATE*(ET + XS-RH + 2)*(XS-1)*(RH + 1)
#       -ATE*(ET-1)*(XS-1)*(RH + 1)
C(2,6,N) = ATE*(ET-XS-RH + 2)*(XS + 1)*(RH + 1)
#       + ATE*(ET-1)*(XS + 1)*(RH + 1)
C(2,7,N) = ATE*(ET + XS + RH-2)*(XS + 1)*(RH + 1)
#       + ATE*(ET + 1)*(XS + 1)*(RH + 1)
C(2,8,N) = -ATE*(ET-XS + RH-2)*(XS-1)*(RH + 1)
#       -ATE*(ET + 1)*(XS-1)*(RH + 1)
C(2,9,N) = -FOR*(XS-1)*(RH**2-1)
C(2,10,N) = FOR*(XS + 1)*(RH**2-1)
C(2,11,N) = -FOR*(XS + 1)*(RH**2-1)
C(2,12,N) = FOR*(XS-1)*(RH**2-1)
C(2,13,N) = -FOR*(XS**2-1)*(RH-1)
C(2,14,N) = ET*FOR*(XS + 1)*(RH-1)*2
C(2,15,N) = FOR*(XS**2-1)*(RH-1)
C(2,16,N) = -ET*FOR*(XS-1)*(RH-1)*2
C(2,17,N) = FOR*(XS**2-1)*(RH + 1)
C(2,18,N) = -ET*FOR*(XS + 1)*(RH + 1)*2
C(2,19,N) = -FOR*(XS**2-1)*(RH + 1)
C(2,20,N) = ET*FOR*(XS-1)*(RH + 1)*2

```

C
C
C

DERIVATIVES WITH RESPECT TO RHO

```

C(3,1,N) = ATE*(ET + XS + RH + 2)*(ET-1)*(XS-1)
#       + ATE*(ET-1)*(XS-1)*(RH-1)
C(3,2,N) = -ATE*(ET-XS + RH + 2)*(ET-1)*(XS + 1)
#       -ATE*(ET-1)*(XS + 1)*(RH-1)
C(3,3,N) = -ATE*(ET + XS-RH-2)*(ET + 1)*(XS + 1)
#       + ATE*(ET + 1)*(XS + 1)*(RH-1)

```

```

C(3,4,N) = ATE*(ET-XS-RH-2)*(ET + 1)*(XS-1)
# -ATE*(ET + 1)*(XS-1)*(RH-1)
C(3,5,N) = -ATE*(ET + XS-RH + 2)*(ET-1)*(XS-1)
# + ATE*(ET-1)*(XS-1)*(RH + 1)
C(3,6,N) = ATE*(ET-XS-RH + 2)*(ET-1)*(XS + 1)
# -ATE*(ET-1)*(XS + 1)*(RH + 1)
C(3,7,N) = ATE*(ET + XS + RH-2)*(ET + 1)*(XS + 1)
# + ATE*(ET + 1)*(XS + 1)*(RH + 1)
C(3,8,N) = -ATE*(ET-XS + RH-2)*(ET + 1)*(XS-1)
# -ATE*(ET + 1)*(XS-1)*(RH + 1)
C(3,9,N) = -RH*FOR*(ET-1)*(XS-1)*2
C(3,10,N) = RH*FOR*(ET-1)*(XS + 1)*2
C(3,11,N) = -RH*FOR*(ET + 1)*(XS + 1)*2
C(3,12,N) = RH*FOR*(ET + 1)*(XS-1)*2
C(3,13,N) = -FOR*(ET-1)*(XS**2-1)
C(3,14,N) = FOR*(ET**2-1)*(XS + 1)
C(3,15,N) = FOR*(ET + 1)*(XS**2-1)
C(3,16,N) = -FOR*(ET**2-1)*(XS-1)
C(3,17,N) = FOR*(ET-1)*(XS**2-1)
C(3,18,N) = -FOR*(ET**2-1)*(XS + 1)
C(3,19,N) = -FOR*(ET + 1)*(XS**2-1)
C(3,20,N) = FOR*(ET**2-1)*(XS-1)

```

```

C
10 CONTINUE
RETURN
END

```

```

C
C
C

```

***** 24 NODE ELEMENT *****

```

SUBROUTINE GPN24
IMPLICIT DOUBLE PRECISION(A-H,O-Z)
COMMON/GPN1/II(48),WXSI(6),WETA(6),WRHO(6),XSI(6),ETA(6),RHO(6)
COMMON/GPN2/EN(48,32),INTXSI,INTETA,INTRHO
FR1 = 1./64.
FR9 = 9./64.
DO 10 I = 1,INTRHO
DO 10 J = 1,INTXSI
DO 10 K = 1,INTETA
N = INTXSI*INTETA*(I-1) + INTETA*(J-1) + K
H(N) = WRHO(I)*WXSI(J)*WETA(K)
RH = RH0(I)
XS = XSI(J)
ET = ETA(K)
XS2 = XS*XS
ET2 = ET*ET
EN(N,1) = FR1*(1.-XS)*(1.-ET)*(1.-RH)*(9.*(XS2 + ET2)-10)
EN(N,20) = FR9*(1.-XS)*(1.-3.*ET)*(1.-RH)*(1.-ET2)
EN(N,12) = FR9*(1.-XS)*(1. + 3.*ET)*(1.-RH)*(1.-ET2)
EN(N,4) = FR1*(1.-XS)*(1. + ET)*(1.-RH)*(9.*(XS2 + ET2)-10)
EN(N,19) = FR9*(1.-3.*XS)*(1. + ET)*(1.-RH)*(1.-XS2)
EN(N,11) = FR9*(1. + 3.*XS)*(1. + ET)*(1.-RH)*(1.-XS2)
EN(N,3) = FR1*(1. + XS)*(1. + ET)*(1.-RH)*(9.*(XS2 + ET2)-10)
EN(N,18) = FR9*(1. + XS)*(1. + 3.*ET)*(1.-RH)*(1.-ET2)
EN(N,10) = FR9*(1. + XS)*(1.-3.*ET)*(1.-RH)*(1.-ET2)
EN(N,2) = FR1*(1. + XS)*(1.-ET)*(1.-RH)*(9.*(XS2 + ET2)-10)
EN(N,17) = FR9*(1. + 3.*XS)*(1.-ET)*(1.-RH)*(1.-XS2)

```

```

EN(N,9) = FR9*(1.-3.*XS)*(1.-ET)*(1.-RII)*(1.-XS2)
EN(N,5) = FR1*(1.-XS)*(1.-ET)*(1. + RH)*(9.*(XS2 + ET2)-10)
EN(N,24) = FR9*(1.-XS)*(1.-3.*ET)*(1. + RII)*(1.-ET2)
EN(N,16) = FR9*(1.-XS)*(1. + 3.*ET)*(1. + RII)*(1.-ET2)
EN(N,8) = FR1*(1.-XS)*(1. + ET)*(1. + RII)*(9.*(XS2 + ET2)-10)
EN(N,23) = FR9*(1.-3.*XS)*(1. + ET)*(1. + RH)*(1.-XS2)
EN(N,15) = FR9*(1. + 3.*XS)*(1. + ET)*(1. + RH)*(1.-XS2)
EN(N,7) = FR1*(1. + XS)*(1. + ET)*(1. + RH)*(9.*(XS2 + ET2)-10)
EN(N,22) = FR9*(1. + XS)*(1. + 3.*ET)*(1. + RH)*(1.-ET2)
EN(N,14) = FR9*(1. + XS)*(1.-3.*ET)*(1. + RII)*(1.-ET2)
EN(N,6) = FR1*(1. + XS)*(1.-ET)*(1. + RII)*(9.*(XS2 + ET2)-10)
EN(N,21) = FR9*(1. + 3.*XS)*(1.-ET)*(1. + RH)*(1.-XS2)
EN(N,13) = FR9*(1.-3.*XS)*(1.-ET)*(1. + RH)*(1.-XS2)

```

```

10 CONTINUE
RETURN
END

```

```

C
C
C

```

***** 24 NODE ELEMENT *****

```

SUBROUTINE DN24 (C)
IMPLICIT DOUBLE PRECISION(A-H,O-Z)
COMMON/GPN1/I(48),WXSI(6),WETA(6),WRHIO(6),XSI(6),ETA(6),RHIO(6)
COMMON/GPN2/EN(48,32),INTXSI,INTETA,INTRHIO

```

```

C
C

```

```

DOUBLE PRECISION C(3,32,80)

```

```

FR1 = 1./64.
FR9 = 9./64.
DO 10 I = 1,INTRHIO
DO 10 J = 1,INTXSI
DO 10 K = 1,INTETA
N = INTXSI*INTETA*(I-1) + INTETA*(J-1) + K
H(N) = WRHIO(I)*WXSI(J)*WETA(K)
RII = RHIO(I)
XS = XSI(J)
ET = ETA(K)

```

```

C
C
C

```

DERIVATIVES WITH RESPECT TO XI

```

C(1,1,N) = FR1*(1.-ET)*(1.-RII)*(10. + 9.*(2.*XS-3.*XS*XS-ET*ET))
C(1,9,N) = FR9*(1.-ET)*(1.-RII)*(9.*XS*XS-2.*XS-3.)
C(1,17,N) = FR9*(1.-ET)*(1.-RII)*(3.-2.*XS-9.*XS*XS)
C(1,2,N) = FR1*(1.-ET)*(1.-RII)*(9.*(3.*XS*XS + ET*ET + 2.*XS)-10.)
C(1,10,N) = FR9*(1.-3.*ET)*(1.-RII)*(1.- ET* ET)
C(1,18,N) = FR9*(1. + 3.*ET)*(1.-RII)*(1.- ET* ET)
C(1,3,N) = FR1*(1. + ET)*(1.-RII)*(9.*(3.*XS*XS + ET*ET + 2.*XS)-10.)
C(1,11,N) = FR9*(1. + ET)*(1.-RII)*(3.-2.*XS-9.*XS*XS)
C(1,19,N) = FR9*(1. + ET)*(1.-RII)*(9.*XS*XS-2.*XS-3.)
C(1,4,N) = FR1*(1. + ET)*(1.-RII)*(10. + 9.*(2.*XS-3.*XS*XS-ET*ET))
C(1,12,N) = FR9*(1. + 3.*ET)*(1.-RII)*( ET* ET-1.)
C(1,20,N) = FR9*(1.-3.*ET)*(1.-RII)*( ET* ET-1.)
C(1,5,N) = FR1*(1.-ET)*(1. + RH)*(10. + 9.*(2.*XS-3.*XS*XS-ET*ET))
C(1,13,N) = FR9*(1.-ET)*(1. + RH)*(9.*XS*XS-2.*XS-3.)
C(1,21,N) = FR9*(1.-ET)*(1. + RH)*(3.-2.*XS-9.*XS*XS)
C(1,6,N) = FR1*(1.-ET)*(1. + RH)*(9.*(3.*XS*XS + ET* ET + 2.*XS)-10.)
C(1,14,N) = FR9*(1.-3.*ET)*(1. + RH)*(1.- ET* ET)

```

```

C(1,22,N) = FR9*(1.+3.*ET)*(1.+RH)*(1.- ET* ET)
C(1,7 ,N) = FR1*(1.+ET)*(1.+RH)*(9.*(3.*XS*XS+ET*ET+2.*XS)-10.)
C(1,15,N) = FR9*(1.+ ET)*(1.+RH)*(3.-2.*XS-9.*XS*XS)
C(1,23,N) = FR9*(1.+ ET)*(1.+RH)*(9.*XS*XS-2.*XS-3.)
C(1,8 ,N) = FR1*(1.+ET)*(1.+RH)*(10.+9.*(2.*XS-3.*XS*XS-ET*ET))
C(1,16,N) = FR9*(1.+3.*ET)*(1.+RH)*( ET* ET-1.)
C(1,24,N) = FR9*(1.-3.*ET)*(1.+RH)*( ET* ET-1.)

```

C
C
C

DERIVATIVES WITH RESPECT TO ETA

```

C(2,1 ,N) = FR1*(1.-XS)*(1.-RH)*(10.+9.*(2.*ET-XS*XS-3.*ET*ET))
C(2,9 ,N) = FR9*(1.-3.*XS)*(1.-RH)*(XS*XS-1.)
C(2,17,N) = FR9*(1.+3.*XS)*(1.-RH)*(XS*XS-1.)
C(2,2 ,N) = FR1*(1.+XS)*(1.-RH)*(10.+9.*(2.*ET-XS*XS-3.*ET*ET))
C(2,10,N) = FR9*(1.+XS)*(1.-RH)*(9.* ET * ET -2.* ET -3.)
C(2,18,N) = FR9*(1.+XS)*(1.-RH)*(3.-2.* ET -9.* ET * ET )
C(2,3 ,N) = FR1*(1.+XS)*(1.-RH)*(9.*(3.*ET*ET+XS*XS+2.*ET)-10.)
C(2,11,N) = FR9*(1.+3.*XS)*(1.-RH)*(1.-XS*XS)
C(2,19,N) = FR9*(1.-3.*XS)*(1.-RH)*(1.-XS*XS)
C(2,4 ,N) = FR1*(1.-XS)*(1.-RH)*(9.*(3.*ET*ET+XS*XS+2.*ET)-10.)
C(2,12,N) = FR9*(1.-XS)*(1.-RH)*(3.-2.* ET-9.*ET*ET)
C(2,20,N) = FR9*(1.-XS)*(1.-RH)*(9.*ET*ET-2.*ET-3.)
C(2,5 ,N) = FR1*(1.-XS)*(1.+RH)*(10.+9.*(2.*ET-XS*XS-3.*ET*ET))
C(2,13,N) = FR9*(1.-3.*XS)*(1.+RH)*(XS*XS-1.)
C(2,21,N) = FR9*(1.+3.*XS)*(1.+RH)*(XS*XS-1.)
C(2,6 ,N) = FR1*(1.+XS)*(1.+RH)*(10.+9.*(2.*ET-XS*XS-3.*ET*ET))
C(2,14,N) = FR9*(1.+XS)*(1.+RH)*(9.* ET * ET -2.* ET -3.)
C(2,22,N) = FR9*(1.+XS)*(1.+RH)*(3.-2.* ET -9.* ET * ET )
C(2,7 ,N) = FR1*(1.+XS)*(1.+RH)*(9.*(3.*ET*ET+XS*XS+2.*ET)-10.)
C(2,15,N) = FR9*(1.+3.*XS)*(1.+RH)*(1.-XS*XS)
C(2,23,N) = FR9*(1.-3.*XS)*(1.+RH)*(1.-XS*XS)
C(2,8 ,N) = FR1*(1.-XS)*(1.+RH)*(9.*(3.*ET*ET+XS*XS+2.*ET)-10.)
C(2,16,N) = FR9*(1.-XS)*(1.+RH)*(3.-2.* ET -9.* ET * ET )
C(2,24,N) = FR9*(1.-XS)*(1.+RH)*(9.* ET * ET -2.* ET -3.)

```

C
C
C

DERIVATIVES WITH RESPECT TO ZETA

```

C(3,1 ,N) = FR1*(1.-XS)*(1.- ET)*(10.-9.*(XS*XS+ ET * ET ))
C(3,9 ,N) = FR9*(1.-3.*XS)*(1.- ET)*(XS*XS-1.)
C(3,17,N) = FR9*(1.+3.*XS)*(1.- ET)*(XS*XS-1.)
C(3,2 ,N) = FR1*(1.+XS)*(1.- ET)*(10.-9.*(XS*XS+ET*ET))
C(3,10,N) = FR9*(1.+XS)*(1.-3.* ET)*( ET * ET -1.)
C(3,18,N) = FR9*(1.+XS)*(1.+3.* ET)*( ET * ET -1.)
C(3,3 ,N) = FR1*(1.+XS)*(1.+ ET)*(10.-9.*(XS*XS+ET*ET))
C(3,11,N) = FR9*(1.+3.*XS)*(1.+ ET)*(XS*XS-1.)
C(3,19,N) = FR9*(1.-3.*XS)*(1.+ ET)*(XS*XS-1.)
C(3,4 ,N) = FR1*(1.-XS)*(1.+ ET)*(10.-9.*(XS*XS+ET*ET))
C(3,12,N) = FR9*(1.-XS)*(1.+3.* ET)*( ET * ET -1.)
C(3,20,N) = FR9*(1.-XS)*(1.-3.* ET)*( ET * ET -1.)
C(3,5 ,N) = -FR1*(1.-XS)*(1.- ET)*(10.-9.*(XS*XS+ET*ET))
C(3,13,N) = -FR9*(1.-3.*XS)*(1.- ET)*(XS*XS-1.)
C(3,21,N) = -FR9*(1.+3.*XS)*(1.- ET)*(XS*XS-1.)
C(3,6 ,N) = -FR1*(1.+XS)*(1.- ET)*(10.-9.*(XS*XS+ET*ET))
C(3,14,N) = -FR9*(1.+XS)*(1.-3.* ET)*( ET * ET -1.)
C(3,22,N) = -FR9*(1.+XS)*(1.+3.* ET)*( ET * ET -1.)
C(3,7 ,N) = -FR1*(1.+XS)*(1.+ ET)*(10.-9.*(XS*XS+ET*ET))

```

```

C(3,15,N) = -FR9*(1.+3.*XS)*(1.+ ET )*(XS*XS-1.)
C(3,23,N) = -FR9*(1.-3.*XS)*(1.+ ET )*(XS*XS-1.)
C(3,8 ,N) = -FR1*(1.-XS)*(1.+ ET )*(10.-9.*(XS*XS+ET*ET))
C(3,16,N) = -FR9*(1.-XS)*(1.+ 3.* ET )*( ET * ET -1.)
C(3,24,N) = -FR9*(1.-XS)*(1.-3.* ET )*( ET * ET -1.)

```

```

10 CONTINUE
RETURN
END

```

```

C
C
C

```

***** 32 NODE ELEMENT *****

```

SUBROUTINE GPN32
IMPLICIT DOUBLE PRECISION(A-H,O-Z)
COMMON/GPN1/II(48),WXSI(6),WETA(6),WRHO(6),XSI(6),ETA(6),RHO(6)
COMMON/GPN2/EN(48,32),INTXSI,INTETA,INTRHO
C0 = 9.0/64.0
C2 = 2.0*C0
DO 10 I = 1,INTRHO
DO 10 J = 1,INTXSI
DO 10 K = 1,INTETA
N = INTXSI*INTETA*(I-1)+INTETA*(J-1)+K
XN = XSI(J)
EA = ETA(K)
ZN = RHO(I)
C1 = C0*(XN**2+EA**2+ZN**2)-19.0/64.0
XP1 = 1.0+XN
XM1 = 1.0-XN
EP1 = 1.0+EA
EM1 = 1.0-EA
ZP1 = 1.0+ZN
ZM1 = 1.0-ZN
XP3 = 1.0+3.0*XN
XM3 = 1.0-3.0*XN
EP3 = 1.0+3.0*EA
EM3 = 1.0-3.0*EA
ZP3 = 1.0+3.0*ZN
ZM3 = 1.0-3.0*ZN
X2 = 1.0-XN*XN
E2 = 1.0-EA*EA
Z2 = 1.0-ZN*ZN
EN(N,1) = C1*XM1*EM1*ZM1
EN(N,28) = C0*XM1*ZM1*EM3*E2
EN(N,20) = C0*XM1*ZM1*EP3*E2
EN(N,4) = C1*XM1*EP1*ZM1
EN(N,27) = C0*EP1*ZM1*XM3*X2
EN(N,19) = C0*EP1*ZM1*XP3*X2
EN(N,3) = C1*XP1*EP1*ZM1
EN(N,26) = C0*XP1*ZM1*EP3*E2
EN(N,18) = C0*XP1*ZM1*EM3*E2
EN(N,2) = C1*XP1*EM1*ZM1
EN(N,25) = C0*EM1*ZM1*XP3*X2
EN(N,17) = C0*EM1*ZM1*XM3*X2
EN(N,9) = C0*XM1*EM1*ZM3*Z2
EN(N,12) = C0*XM1*EP1*ZM3*Z2
EN(N,11) = C0*XP1*EP1*ZM3*Z2
EN(N,10) = C0*XP1*EM1*ZM3*Z2

```

```

EN(N,13) = C0*XM1*EM1*ZP3*Z2
EN(N,16) = C0*XM1*EP1*ZP3*Z2
EN(N,15) = C0*XP1*EP1*ZP3*Z2
EN(N,14) = C0*XP1*EM1*ZP3*Z2
EN(N,5) = C1*XM1*EM1*ZP1
EN(N,32) = C0*XM1*ZP1*EM3*E2
EN(N,24) = C0*XM1*ZP1*EP3*E2
EN(N,8) = C1*XM1*EP1*ZP1
EN(N,31) = C0*EP1*ZP1*XM3*X2
EN(N,23) = C0*EP1*ZP1*XP3*X2
EN(N,7) = C1*XP1*EP1*ZP1
EN(N,30) = C0*XP1*ZP1*EP3*E2
EN(N,22) = C0*XP1*ZP1*EM3*E2
EN(N,6) = C1*XP1*EM1*ZP1
EN(N,29) = C0*EM1*ZP1*XP3*X2
EN(N,21) = C0*EM1*ZP1*XM3*X2
10 CONTINUE
RETURN
END
C
C          ***** 32 NODE ELEMENT *****
C
SUBROUTINE DN32 (C)
IMPLICIT DOUBLE PRECISION(A-H,O-Z)
COMMON/GPN1/IH(48),WXSI(6),WETA(6),WRHO(6),XSI(6),ETA(6),RHO(6)
COMMON/GPN2/EN(48,32),INTXSI,INTETA,INTRHO
C
DOUBLE PRECISION C(3,32,80)
C0 = 9.0/64.0
C2 = 2.0*C0
DO 10 I = 1,INTRHO
DO 10 J = 1,INTXSI
DO 10 K = 1,INTETA
N = INTXSI*INTETA*(I-1) + INTETA*(J-1) + K
H(N) = WRHO(I)*WXSI(J)*WETA(K)
XN = XSI(J)
EA = ETA(K)
ZN = RHO(I)
C1 = C0*(XN**2 + EA**2 + ZN**2) - 19.0/64.0
XP1 = 1.0 + XN
XM1 = 1.0 - XN
EP1 = 1.0 + EA
EM1 = 1.0 - EA
ZP1 = 1.0 + ZN
ZM1 = 1.0 - ZN
XP3 = 1.0 + 3.0*XN
XM3 = 1.0 - 3.0*XN
EP3 = 1.0 + 3.0*EA
EM3 = 1.0 - 3.0*EA
ZP3 = 1.0 + 3.0*ZN
ZM3 = 1.0 - 3.0*ZN
X2 = 1.0 - XN*XN
E2 = 1.0 - EA*EA
Z2 = 1.0 - ZN*ZN
C          *****
C

```

C
C

DERIVATIVES WITH RESPECT TO XSI

C(1,1,N) = EM1*ZM1*(-C1 + C2*XN*XM1)
 C(1,28,N) = -C0*ZM1*EM3*E2
 C(1,20,N) = -C0*ZM1*EP3*E2
 C(1,4,N) = EP1*ZM1*(-C1 + C2*XN*XM1)
 C(1,27,N) = C0*EP1*ZM1*(-3.0-2.0*XN + 9.0*XN**2)
 C(1,19,N) = C0*EP1*ZM1*(3.0-2.0*XN-9.0*XN**2)
 C(1,3,N) = EP1*ZM1*(C1 + C2*XN*XP1)
 C(1,26,N) = C0*ZM1*EP3*E2
 C(1,18,N) = C0*ZM1*EM3*E2
 C(1,2,N) = EM1*ZM1*(C1 + C2*XN*XP1)
 C(1,25,N) = C0*EM1*ZM1*(3.0-2.0*XN-9.0*XN**2)
 C(1,17,N) = C0*EM1*ZM1*(-3.0-2.0*XN + 9.0*XN**2)
 C(1,9,N) = -C0*EM1*ZM3*Z2
 C(1,12,N) = -C0*EP1*ZM3*Z2
 C(1,11,N) = C0*EP1*ZM3*Z2
 C(1,10,N) = C0*EM1*ZM3*Z2
 C(1,13,N) = -C0*EM1*ZP3*Z2
 C(1,16,N) = -C0*EP1*ZP3*Z2
 C(1,15,N) = C0*EP1*ZP3*Z2
 C(1,14,N) = C0*EM1*ZP3*Z2
 C(1,5,N) = EM1*ZP1*(-C1 + C2*XN*XM1)
 C(1,32,N) = -C0*ZP1*EM3*E2
 C(1,24,N) = -C0*ZP1*EP3*E2
 C(1,8,N) = EP1*ZP1*(-C1 + C2*XN*XM1)
 C(1,31,N) = C0*EP1*ZP1*(-3.0-2.0*XN + 9.0*XN**2)
 C(1,23,N) = C0*EP1*ZP1*(3.0-2.0*XN-9.0*XN**2)
 C(1,7,N) = EP1*ZP1*(C1 + C2*XN*XP1)
 C(1,30,N) = C0*ZP1*EP3*E2
 C(1,22,N) = C0*ZP1*EM3*E2
 C(1,6,N) = EM1*ZP1*(C1 + C2*XN*XP1)
 C(1,29,N) = C0*EM1*ZP1*(3.0-2.0*XN-9.0*XN**2)
 C(1,21,N) = C0*EM1*ZP1*(-3.0-2.0*XN + 9.0*XN**2)

DERIVATIVES WITH RESPECT TO ETA

C
C
C

C(2,1,N) = XM1*ZM1*(-C1 + C2*EA*EM1)
 C(2,28,N) = C0*XM1*ZM1*(-3.0-2.0*EA + 9.0*EA**2)
 C(2,20,N) = C0*XM1*ZM1*(3.0-2.0*EA-9.0*EA**2)
 C(2,4,N) = XM1*ZM1*(C1 + C2*EA*EP1)
 C(2,27,N) = C0*ZM1*XM3*X2
 C(2,19,N) = C0*ZM1*XP3*X2
 C(2,3,N) = XP1*ZM1*(C1 + C2*EA*EP1)
 C(2,26,N) = C0*XP1*ZM1*(3.0-2.0*EA-9.0*EA**2)
 C(2,18,N) = C0*XP1*ZM1*(-3.0-2.0*EA + 9.0*EA**2)
 C(2,2,N) = XP1*ZM1*(-C1 + C2*EA*EM1)
 C(2,25,N) = -C0*ZM1*XP3*X2
 C(2,17,N) = -C0*ZM1*XM3*X2
 C(2,9,N) = -C0*XM1*ZM3*Z2
 C(2,12,N) = C0*XM1*ZM3*Z2
 C(2,11,N) = C0*XP1*ZM3*Z2
 C(2,10,N) = -C0*XP1*ZM3*Z2
 C(2,13,N) = -C0*XM1*ZP3*Z2
 C(2,16,N) = C0*XM1*ZP3*Z2
 C(2,15,N) = C0*XP1*ZP3*Z2

```

C(2,14,N) = -C0*XP1*ZP3*Z2
C(2,5 ,N) = XM1*ZP1*(-C1 + C2*EA*EM1)
C(2,32,N) = C0*XM1*ZP1*(-3.0-2.0*EA + 9.0*EA**2)
C(2,24,N) = C0*XM1*ZP1*( 3.0-2.0*EA-9.0*EA**2)
C(2,8 ,N) = XM1*ZP1*(C1 + C2*EA*EP1)
C(2,31,N) = C0*ZP1*XM3*X2
C(2,23,N) = C0*ZP1*XP3*X2
C(2,7 ,N) = XP1*ZP1*(C1 + C2*EA*EP1)
C(2,30,N) = C0*XP1*ZP1*( 3.0-2.0*EA-9.0*EA**2)
C(2,22,N) = C0*XP1*ZP1*(-3.0-2.0*EA + 9.0*EA**2)
C(2,6 ,N) = XP1*ZP1*(-C1 + C2*EA*EM1)
C(2,29,N) = -C0*ZP1*XP3*X2
C(2,21,N) = -C0*ZP1*XM3*X2

```

DERIVATIVES WITH RESPECT TO RIHO

```

C(3,1 ,N) = XM1*EM1*(-C1 + C2*ZN*ZM1)
C(3,28,N) = -C0*XM1*EM3*E2
C(3,20,N) = -C0*XM1*EP3*E2
C(3,4 ,N) = XM1*EP1*(-C1 + C2*ZN*ZM1)
C(3,27,N) = -C0*EP1*XM3*X2
C(3,19,N) = -C0*EP1*XP3*X2
C(3,3 ,N) = XP1*EP1*(-C1 + C2*ZN*ZM1)
C(3,26,N) = -C0*XP1*EP3*E2
C(3,18,N) = -C0*XP1*EM3*E2
C(3,2 ,N) = XP1*EM1*(-C1 + C2*ZN*ZM1)
C(3,25,N) = -C0*EM1*XP3*X2
C(3,17,N) = -C0*EM1*XM3*X2
C(3,9 ,N) = C0*XM1*EM1*(-3.0-2.0*ZN + 9.0*ZN**2)
C(3,12,N) = C0*XM1*EP1*(-3.0-2.0*ZN + 9.0*ZN**2)
C(3,11,N) = C0*XP1*EP1*(-3.0-2.0*ZN + 9.0*ZN**2)
C(3,10,N) = C0*XP1*EM1*(-3.0-2.0*ZN + 9.0*ZN**2)
C(3,13,N) = C0*XM1*EM1*( 3.0-2.0*ZN-9.0*ZN**2)
C(3,16,N) = C0*XM1*EP1*( 3.0-2.0*ZN-9.0*ZN**2)
C(3,15,N) = C0*XP1*EP1*( 3.0-2.0*ZN-9.0*ZN**2)
C(3,14,N) = C0*XP1*EM1*( 3.0-2.0*ZN-9.0*ZN**2)
C(3,5 ,N) = XM1*EM1*(C1 + C2*ZN*ZP1)
C(3,32,N) = C0*XM1*EM3*E2
C(3,24,N) = C0*XM1*EP3*E2
C(3,8 ,N) = XM1*EP1*(C1 + C2*ZN*ZP1)
C(3,31,N) = C0*EP1*XM3*X2
C(3,23,N) = C0*EP1*XP3*X2
C(3,7 ,N) = XP1*EP1*(C1 + C2*ZN*ZP1)
C(3,30,N) = C0*XP1*EP3*E2
C(3,22,N) = C0*XP1*EM3*E2
C(3,6 ,N) = XP1*EM1*(C1 + C2*ZN*ZP1)
C(3,29,N) = C0*EM1*XP3*X2
C(3,21,N) = C0*EM1*XM3*X2

```

```

10 CONTINUE
RETURN
END

```

C
C CALCULATES AN ELEMENT STIFFNESS MATRIX,
C

SUBROUTINE ELKAY (D,ELXYZ,ak,C,R,dteta,dphi)
IMPLICIT DOUBLE PRECISION(A-H,O-Z)

```

COMMON/GPN1/II(48),WXSI(6),WETA(6),WRHIO(6),XSI(6),ETA(6),RHO(6)
COMMON/GPN2/EN(48,32),INTXSI,INTETA,INTRHIO
COMMON/IDAT/NNOD,NDOF,NGAUSS

```

```

C
DOUBLE PRECISION B(6,96,600),C(3,32,80),S(96,96),ELXYZ(32,3)
DOUBLE PRECISION BT(96,6),BTD(96,6),GJ(3,3),GJI(3,3),teta,tetar
DOUBLE PRECISION D(6,6),ak(3,3,528),t1(6,6),t2(6,6),dd(6,6)
REAL R(162,60),dteta,dphi
tetr = dble(dteta)
phir = dble(dphi)
teta = -tetr
phi = -phir
call t (1,teta,phi,t1)
c call t (2,tetr,phir,t2)
c do 123 i = 1,6
c do 123 j = 1,6
c d(i,j) = 0.0
c do 123 k = 1,6
c d(i,j) = d(i,j) + dd(i,k)*t2(k,j)
c 123 continue
DO 5 I = 1,ndof
DO 5 J = 1,ndof
S(I,J) = 0.d0
5 CONTINUE
n1 = ngauss*6
DO 130 I = 1,n1
DO 130 J = 1,NDOF
R(i,j) = 0.0
130 CONTINUE
n1 = nnod/2*(nnod + 1)
do 125 i = 1,3
do 125 j = 1,3
do 125 k = 1,n1
ak(i,j,k) = 0.d0
125 continue
do 10 i = 1,ngauss
xgp = 0.0
ygp = 0.0
zgp = 0.0
do 20 j = 1,nnod
xgp = xgp + en(i,j)*elxyz(j,1)
ygp = ygp + en(i,j)*elxyz(j,2)
zgp = zgp + en(i,j)*elxyz(j,3)
20 continue
write(6,200) xgp,ygp,zgp
200 format(t5,3(5x,f12.5))
10 continue
IBMAT = 0
c
DO 30 NG = 1,NGAUSS
IBMAT = IBMAT + 1
DO 40 I = 1,3
DO 40 J = 1,3
GJ(I,J) = 0.0
DO 44 K = 1,NNOD

```

```

      GJ(I,J) = GJ(I,J) + C(I,K,NG)*ELXYZ(K,J)
44      CONTINUE
40      CONTINUE
C
      DETJ = GJ(1,1)*GJ(2,2)*GJ(3,3) + GJ(1,2)*GJ(2,3)*GJ(3,1)
C      + GJ(1,3)*GJ(2,1)*GJ(3,2) - GJ(1,3)*GJ(2,2)*GJ(3,1)
C      - GJ(1,1)*GJ(2,3)*GJ(3,2) - GJ(1,2)*GJ(2,1)*GJ(3,3)
C
      IF ( DETJ.LT. .00000001) THEN
300      WRITE(6,300) NG
C      FORMAT(/5X,'ZERO OR NEGATIVE JACOBIAN DETERMINANT',
C      //,5X,'GAUSS POINT NO.',I3)
      STOP 3
      END IF
      DETINV = 1./DETIJ
      GJI(1,1) = ( GJ(2,2)*GJ(3,3) - GJ(2,3)*GJ(3,2) )*DETIJ
      GJI(2,1) = ( GJ(2,3)*GJ(3,1) - GJ(2,1)*GJ(3,3) )*DETIJ
      GJI(3,1) = ( GJ(2,1)*GJ(3,2) - GJ(2,2)*GJ(3,1) )*DETIJ
      GJI(1,2) = ( GJ(3,2)*GJ(1,3) - GJ(1,2)*GJ(3,3) )*DETIJ
      GJI(2,2) = ( GJ(1,1)*GJ(3,3) - GJ(1,3)*GJ(3,1) )*DETIJ
      GJI(3,2) = ( GJ(1,2)*GJ(3,1) - GJ(1,1)*GJ(3,2) )*DETIJ
      GJI(1,3) = ( GJ(1,2)*GJ(2,3) - GJ(2,2)*GJ(1,3) )*DETIJ
      GJI(2,3) = ( GJ(2,1)*GJ(1,3) - GJ(1,1)*GJ(2,3) )*DETIJ
      GJI(3,3) = ( GJ(1,1)*GJ(2,2) - GJ(1,2)*GJ(2,1) )*DETIJ
C
      DO 55 I = 1,6
        DO 55 J = 1, NDOF
55      B(I,J,IBMAT) = 0.0
C
      DO 60 I = 1,3
        DO 60 K = 1, NNOD
          NN = (K-1)*3 + I
          DO 60 J = 1,3
60      B(I,NN,IBMAT) = B(I,NN,IBMAT) + GJI(I,J)*C(J,K,NG)
C
      DO 70 K = 1, NNOD
        NN = 3*(K-1) + 1
        DO 70 J = 1,3
          B(4,NN + 1,IBMAT) = B(4,NN + 1,IBMAT) + GJI(3,J)*C(J,K,NG)
          B(4,NN + 2,IBMAT) = B(4,NN + 2,IBMAT) + GJI(2,J)*C(J,K,NG)
          B(5,NN,IBMAT) = B(5,NN,IBMAT) + GJI(3,J)*C(J,K,NG)
          B(5,NN + 2,IBMAT) = B(5,NN + 2,IBMAT) + GJI(1,J)*C(J,K,NG)
          B(6,NN,IBMAT) = B(6,NN,IBMAT) + GJI(2,J)*C(J,K,NG)
          B(6,NN + 1,IBMAT) = B(6,NN + 1,IBMAT) + GJI(1,J)*C(J,K,NG)
70      C
      DO 79 I = 1, NDOF
        DO 79 J = 1,6
          BT(I,J) = B(J,I,IBMAT)
79      CONTINUE
C
      DO 81 I = 1, NDOF
        DO 81 J = 1,6
          BTD(I,J) = 0.0
          DO 80 K = 1,6
            BTD(I,J) = BTD(I,J) + BT(I,K)*D(K,J)

```

```

80   CONTINUE
81   CONTINUE
C
WEIGHT = H(NG)*DETJ
DO 90 I = 1,NDOF
  DO 90 J = I,NDOF
    DO 90 L = 1,6
      S(I,J) = S(I,J) + WEIGHT*BTD(I,L)*B(I,J,IBMAT)
90   CONTINUE
30   DO 118 I = 1,NDOF
      DO 118 J = I,NDOF
        S(J,I) = S(I,J)
118  CONTINUE
C
  NN = 1
  DO 110 N = 1,NNOD
    NN = NN + N - 1
    N1 = NN + N - 1
    DO 110 L = NN,N1
      DO 110 M1 = 1,3
        DO 110 M2 = 1,3
          I = (N-1)*3 + M2
          J = (L-NN)*3 + M1
          AK(M1,M2,L) = S(j,i)
110  CONTINUE
      do 122 i = 1,6
        do 122 j = 1,6
          dd(i,j) = 0.0
          do 122 k = 1,6
            dd(i,j) = dd(i,j) + t1(i,k)*d(k,j)
122  continue
      DO 120 NG = 1,NGAUSS
        DO 120 ND = 1,NDOF
          DO 120 I = 1,6
            k = (ng-1)*6 + i
            r(k,nd) = 0.0
            DO 120 J = 1,6
              R(K,ND) = R(K,ND) + dD(I,J)*B(J,ND,NG)
120  CONTINUE
      RETURN
      END
C
C      TO CALCULATE D, THE STRESS-STRAIN MATRIX
c
SUBROUTINE DMAT (E,D,ateg)
IMPLICIT DOUBLE PRECISION(A-H,O-Z)
DOUBLE PRECISION T1(6,6),T2(6,6),DT2(6,6),D(6,6)
REAL E(15)
E11 = E(1)
E22 = E(2)
E33 = E(3)
G12 = E(4)
G13 = E(5)
G23 = E(6)
V12 = E(7)
V13 = E(8)

```

```

V23 = E(9)
THETA = E(10)/57.29577951
phi = e(11)/57.29577951
del = theta-ateg
V21 = V12*E22/E11
V31 = V13*E33/E11
V32 = V23*E33/E22
POISON = 1./(1-V12*V21-V13*V31-V23*V32-V12*V23*V31-V21*V13*V32)
DO 10 I = 1,6
  DO 10 J = 1,6
    D(I,J) = 0.0
10 CONTINUE
D(1,1) = (1-V23*V32)*E11*POISON
D(1,2) = (V12 + V13*V32)*E22*POISON
D(1,3) = (V13 + V12*V23)*E33*POISON
D(2,2) = (1-V13*V31)*E22*POISON
D(2,3) = (V23 + V21*V13)*E33*POISON
D(3,3) = (1-V12*V21)*E33*POISON
D(4,4) = G23
D(5,5) = G13
D(6,6) = G12
DO 20 I = 1,6
  DO 20 J = 1,6
    D(J,I) = D(I,J)
20 CONTINUE
c REVT = -THETA
c revp = -phi
revt = -del
revp = -phi
CALL T(1,REVT,revp,T1)
c CALL T(2,THETA,phi,T2)
CALL T(2,del,phi,T2)
DO 30 I = 1,6
  DO 35 J = 1,6
    DT2(I,J) = 0.0
    DO 35 K = 1,6
      DT2(I,J) = DT2(I,J) + D(I,K)*T2(K,J)
35 CONTINUE
30 CONTINUE
DO 40 I = 1,6
  DO 40 J = 1,6
    D(I,J) = 0.0
    DO 40 K = 1,6
      D(I,J) = D(I,J) + T1(I,K)*DT2(K,J)
40 CONTINUE
RETURN
END

C
C
C          TO CALCULATE STRESS AND STRAIN
C          TRANSFORMATION MATRICES
C
SUBROUTINE T(N,THETA,PHI,T1)
IMPLICIT DOUBLE PRECISION(A-H,O-Z)
DOUBLE PRECISION T1(6,6)
C

```

```

DO 10 I= 1,6
  DO 10 J= 1,6
    T1(I,J)= 0.0
10 CONTINUE
S= DSIN(THETA)
C= DCOS(THETA)
S2= S**2
C2= C**2
T1(1,1)= C2
T1(2,2)= C2
T1(1,2)= S2
T1(2,1)= S2
T1(3,3)= 1
T1(4,4)= C
T1(5,5)= C
T1(4,5)= -S
T1(5,4)= S
T1(6,6)= C2-S2
T1(1,6)= 2.*C*S/FLOAT(N)
T1(2,6)= -2.*C*S/FLOAT(N)
T1(6,1)= -FLOAT(N)*C*S
T1(6,2)= FLOAT(N)*C*S
RETURN
END
C
C
C= END FORTRAN

```

**The vita has been removed from
the scanned document**